5-2018

# Tissue engineered micro and macrovasculature utilizing stromal vascular fraction.

Joseph Samir Zakhari
*University of Louisville*

# TISSUE ENGINEERED MICRO AND MACROVASCULATURE UTILIZING STROMAL VASCULAR FRACTION

by

Joseph Samir Zakhari
B.S., Wake Forest University, 2009
M.A., Boston University School of Medicine, 2013

A Dissertation
Submitted to the Faculty of the
School of Medicine of the University of Louisville
In Partial Fulfillment of the Requirements
For the Degree of

Doctor of Philosophy in Physiology and Biophysics

Department of Physiology
University of Louisville
Louisville, KY

May 2018

TISSUE ENGINEERED MICRO AND MACROVASCULATURE UTILIZING STROMAL VASCULAR FRACTION

by

Joseph Samir Zakhari
B.S., Wake Forest University, 2009
M.A. Boston University School of Medicine, 2013

A Dissertation Approved on

April 19, 2018

by the following Dissertation Committee

_____
Stuart K. Williams, Ph.D., Dissertation Director

_____
James B. Hoying, Ph.D.

_____
Amanda J, LeBlanc, Ph.D.

_____
Mark S. Slaughter, M.D.

_____
Irving G. Joshua, Ph.D.

# DEDICATION

This dissertation is dedicated to my family for their continual support towards my pursuit of my two graduate degrees; to my father Samir Zakhari, my mother Beatrix Zakhari, and my sisters Julia and Lydia Zakhari. It is not without their help that I am where I am today, and I thank them for their love, words of wisdom, encouragement, and pride in my accomplishments.

ACKNOWLEDGEMENTS

Dr. Stuart Williams and I met over 3 years ago when my interest in molecular cardiology and bioengineering led me to his Biofical Organs research program. I want to thank him for him for his patience and guidance during my time struggling over experiments or trying to grasp new knowledge and techniques. He always gave me enough mentorship to stimulate my scientific questioning without depriving me of intellectual independence or the pursuit of individuality in his lab, ultimately mending me to become an independent researcher with the hopes of one day running my own lab. I thank Dr. James Hoying for never letting me get the easy answer and always making me think when it comes to vascular biology, cellular mechanisms, and experimental design. He always pushed me to the limits and because of that I feel a great sense of accomplishment, albeit once I finally figured out the answers to his difficult questions. I thank Dr. Amanda LeBlanc for her expertise in *in vivo* surgical approaches and I will always feel welcome asking her help and guidance when it comes to small animal model experiments. I thank Dr. Mark Slaughter for stimulating the clinical side of my brain and always asking if my research is translatable. His keen questioning has continually kept me on course towards my pursuit of becoming a physician scientist where one day I hope to bring research from the bench to the bedside. Finally, I'd like to thank Dr. Irving Joshua, Dr. Binks Wattenberg, and Dr. Donald Miller whom afforded me the opportunity to join the Physiology department for my studies in addition to joining U of L's combined MD-PhD program.

ABSTRACT

TISSUE ENGINEERED MICRO AND MACROVASCULATURE UTILIZING STROMAL VASCULAR FRACTION

Joseph Samir Zakhari

April 19, 2018

This dissertation describes the use of stromal vascular fraction to tissue engineer 3D microvasculature and macrovasculature. Stromal vascular fraction is an easily isolatable cell source from adipose tissue depots. It has demonstrated remarkable potential both *in vitro* and *in vivo* for forming microcirculation capable of perfusion upon implantation. SVF is clinically utilized as a therapeutic cell source for anti-inflammation for osteoarthritis and is being studied for ischemic tissue application to stimulate revascularization.

The work described herein is divided within four chapters. Chapter I provides an introductory overview and lists the aims and hypothesis for the dissertation. Chapter II describes experiments towards elucidating specific aim 1: **determine the mechanism by which SVF forms neovascular networks in 3D fibrin gels *in vitro*.** This was accomplished through a multitude of experiments describing SVF undergoing vasculogenesis and angiogenesis in a 2D automated *in vitro* assay, and the ability to inhibit these processes via NOTCH and PDGF-B/PDGFR-β interruption. These mechanisms, as well as integrin dependent mechanisms, were analyzed within 3D fibrin and 3D collagen I culture systems

as well. It is believed that the activation of the fibrin specific integrin $\alpha_V\beta_3$ plays a role in hyper-stimulating fibrin-embedded endothelial cells in a VEGF dependent manner.

Chapter II describes experiments towards understanding specific aim 2: **create deliverable tissue units of SVF-derived microvasculature or macrovasculature utilizing bioprinting, and electrospinning technologies.** This was accomplished through bioprinting spheroids containing cells embedded in collagen I or fibrin using superhydrophobic surface technology or electrospinning varying porosities of PCL and pressure sodding SVF cells into the material. It is possible to automate and create dosable units of microvascular tissue in spheroid format using SVF cells, ECM such as fibrin or collagen I, and bioprinting technologies. Additionally, it is possible to create blood vessel mimics of multiple porosities in order to retain and allow cellular infiltration within the biomaterial. Chapter IV is an overall summary and conclusion of the dissertation. These studies could hopefully generate more knowledge on the creation of tissue engineered microvasculature and microvasculature for use in treating ischemic cardiomyopathies.

TABLE OF CONTENTS

LIST OF TABLES

LIST OF FIGURES

# CHAPTER I

# INTRODUCTION

## Ischemic Cardiovascular Disease

Cardiovascular disease is a growing concern in the western world. The American Heart Association in 2017 states that an estimated 92.1 million adults in the United States have at least one type of cardiovascular disease (CVD), and by 2030, 43.9% of the population is projected to have some form of cardiovascular disease[1]. Due to increase in treatments of acute conditions and better therapies, death rates due to CVD have declined by 25.3% since 2004[1]. While deaths have declined, the growing rates of cardiovascular disease can still be attributable to smoking and tobacco use, physical inactivity, poor nutrition, obesity, high blood cholesterol, high blood pressure, and increases in type II diabetes and metabolic syndrome.

Smoking and tobacco usage has decreased over the past ten years, (15.2%) but with changing technology, there has been increases in e-cigarette usage especially in middle school (5.3%) and high school (16.0%) students. In addition to tobacco usage, only 27.1% of high school students meet the 60 minutes or more per day physical activity recommendations in 2015[1]. The increase in obesity from 2000 to 2013 was significant in adults and youth, however, obesity rates have begun to level off, according to the most recent AHA statistics. Cholesterol lowering drugs such as statins have increased in usage from 7 to 17% from the years 1999 – 2012 alone, trending with the decrease in the age-

adjusted blood levels of low-density lipoprotein cholesterol (126mg/dL to 111mg/dL; 1999 to 2014) as well as the age-adjusted prevalence of high-density lipoprotein cholesterol (42.9% to 28.5%, 1999 to 2014 respectively). Hypertension in US adults in 2014 was estimated to be 34%, totaling 85.7 million adults, and in children to adolescents 8 to 17 years old, the prevalence of borderline to high blood pressure was noted at 11%. Controlling hypertension in both adults and adolescents with stage 2 hypertension is a foundational therapy which can potentially be cost saving for CVD associated hospitalizations in the future. The most recent statistics show that an estimated 23.4 million US adults have diabetes mellitus with 7.6 million remaining undiagnosed and 81.6 million having prediabetes[1]. Even with some promising statistics, it should be noted however that CVD and associated hospital costs can provide a devastating burden to the socioeconomic structure of the American health care system in years to come.

There are many types of CVD, but of the acute types, where the majority of hospitalizations are required, these can be attributed to myocardial infarction brought on by coronary artery disease or acute coronary syndrome. Coronary artery disease is described as a pathogenesis in which an atherosclerotic plaque high in low-density lipoprotein builds up on the intimal surface of the coronary artery in areas of endothelial cell damage, causing increased inflammation, lipoprotein retention, and foam cell formation with subsequent luminal narrowing and thrombosis or rupture of plaque, sending lipid-rich emboli distally, leading to incomplete or complete occlusion of downstream coronary branches and loss of oxygen rich blood delivery to the myocardium. Atherosclerosis can affect the coronary arteries, abdominal aorta, thoracic aorta, circle Willis, and popliteal arteries.

However, regardless of location, the pathogenesis remains the same. Atherosclerosis begins with the depositing of fatty streaks at areas of significant turbulent blood flow causing additional hemodynamic stress and damage to the underlying endothelium. These damaged cells subsequently upregulate adhesion molecules for neutrophilic and monocytic binding and infiltration[2] as well as lose functional adherens junctions between cells allowing for increased LDL entry into the sub-intimal space[3]. Increase in LDL stores sub-intimally leads to inappropriate oxidation of LDL which exacerbates monocyte recruitment to the area. The oxidized LDL along with Apolipoprotein B are phagocytosed by the recruited monocytes/macrophages, however, the enzymatic ability of the cells become limited and as such, huge deposits of oxidized LDL remain within the cell giving the cell a histological 'foamy' appearance, thus termed foam cells[4]. Foam cells indeed are highly inflammatory due to increased cytokine production and release, ultimately stimulating local smooth muscle cell proliferation and production and secretion of collagen. As such, a positive feedback loop occurs causing increased recruitment of monocytes, increased LDL storage, increased damage to underlying smooth muscle cells, and pathophysiologic change from a 'fatty streak' to an atherosclerotic plaque[5]. The developing atherosclerotic lesion can itself reduce luminal size, reduce distal blood flow via occlusion or thrombotic formation at the lesion as well as weaken and rupture sending emboli distally all while increasing vessel wall stress and proximal aneurysm formation. Regardless of late stage rupture or thrombosis, both ultimately lead to cessation of physiologic blood flow, infarction and tissue necrosis.

At the coronary artery, non-restorative loss of blood flow leads to tissue apoptosis and necrosis, termed clinically a transmural infarct if involvement occurs from

endocardium through the myocardium, i.e., greater than 50% of the thickness of the ventricular wall. Initial infarct size grows in a waveform state in which collateral microvessels cannot support the needs of the surrounding tissue to the primary infarct zone and subsequently undergo apoptosis and necrosis as well, termed the 'border zone' of infarct where it is argued that this tissue is most responsive to clinical revascularization.

Cell viability may be preserved if blood flow is restored immediately post infarct (20-40min). Indeed, within seconds of loss of myocardial blood supply, cardiomyocytes' aerobic glycolysis ceases leading to inadequate ATP and production of lactic acid with a functional loss of contraction within just a minute of ischemic insult. On a subcellular level, mitochondrial swelling is noticed along with myofibrillar relaxation and glycogen depletion. If the ischemic insult lasts more than 40 minutes, coagulative necrosis takes place. Overtime, both gross and microscopic findings of the affected tissue demonstrate an infarct that remodels first through a highly infiltrated granulation tissue, subsequent robust angiogenesis but latter angioregression[6,7], and finally, a dense, avascular collagenous scar, ultimately affecting multiple functions, including contractility as well as signal transduction from pacemaker cells[8,9].

If patients do survive the initial infarct, remodeling of the tissue occurs and can lead to infarct expansion, loss of muscle density, and left ventricular systolic failure potentially leading to congestive heart failure if chronically left untreated. What governs the location, size, and morphological features of acute MI ultimately depend on 1) location, severity and rate of coronary occlusion, 2) size of the vascular bed perfused by the obstructed vessel(s), 3) duration of the occlusion, 4) metabolic demands of the myocardium, and 5) the extent of collateral blood supply that may provide support to the ischemic tissue.

While most attribute MI to coronary artery atherosclerosis, the microvasculature of the heart and the downstream reperfusion even after surgical coronary artery bypass grafting (CABG) are instrumental in functional retention of the myocardium. Indeed, because of the high metabolic demand of the heart, the microvasculature makes up 37% of the total volume of the heart[10]. Even post CABG, a phenomenon called no-reflow may occur in which conduit vessel perfusion is not satisfactory to perfuse downstream microvasculature in the affected tissue[11]. While this phenomenon is not well understood, it is hypothesized that redistribution of flow via microvessels away from the necrotic core is a saving mechanism for the surrounding host tissue not damaged by ischemic insult, and that the redirection of flow increases areas in which microvessels can rupture or form aneurysms within the necrotic zones. However, the border zone infarct is significantly depleted of oxygen rich blood in severe cases of no-flow as well[12].

Current approved therapies for acute myocardial infarction include surgical and non-surgical techniques in order to correct the coronary artery insult. Of the surgical techniques coronary artery bypass grafting is a predominant treatment today in which either the saphenous vein or the left internal mammary artery (LIMA) is harvested to use as a conduit vessel to circumvent the blockage within the native coronary vessel. The LIMA is the vessel of choice with greater than 90% of patients retaining patency over a 10-year period and less than 4% developing any atherosclerosis of hemodynamic significance. Saphenous vein is a secondary vessel used, however, as current statistics demonstrate, up to 25% of saphenous grafts occlude within 1 year post-operatively[13]. The procedure was first established by Debakey and Favaloro in 1968 and is still the predominant surgical

procedures used today[14-16]. The peak number of operations were roughly 519,000 in 2000 and has declined to about 300,000 in 2012[13].

Non-surgically, percutaneous transluminal coronary angioplasty or stenting is a common treatment to relieve angina as well as acute MI due to coronary occlusion. Briefly, a catheter is inserted into the arterial circulation usually through the groin or femoral artery and advanced retrograde against blood flow into the coronary artery of interest. After angiography, a balloon at the end of the catheter is inflated widening the lumen of the vessel at the point of plaque narrowing, in addition, expandable mesh stents can be deployed intra-arterially around the balloon and be retained within the vessel wall to provide mechanical integrity in order to keep the lumen patent. PTCA was first performed by Andreas Gruntzig in 1977 and is still used today[17-19].

More recent efforts to elucidate stem cell therapies and other cellular transplantation have been forefront in cardiac regenerative medicine as of recent. Most of these therapies involve isolating adult cardiac stem cells from patient tissue such as atrial appendage in order to culture expand and reintroduce to the damaged myocardium. The idea being that the ckit positive adult cardiac stem cells will localize to areas of insult and replenish damaged cardiomyocytes, indeed, endogenous cardiac myocytes cannot replicate and self-heal. A key phase one clinical trial called SCIPIO was performed in which patient's own ckit$^{+}$ adult cardiac stem cells were isolated, expanded, and reintroduced to the damaged myocardium through coronary balloon occlusion and release of cells intravascularly. However, less than 2% of the cells homed and resided in the heart tissue with most localizing to the liver, lungs and kidneys. As such, while some patients experienced increases in ejection fraction and other beneficial hemodynamic measures, it

was concerning that the cell-based therapies were not retained, and rather, paracrine mechanisms may be at play[20-22].

The SCIPIO trial, and others utilizing stem cells, focus on the endpoint of ejection fraction due to functional mass increase of myocardium without addressing a key concern post MI as alluded to prior: the dysfunction of microcirculation within the ischemic tissue. It is imperative to restore vascular supply to retain and support endogenous cardiac myocytes as well, and as such, seems logical to introduce cells that reproduce microvasculature as well. Indeed, animal studies utilizing heterogenous cell populations like SVF contained within tissue engineered constructs retain cell populations at areas of surgical implant. Leblanc and colleagues created a hybrid vascular graft patch for the pericardium of animals undergoing left coronary artery ligation to aid in systolic function of the ischemic tissue. This graft was made of a vicryl™ mesh support system housing adipose-derived stromal vascular fraction cells (SVF) embedded within the pores. In the presence of both vicryl™ and cells, increased hemodynamic pressures specifically demonstrating improved systolic function were noted in addition to increased microvessel density and perfusion at site of SVF patch implant[23]. As such, tissue engineered microvasculature may be an alternative roadmap to follow for future cell-based therapies for ischemic cardiomyopathies.

**The Circulatory System**

The vasculature is a complex organ within the body that serves to provide oxygenated blood to tissues and remove waste and metabolites as well as circulate deoxygenated blood back to the heart and lungs. It is a complex system made up of a

multitude of cell types that form distinct hierarchical structures including arteries, arterioles, veins, venules, and capillaries.

Arteries function to carry oxygenated blood from the lungs and heart to deliver to the peripheral and visceral organs. As mainly conduit vessels, their structure resembles their function. At the macroscopic level, arteries can be divided into 3 main layers. These layers are the tunica intima, the tunica media, and the tunica adventitia. The tunica intima is comprised of a single layer of endothelial cells as well as a basement membrane/internal elastic membrane, the latter of which provides polarity and a diffusion barrier to proteins crossing the endothelial cell layer from the lumenal blood.

Adjacent to the internal elastic lamina resides the tunica media composed predominantly of smooth muscle cells. The tunica media functions to respond to luminal sheer and pressure signals sent from the endothelium, as well as juxtacrine and paracrine signaling to either contract or relax, thereby changing the diameter of the vessel. These smooth muscle cells maintain what is known as vascular tonicity. The tunica media is physically separated by the external elastic membrane or external elastic lamina from the final layer, the tunica adventitia.

The tunica adventitia is the outermost layer of the vessel and is made up of fibroblasts, resident immune cells, connective tissue, and perivascular nerves. It was once believed to be a layer of purely structure and separation from surrounding tissues, but now there is much debate regarding resident immune cell signaling as important mediators of vascular function in both diseased and non-diseased states[24].

If we continue to follow blood flow from the arteries we move to arterioles which have decreased diameters and regulate the flow of blood to a higher extent due to their

thick tunica media with smooth muscle cells aligned concentrically as well. They are known as the resistance vessels within the body. Upon constriction or dilation, arterioles can regulate the flow of blood into the downstream capillary beds. It is here at the capillary where nutrient and gas exchange predominantly occurs. Capillary lumens are quite small ranging from about 5-10 μm in diameter, roughly the size of a single red blood cell. The diameter change allows for blood cells to pass through at low velocity such that gaseous material and small molecules could be transferred between the blood cell, endothelium, and tissue to allow for tissue oxygenation and waste removal.

Capillary beds are highly specialized for certain functions depending on the organ in which they perfuse. More specifically, there are three types of capillaries: continuous, fenestrated, and sinusoidal. Continuous capillaries are those in which endothelial cells retain tight junctions or zonula occludens/adherens where the junctions exhibit vascular cadherins (i.e. VE-cadherin), proteins which link adjacent cells together in a fashion that restricts the ability of large proteins to cross between cells. Along with tight junctions, continuous capillaries also have a continuous basement membrane on the basal side of the cell. Basement membranes are proteinaceous complexes made of collagen IV, laminins, hyaluronic acid, and other proteins. They present an additional physical as well as charge barrier to any large molecule or protein trying to cross from luminal space to tissue space, and vice versa. These structural barriers are important in areas of the body that have to limit protein or large molecule movement from the circulation into the tissue. Such an example would be the blood brain barrier which is predominantly made up of continuous capillaries that exhibit zonula occludens. The next type of capillary is the fenestrated capillary. Fenestrated capillaries like continuous capillaries have a continuous,

uninterrupted basement membrane, however, there exists windows within endothelial cells, small openings on the order of 60-80 nm which allow transvascular exchange of small molecules and proteins. Such capillaries can be found in organs such as the small intestine, pancreas, and kidney where proteins and hormones need to transfer from tissue space into circulation and vice versa. The final type of capillary is sinusoidal capillaries. Unlike fenestrated and continuous capillaries, sinusoidal capillaries have discontinuous basement membranes and endothelial junctions which allow for the passage of large substances, as large as 30-40 μm to cross, such as red blood cells, white blood cells, albumin and other plasma proteins, bilirubin, etc. Organs that contain sinusoidal capillaries include the spleen, liver, lymph nodes, and bone marrow.

After nutrient exchange occurs at the capillaries, deoxygenated blood returns through venules and veins back to the right heart to be pumped into the lungs for reoxygenation. Venules and veins contain the same cell types as arterioles and arteries, however they are more compliant usually with less smooth muscle cells. In other words, they store a lot of the blood volume and can stretch to accommodate larger volumes. Interestingly, returning deoxygenated blood back to the heart would be a concern when working against gravity, however, this is mitigated by the presence of one-way valves in conjunction with skeletal muscle pumps that facilitate unidirectional movement back towards the inferior and superior vena cava. These valves are endothelial flaps that are unique to the venous and lymphatic side of the circulatory system.

**Development of the Circulatory System; Vasculogenesis and Angiogenesis**

The mammalian circulatory system develops initially utilizing two processes: vasculogenesis and angiogenesis. Vasculogenesis is the differentiation and assembly of individual endothelial cells into blood vessels *in situ*. Usually this event is initiated extraembryonically, associated with the formation of blood islands within the yolk sac. Blood islands are groupings of hemangioblasts, cells that are hematopoetic precursors as well as angioblasts which form the vessel proper. The other type of vasculogenesis occurs intraembryonically. More specifically, intraembryonic vasculogenesis occurs when angioblasts within the aorta-gonad-mesonephros differentiate to form the dorsal aorta and the cardinal veins. The dorsal aorta fuses with differentiated angioblasts that arose from the cranial mesoderm, which at this point in embryonic development forms the endocardium of what will be the heart. These two systems fuse and ultimately remodel to the endocardial tube, the plexus of endothelial cells that ultimately will form the heart and aorta. It is argued from this point forward that intraembryonic development is primarily through angiogenesis, the growth of new blood vessels from preexisting ones.

Angiogenesis occurs through predominantly two mechanisms. The classical mechanism is sprouting, where endothelial cells migrate away from nascent vasculature into the tissue to establish a new vascular bed. Sprouting occurs via production and secretion of matrix metalloproteases, enzymes which help degrade surrounding matrix outside the vessel within the tissue of interest, as well as parts of the vessel connective tissue itself, to subsequently allow endothelial cell migration through a more porous microenvironment. Sprouting angiogenesis is activated via a chemotactic gradient of specific growth factors such as hypoxia inducible factor 1 alpha (HIF1$\alpha$) and vascular

endothelial growth factor (VEGF), which stimulate endothelial cells to migrate into low oxygen tension, avascular tissues, mechanisms which will be described in detail further. The second type of angiogenesis is known as intussusception, which is the mechanism in which existing blood vessels, usually, smaller vessels such as capillaries, pinch inward within the lumen, splitting one vessel into two or more vessels, a phenomenon highly dependent upon pericytyes and surrounding matrix interaction and stability. The initial description and use of the term angiogenesis was by John Hunter in the 1780's. Judah Folkman and colleagues in the early 1970s proposed that angiogenesis was a major contributor to the expansion of solid tumors[25-27].

The molecular mechanisms involved in vascuologenesis and angiogenesis are quite complex, however, several known growth factors are key players in both events. Beginning early in vasculogenesis, hemangioblasts must get signaling to differentiate from the mesoderm and follow a path to nascent vessel formation. Fibroblast growth factor (FGF) and bone morphogenic protein (BMP) families of growth factors are the primary cue for this differentiation cascade to occur[28-31]. Fibroblast growth factor consists of two predominant forms, acidic and basic FGF. There are a total of 15 FGF members, all containing heparin-binding motifs[32]. To understand FGF's role in vascular development, FGF2 knockout animals were studied. Interestingly, the knockout was not lethal, however, mice had decreased vascular tone and low blood pressure as compared to wild type [33,34]. On the other hand, overexpression of the gene led to tumors that were highly angiogenic in nature [35].

An extremely important factor regulating angiogenesis both during embryonic development and throughout life is the secretion of vascular endothelial growth factor

(VEGF). The VEGF family contains 7 members: VEGF-A (5 isoforms 121, 145, 165, 189, and 206 amino acids), VEGF-B, VEGF-C, VEGF-D, VEGF-E, svVEGF, and placental growth factor (PlGF) with VEGF-A the most notable upregulated form found in a variety of solid human cancers and lymphomas. The cells that respond to VEGF are those that have VEGF-Receptor 1 (FLT-1) and VEGFR-2 (FLK-1), which happen to be restricted to only endothelial cells[36]. VEGF initially was discovered in the early 1980s by Senger and colleagues where they witnessed tumor cells secreting a substance that made vasculature leaky and increased the production of ascites fluid. As such, VEGF was initially described as Vascular Permeabilty Factor (VPF) [37]. Continually studies into the late 1980s changed the name from VPF to VEGF. Indeed, it was found that VPF was a mitogen that played a key role in tumor angiogenesis[38]. VEGF, unlike FGF is instrumental to embryo survival. Loss of a single copy of the VEGF gene results in embryonic lethality. VEGF is such an incredible inducer of angiogenesis that inhibitors of the molecule have been studied clinically as treatments for highly vascularized tumors and metastatic cancers. Avastin (bevacizumab) is a well-known example cleared for use by the FDA in 2004 for metastatic cancer of the colon and rectum[39].

Angiogenesis as aforementioned is the sprouting and migration of endothelial cells away from an established vessel in order to infiltrate new tissue, lumenize and create a new branch or vessel to provide the oxygen and nutrients necessary to that tissue. The original endothelial cell migrating is known as the tip cell, where the subsequent endothelial cell following behind is known as the stalk cell. Local hypoxia is a key trigger of angiogenesis where HIF1$\alpha$ stimulates the production of VEGF which acts as a chemoattractant to endothelial cells. The first cell migrates away due to the high production of matrix

metalloproteases and active cytoskeletal rearrangement with high presence of filipodia on the cell surface. Intricate signaling takes place between the tip cell and the subsequent stalk cell behind which dictates phenotype of each endothelial cell. Specifically, VEGF binding to VEGFR2 increases the expression of delta-like ligand 4 (Dll4) on tip cells which activates NOTCH signaling on the adjacent stalk cell. Notch is cleaved by ADAM and γ-secretase which solubilizes the intracellular domain NICD, a transcription factor which downregulates VEGFR2 and upregulates Wnt and VEGFR1, pushing the cell to retain a stalk cell phenotype; unlike the tip cell which has high filipodia, motility, and expression of VEGFR2 on the cell surface[40].

Individual tip and stalk cells undergo tubulogenesis as well to establish a lumen. Cell hollowing and cord hollowing are the established models for tubulogenesis. In cell hollowing, endothelial cells undergo pinocytosis, vacuolar formation and continual fusion to create a hole or lumen within and individual endothelial cell. Exocytosis between cells at basolateral surfaces create a continuous lumen. Polarity is established upon complete lumen formation of single endothelial cells aligned next to one another. In cord hollowing, endothelial cells lose apical to basal polarity. Signaling externally, pinocytotic vesicles carry apical markers and fuse between multiple endothelial cells' membranes. A tube in cross section in the cord model will be made of two or more endothelial cells while a tube in cross section in the cell hollowing model will only contain one nucleus, one endothelial cell[41].

The endothelial cell in addition to forming the lining of the vasculature also modulates vasodilation, vasoconstriction, inflammation, oxidative phosphorylation and thrombosis in order to maintain homeostasis of the local microenvironment. Vasodilation

and vasoconstriction are predominantly through endothelial cell production of nitric oxide, a potent vasodilator produced through the enzyme endothelial nitric oxide synthase (eNOS)[42]. Nitric oxide diffuses into the smooth muscle layer of the vessel and promotes recycling of ADP and ATP to relax smooth muscle cells. On the other end, endothelial cells produce endothelin and prostanoids which are potent vasoconstrictors. eNOS itself can be increased in the presence of VEGF, serotonin, adenosine, and bradykinin[43,44]. Nitric oxide also can decrease inflammation and oxidative phosphorylation leading to a decrease in reactive oxygen species[45]. The endothelial cell in addition, regulates diapedesis and the transfer of white blood cells from the circulation into the surrounding tissue under inflammatory responses by upregulating cell surface adhesion molecules Selectin and ICAM[46].

A final set of mechanisms to discuss that are pivotal to formation of functional, non-leaky microvasculature is the paradigm in which newly formed endothelial tubes recruit and communicate with perivascular support cells, pericytes in order for vessel maturation to occur. During sprouting angiogenesis, endothelial cells secrete the ligand platelet-derived growth factor B. The concomitant receptor for this ligand is PDGFRβ which is found on co-migrating pericytes. In studies where mice had knockout PDGFRβ or PDGFB, mural cell deficiency and widespread vascular leakage led to perinatal lethality, in addition to the absence of glomerular tufts within the kidneys[47].

Once pericytes are recruited to endothelial networks they produce tight adhesions, N-Cadherins to maintain position with the endothelial cell. Additional signaling occurs where the pericyte or mural cell now produces angiopoetin-1, a paracrine factor stimulating the production of the Tie 2 receptor on the endothelial cell which is imperative for continual

endothelial cell survival, angiogenesis, and additional mural cell attachment and retention. Mice lacking the Tie2 receptor develop cardiac defects, edema, and hemorrhage and die in utero[48].

A sphingosine, lipid derived molecule known as S1P is produced by platelets and hematopoetic cells to activate endothelial differentiation gene (Edg) receptors on endothelial cells. Upon Edg activation, G-protein coupled signaling and downstream MAPK and Rac cascades are activated in order to increase production and trafficking of N-Cadherin to adherens junctions in order to maintain tight association with mural cells. Additionally, however, in a g protein coupled independent manner, Rho cascades are also activated to increase the production and trafficking of VE-Cadherin. Indeed, S1P mutants in utero between weeks 14 and 15 develop severe edema and fatal hemorrhages[49].

Pericytes can differentiate into mural cells and subsequently smooth muscle cells through the induction of TGF-β signaling through the activing receptor kinase Alk5. Activation of Alk5 leads to phosphorylation of Smads 2/3, transcription factors that regulate genes such as SM22α, connexin 37, fibronectin, and others which decrease cell migration and proliferation while increasing smooth muscle differentiation and subsequent vessel maturation[50]. All these intricate mechanisms are important to develop functional, non-leaky vasculature through vascuolgeneis and angiogenesis.

**Tissue Engineering Vascular Structures**

Tissue engineering utilizes concepts from biology and bioengineering to produce biomass *in vitro* resembling endogenous tissues for potential therapeutic benefit. Usually, experiments involve the use of highly adaptive and specific cells grown in an extracellular

matrix that allows for cell function to occur as well as provide a 3D microenvironment resembling native tissue stroma, with the hopes that post maturation *in vitro*, the engineered tissue when implanted may reform, refunction, or replace the pathological tissue.

Specifically, vascular tissue engineering can be divided into microvascular and macrovascular engineering. Microvascular tissue engineering tries to recreate microvessels (~ < 200μm in diameter) such as arterioles, capillaries, and venules utilizing sourced endothelial, stem, or heterogenous cell populations grown within a matrix that supports proliferation, differentiation, and angiogenesis. That matrix can be proteinaceous mixtures resembling endogenous extracellular matrix, non-proteinaceous complexes forming what are called hydrogels that are highly viscous for mechanical rigidity and structure, or finally hybrids of protein and non-protein complexes. The most common biomaterials used include alginates[51], agarose[52], collagen and fibrin[53], methacrylated gelatin (GelMA)[54], and poly (ethylene glycol) dimethacrylate (PEGDMA)[55].

A common misconception within the bioengineering community is that these matrices are commonly referred to as 'scaffolds', suggesting that they only provide mechanical integrity and structure in an intended 3D orientation, however, they must also provide a microenvironment that can allow for cell-to-cell communication, chemotactic signaling, nutrient diffusion, porosity for cell migration, binding sites for cell adhesion, induction of intracellular signaling driving angiogenesis and growth, and finally, upon implantation, biocompatibility with host tissue leading to functional reperfusion and/or replacement of pathologic tissue. Therefore, it is safe to assume that the use of the term 'scaffold', when referring to microvascular engineering, from this point forward

encompasses the entire components necessary, devoid of cells, both biological and non-biological, to form microvessels *in vitro*.

There are two general theories regarding the bioengineering of microvessels. The first is the utilization of techniques such as sterolithography, laser etching, or creation of molds to produce specific channel geometries resembling capillary beds onto a gel or plastic substrate, and secondarily addition of endothelial or other cells to line the aforementioned channels. This process is known as microvessel patterning and was first developed by Tien and colleagues in the early 2000's[56,57]. Zheng and colleagues utilized such a technique to create a patterned stamp which imprinted in collagen hydrogels and subsequent sandwiching of hydrogels led to the formation of hollow tubes which were then seeded with human umbilical vein endothelial cells (HUVECs)[58]. Similarly, 'negative molds' where created as well by the Tien group using polymers such as pluronic that can undergo phase change and allow removal at specific temperatures leaving channels behind[59]. Pre-patterning using molds or etchings create microarchitectures for endothelial cells to line, artificially producing specific geometric tubes of endothelium. Interestingly, using pre-patterning, hemodynamic stresses can be calculated precisely, thus limiting unknown shear effects on endothelial tubes post formation when exposed to flow.

However, there are several drawbacks using these techniques which include 1) difficulty creating channels less than 50μm in diameter, 2) assuming pre-patterned channel architectures are necessary to create microvessels that will retain structure, recapitulate native microvessels, and undergo appropriate inosculation without extensive pruning or loss of vessel mass upon implantation, and 3) using highly modified plastics and hydrogels that are not FDA approved for medical device implants. Indeed, pre-patterning can limit

biological derived movement of cells via chemotaxis, and when only seeded with endothelial cells, 'man-made microvessels' do not recapitulate native microvasculature[60]. While *in vitro* experiments may benefit from utilizing these systems, they are insufficient to create implantable microvessel rich tissue for therapeutic applications[61].

The second theory for the bioengineering of microvessels sources heterogenous cell populations grown in a biologically derived, 3D extracellular matrix exposed to certain growth factors promoting formation of microvessels that more closely resembles vasculogenesis and angiogenesis *in vivo*. Indeed, in native tissue there are complex interwoven stimuli that act both locally and systemically in order for functional microvasculature production. Autocrine and paracrine growth factors and cytokines dictate chemical gradients driving endothelial cell sprouting and motility. Additionally, mechanical constraints and physical space play a huge role as both a barrier and a stimulus to allow for coordinated guidance and microvascular position and alignment[62-64]. For example, the presence of extracellular matrix proteins collagen IV, collagen VIII and laminin help establish cell polarity and restriction and are the main components of the underlying basement membrane[65,66]. However, extravascular space collagen type I and fibrin have demonstrated robust angiogenesis possibly due to integrin specific binding and activation on EC membranes, as well as respond to MMPs in order to degrade and remodel fibrils for endothelial cell migration, as well as retention of soluble growth factors such as VEGF and bFGF[63,67]. Both the extracellular matrix and the paracrine and autocrine signaling it supports allows for the formation of a stable heterogeneic microcirculation to develop, in other words, vessel caliber and diameter can vary allowing the expansion, production, pruning, and remission of microvessels to encompass arterioles, capillaries,

and venules, a system not supported in the aforementioned pre-patterned micro-etching standards for bioengineering.

Additionally, endothelial and other cells not only experience contact inhibition via active grouping and coupling between cells, but also through mechano-chemical coupling which can be described as stresses and tensions cells provide to their microenvironment through focal adhesion kinases, and also through mechanical compression and tension that the local microenvironment can play on the cell as well[68-70]. Specifically, these forces can maintain endothelial cell shape as well as cell alignment which can determine capillary bed 3D microarchitecture within tissues[71-73]. This interplay is crucial such that mechanical barriers provided within ECM must be broken down and remodeled to allow for sprout formation in angiogenesis and subsequent tip cell motility and migration via secretion of matrix metallo-proteases.

Our group and others focus on production of bioengineered microvessels utilizing predominantly 3D endogenous ECM systems encompassing adipose-derived stromal vascular fraction cells (SVF) as the cell population necessary to reform microcirculation *in vitro*, the composition of which will be described in detail further.

Macrovascular engineering refers to the production of blood vessel mimics usually greater than 1 mm in diameter in the hopes of replacing diseased arteries and veins. Large vessel prosthesis currently approved for clinical use for vessel grafting greater than 6mm in diameter are predominantly made of materials such as polyethylene terephthalate (PTFE) also known as Dacron®. Dacron was first discovered in 1941 by Whinfield whom was developing the polymer as polyester film Mylat® for DuPont. It was adapted for medical use in the 1950s when West and colleagues utilized tube formations of woven

PTFE to treat arteriosclerotic occlusions of the femoral artery[74]. Dacron to this day is used clinically in cases of femoral artery repair, aortic aneurisms and resections, and large vessel substitutes surgically. However, its use is limited for smaller artery and vein anastomoses because if the diameter is less than 6mm, thrombosis and occlusion predominate and can halt physiologic blood flow. As such, currently there are still no artificial coronary artery substitutes approved by the FDA for CABG. There has been a recent push by the bioengineering community to produce blood vessel mimics utilizing multiple methods, including but not limited to cell-sheet rolling and electrospinning tubular scaffolds that may or may not be cellularized *ex vivo*.

The first to describe the process of electrospinning a biodegradable nanofibrous structure for a blood vessel mimic was Ramakrishna and colleagues in 2003. Electrospinning is a fiber production method in which electric force is utilized to draw threads from liquefied polymer solutions onto a rotating, grounded mandrel. Specifically, once the liquid droplet exiting the needle becomes sufficiently charged, electrostatic repulsion occurs and is greater than the surface tension of the tip of the dispenser. The droplet subsequently becomes stretched and exudes in what is called the 'Taylor cone.' The volatile solvent evaporates and the fibrous polymer deposits in random orientation in nanometer sized fibers onto a grounded collector. Ramakrishna and colleagues were the first to describe the use of the biodegradable polymer poly(L-lactid-co-ε-caprolactone [P(LLA-CL)] to electrospin BVMs. In their experiments they claimed that the alignment of the deposited fibers (~ 500nm in diameter) where in such a manner that they mimicked circumferential orientation of cells and fibrils around the medial layer of a native artery. They indeed cultured large vessel derived smooth muscle cells onto the electrospun

scaffold to note cell attachment, growth and alignment. They concluded that the cells attached and aligned in the orientation of the deposited electrospun fibers and as such provided a favorable morphology to produce blood vessel mimics in the future[75]. While these early experiments did not produce vessel mimics resembling native arteries or veins, they provided a foundation in order to study electrospinning and cell sodding methods further.

Many others went on to study electrospinning using solutions containing additional biodegradable plastics as well as mixtures with extracellular matrix proteins such as collagen and elastin in the hopes of increased retention and cell binding to native ligands[76]. Cell sheet engineering creating monolayers of cells *in vitro*, then subsequently rolling them onto electrospun tubes is an additional method studied for bioengineering BVMs. Ahn *et al*. described creating a smooth muscle cell sheet one layer thick, which was removed from culture via a thermosensitive poly(N-isopropylacrylamide) coated culture dish, hand rolled onto polycaprolactone (PCL) electrospun tubes, and placed in a pulsatile flow bioreactor. They concluded that the cells retained tight junctions with one another, were able to infiltrate into the electrospun scaffold, and had increased viability due to pulsatile flow over non-flow and non-cell-sheet controls[77]. While most of the early studies utilized smooth muscle cells as the cell population of choice to line electrospun grafts[78,79], our group and others studied stromal vascular fraction cells as potential endothelial precursors for graft lining and large blood vessel tissue production[80-82].

**The Stromal Vascular Fraction**

Stromal Vascular Fraction is a dynamic, complex group of cells that can be derived from adipose tissue depots in both humans and other mammals. It was discovered as a potential therapeutic cell source to form fully functional vascularized tissue by Wagner and Mathews in the 1970s, whom adopted the use of collagenase to digest tissues to release cellular components as previously described by Rodbell[83]. The enzymatic digestion of fat tissue allowed for the production and separation of tissue components via centrifugation, ultimately providing the ability to isolate buoyant adipocytes and dense cellular pellets, the latter of which would be described as stromal vascular fraction. Within this dense cellular pellet there are a multitude of cell types including endothelial cells, smooth muscle cells, fibroblasts, pericytes, perivascular cells, immune cells, adipose stem cells, and mesenchymal stem cells[84-88].

The analysis of lipoaspirate-derived SVF was first described by Williams and colleagues where they state that of the cells left intact after collagenase digestion, seventy-five percent expressed von Willebrand factor (vWF) while almost six percent expressed alpha smooth muscle actin, and seventy-four percent expressed EN4, a specific antigen found on endothelial cells[86]. Indeed, other groups went on to characterize the cell types found in both freshly isolated stromal vascular fraction and passaged cultures. More specifically, it was noted that freshly isolated SVF had a relatively low number of stromal cells as characterized by markers CD13, CD29, CD44, CD63, CD73, CD90, and CD166, however these cells seemed to proliferate rapidly during successive passages. More interestingly, endothelial cell markers such as CD31, CD144, VE-cadherin, vascular endothelial growth factor receptor 2 (VEGFR2), and vWF were not changed significantly

during cell culture and passage[89]. These data suggested that freshly isolated SVF could be a source of endothelial cells and perivascular cells, which may have therapeutic potential for re-vascularizing tissues.

However, there is discrepancy between groups characterizing the proportions of each cell type found in SVF. This can be attributed to experimental variability in which adipose isolation sites are different, enzymes used for digestion are different, and patients' wide variability in comorbidities and unknown pathologies. Our group more recently has characterized rodent SVF cells through fluorescence-activated cell sorting at freshly isolated time points as well as post culturing. Interestingly 33% of the freshly isolated SVF cells were endothelial cells which reduced to just 10% of the total population after culture and passage. $CD14^+$ monocytes and macrophages declined from 22% to 18%, $ckit^+$ progenitor cells declined from 5% to 1% and PDGFR-$B^+$ perivascular cells declined from 20% to 18%[90]. These data along with others undoubtedly demonstrates the vast variety in SVF cell composition, but maybe more importantly, culturing and expansion can greatly vary the cell type and differentiation status of sub populations of cells found within SVF. Freshly isolated SVF as such may have greater consistency and more vasculogenic potential due to higher amounts of endothelial and perivascular cells at the time of isolation. In addition, freshly isolated SVF is arguably a more clinically viable cell product due to its minimal manipulation which may translate at the bedside.

While composition may vary, endothelial cell function within SVF seems to remain. Monsuur and colleagues went on to study the properties of SVF-derived endothelial cells to compare with other endogenous endothelial cells, more specifically, dermal endothelium. They characterized endothelial cells isolated from adipose-derived

SVF and from the dermis. Indeed, both populations expressed the typical endothelial markers PECAM-1, ECAM-1, Endoglin, VE-cadherin and VEGFR2[91]. They concluded there were vast similarities between the two endothelial cultures and the ability of SVF-derived endothelial cells to respond to bFGF and VEGF was similar to that of dermal endothelial cells[91]. SVF may be an excellent source of endothelium for tissue engineering, due to its abundance and relative ease of isolation. These early *in vitro* experiments provided an amalgam of data necessary to continue studies on SVF for regenerative vascular therapeutics.

SVF can undergo angiogenesis and spontaneously self-assemble into vascular networks when grown *in vitro*[67,84,85]. If we look at our own vascular tree within our bodies, we notice that blood vessels are hierarchical giving off branches with changing diameters of the lumen to facilitate nutrient and waste exchange at the single cell level, all the way down to capillaries[92]. This structure is required for function, where larger more smooth muscle containing vessels, resistance vessels, dictate flow of oxygenated blood, and smaller, mostly endothelial only vessels dictate nutrient exchange[27]. The unique properties of SVF demonstrate these phenomena after vasculogenesis and angiogenesis, even when cultured *in vitro*. Koh and colleges found that the endothelial cells within SVF are imperative to form microvascular structures *in vitro*, and their depletion destroys any phenotypic reorganization[85]. However, if only endothelial cells are used in culture, while tube-like structures do occur, these immature microvessels are uniform in diameter and do not approximate endogenous vasculature. As aforementioned, SVF contains perivascular cells, endothelial cells, adipose stem cells, as well as many other cell types. Focusing on a two-cell system, Merfeld-Clauss and others isolated adipose stem cells as well as

endothelial cells from SVF to co-culture in order to understand signaling and differentiation effects the two cell populations may have upon one another *in vitro*. Interestingly, experimental groups in which both cell populations were cultured together yielded the highest degree of diverse endothelial network formation. Adipose stem cells took on a slight smooth-muscle cell phenotype with increased alpha smooth muscle actin expression while endothelial cells increased expression of CD31[93]. This interplay between perivascular support cells, stem cells, and endothelial cells is critical to form microvasculature both *in vitro* and *in vivo*, especially microvasculature that resembles native host vasculature. SVF as a heterotypic cell population is unique in that it contains all the cells necessary to reform hierarchical vasculature including but not limited to smooth muscle cells, pericytes, endothelial cells, and stem cells. SVF affords an easily harvested cell population with potential for regenerative vascular therapeutics[94].

SVF also forms fully functional, perfusable microvasculature when implanted *in vivo*[66,95]. More specifically, retained microvessel fragements isolated from adipose tissue retain angiogenic capacity when implanted *in viv*o in a three-dimensional collagen gel. Within the first 5 days of culture, rat microvascular fragments undergo angiogenic sprouting; these "activated" fragments will then seek out endogenous microvasculature and inosculate, in order to allow blood flow through the lumens of host vasculature and newly implanted vasculature. Post inosculation, implanted SVF-derived microvasculature undergoes phenotypic remodeling and functional response to blood flow and shear stress and can differentiate into a full range of vessel types including arteries, arterioles, capillaries, venules, and veins[95].

Due to the neovascularization capacity of SVF both *in vitro* and *in vivo*, many groups have sought after means to automate cell isolation for application in a clinical setting. As an example, post minimally invasive surgery, lipoaspiration can be delivered to the tissue genesis incorporated, TGI 1000 Cell Isolation System™, that has a fully enclosed loop where contamination and personnel handling are at a minimum. In a study utilizing lipoaspirate from patients, the TGI instrument yielded $1x10^5$ SVF cells per cc of fat with endotoxin levels below FDA recognized standards. Cells were subsequently sodded on expanded polytetrafluoroethylene peripheral vascular bypass grafts and re-implanted into 7 patients yielding 60% patency post 1 year implant[96]. Many other groups have also developed similar systems with positive results of cell isolation with no contamination and variable yields of total cells from lipoaspirate[80,97-102].

SVF has been used clinically to treat a variety of diseases. The highest clinical usage in terms of patients treated with SVF cells are mostly for degenerative cartilage diseases such as osteoarthritis, where SVF are reinjected into the inflamed site and modulate inflammation as well as stimulate regenerating chondrocytes[103-107]. The presence of adipose stem cells and mesenchymal stem cells within SVF potentially allows for differentiation into tissues of multiple lineages, which may have therapeutic potential for treatment of degenerative diseases where multiple tissue types are involved. Zuk *et al*. were the first to demonstrate that processed lipoaspirate could differentiate under certain growth conditions to cells of osteogenic, adipogenic, chondrogenic, and myogenic lineages[108]. Adipose derived stromal vascular fraction has been utilized clinically whether through clinical trials or individual cases as cellular injections for breast augmentation[109-111], craniofacial defects[110,112-114], irradiation fibrosis[115], Crohn's disease[116-121], and

multiple/systemic sclerosis[122]. While the heterogeneity as well as variability between SVF samples does not help to elucidate specific mechanisms involved, osteoarthritic patients have seen positive changes in flexion and extension capacities as well as reduced pain and inflammation over no cell controls[104]. SVF as a tissue source has generated a lot of hype in the field of regenerative medicine, however additional studies are necessary to elucidate specific mechanisms in play.

# SIGNIFICANCE AND RESEARCH PLAN

Myocardial infarction due to ischemic injury is the leading cause of congestive heart failure and subsequent death in the United States[123]. There has been a significant amount of research to produce therapies to mitigate ventricular wall remodeling, fibrosis, and dilation. Many therapies include the use of acellular hydrogel materials injected into ischemic myocardium to provide mechanical support, cellular populations including differentiated or non-differentiated stem cells injected to produce viable myocytes, or epicardial wraps made of cellularized and non-cellularized sheets to provide external mechanical and cellular support. These therapeutic strategies are different in approach and have varying efficacies including rates of cellular and material retention and improvement in cardiac function. It is possible that the underlying pathology is not being addressed with many of the injectable therapies or external wraps and needs to be further assessed.

Damaged myocardium due to ischemic injury from coronary occlusion requires reperfusion and retention of functional microvasculature to mitigate damage at the cellular level of the infarct. Ventricular necrosis and fibrosis are directly correlative to the loss of blood supply and subsequent nutrient delivery to starved myocardium. As such, restorative microvascular perfusion could alleviate cellular damage that ensues post myocardial infarction. Stromal vascular fraction (SVF) is a dynamic mixture of endothelial cells, smooth muscle cells, pericytes, adipocyte progenitors, immune cells, fibroblasts, stromal cells, as well as unidentified circulating progenitor cells. This complex yet relatively abundant cell population has successfully been differentiated into multiple cell types including adipocytes, osteoblasts, chondrocytes, pericytes and myocyctes under certain conditions. Adipose derived stromal vascular fraction has also been implemented in multiple clinical trials for regenerative medicine. However, vascular self-assembly or

neovascularization from SVF *in vitro* as an implantable model is not fully understood. Our lab and others have studied the effects of SVF and microvascular network formation both *in vivo* and *in vitro*. Currently, the recapitulation and ability of SVF to form microvascular networks *in vitro* depends on certain medias and growth factors that cannot be used in a clinical implantation model. However, SVF when injected with extracellular matrix components, as a heterogeneous cellular mileu, can form functional microvasculature *in vivo*. We hope to understand and recreate functional microcirculation utilizing SVF in an *in vitro* system, that after maturation can be implanted along with a tissue engineered conduit vessel to provide reperfusion to ischemic tissues. It is imperative to provide a functional microcirculation for tissue that is implanted or starved of blood flow in regenerative medicine. **It is hypothesized, and a long-term goal for these studies is that a tissue engineered macro and microcirculation can be anastamosed to endogenous vasculature and provide reperfusion to damaged tissues and mitigate the pathogenesis involved in diseases such as myocardial infarction**.

**Specific Aim 1: Determine the mechanism by which SVF forms neovascular networks in 3D fibrin gels *in vitro*.** SVF can undergo vasculogenesis and produce neovasculature in two dimensions (2D) *in vitro*, utilizing commercially available Matrigel®, a heterogenous biomaterial made up of multiple extracellular matrix (ECM) proteins produced from Engelbreth-Holm-Swarm mouse sarcoma cells. SVF as well as endothelial pure cell populations have been able to form patent tubular networks on Matrigel®-coated *in vitro* models, however, Matrigel® is not a clinically relevant or translatable biomaterial. Thus, it is imperative to explore other biomaterials and hydrogels as a means for clinical implementation. Our group has shown that intact isolated microvessel fragments, obtained from human adipose tissue, can be cultured in three dimensional (3D) polymerized type I collagen gels and undergo angiogenesis as well as inosculation events with other sprouting microvessels *in vitro*; and when implanted *in vivo*, inosculation between host and

implant allows for a functional microcirculation to develop[67]. It can be argued that in order for mature functional neovessels to form *in vitro* as well as *in vivo*, the entire cellular milieu composing the microcirculation (arterioles, capillaries, venules) must be present; including endothelial cells, smooth muscle cells, pericytes and associated immune and stromal cells. However, SVF digested longer than 35 minutes to release individual cells from one another, and devoid of microvascular fragments, can form microvascular networks in 3D fibrin but not 3D collagen I *in vitro* over a 7-day culture period.

**Hypothesis 1:** ***Specific ECM proteins are required to guide and stimulate SVF EC to undergo vasculogenesis, which is dependent upon the binding and activation of the fibrin-specific integrins $\alpha_v\beta_3$ and $\alpha_5\beta_1$ and not collagen specific integrins.*** Activation of fibrin specific integrins promotes angiogenic events on endothelial cells within SVF to hyper-stimulate endothelial tube formation and perivascular recruitment within 3D fibrin *in vitro* systems.

**Specific Aim 2: Create deliverable tissue units of SVF-derived microvasculature or macrovasculature utilizing bioprinting, and electrospinning technologies.** Our group and others have successfully created 3D implants utilizing microvessels derived from adipose tissue and collagen I gels, however, these approaches require manipulation and handling that does not afford clinical translatability. As such, it is necessary to discover techniques with minimal manipulation, and high automation to create tissue units using SVF for implantation in a clinical setting.

**Hypothesis 2: Microvessel tissue units created via SVF embedded in either fibrin or collagen I gels can be bioprinted into discreet dosage units with minimal manipulation and handling for therapeutic purposes. Macrovessel structures can also be created utilizing electrospinning technologies, however, specific porosities within electrospun conduits are necessary to allow for adequate cellular infiltration and retention *in vitro*.** Correct dosing of cells may be imperative to restore reperfusion in ischemic tissues, as well as retain cells at sites of implantation. It is possible that mature microvascular units contained within 3D ECM may provide more therapeutic relevance than individual cells suspended in solution for injection. Discreet microvessel-rich tissue units with known concentrations of cells can thusly be produced in a format that does not create zones of ischemia or necrotic cores *in vitro*. Macrovascular structures as well can be produced utilizing SVF, however cellular retention under physiological flow is imperative for graft success. Cellular retention may be modified by creating porosities relevant for cellular infiltration and migration in an *in vitro* setting.

# CHAPTER II

# STROMAL VASCULAR FRACTION FORMS DENSE MICROVASCULAR NETWORKS IN 3D FIBRIN BUT NOT 3D COLLAGEN I

## An Automated *In Vitro* Assay to Determine Vasculogenesis and Angiogenesis of SVF Cell Populations

### Introduction

Tissue engineering the microvasculature is a novel approach towards therapeutic reperfusion for ischemic disease states such as peripheral vascular disease and acute myocardial infarction[124-130]. Microvascular engineering requires both cellular and extracellular components to recapitulate the microenvironment and tissue organization of endogenous microcirculation. Indeed, many researchers have isolated vascular components from a variety of tissues including endothelial-only populations from both large vessel (human umbilical vein and other large adult vessels) and microvascular tissues[131-133]. *In vitro* studies have established the ability of these endothelial cells to undergo the formation of tube-like structures, a process that is highly dependent on the extracellular matrix used as a substrate[134].

Additionally, adipose derived stromal vascular fraction cells (SVF) have been proposed as a source of cells for microvascular tissue engineering[23,84,135,136]. Adipose derived SVF represents a heterogeneous cell population [137,138] that has demonstrated efficacy in the formation of functional microcirculation following implantation[92,139-141]. These *in vivo* studies are based, in part, on the observed ability of SVF-derived, cultured, microvascular endothelial cells to undergo tube formation *in vitro*[134]; however, and the impetus for the studies reported here, the *in vitro* formation of tube-like structures by freshly isolated, heterogenenous SVF cell populations has not been reported.

Previous *in vitro* "angiogenesis" assays have utilized endothelial cell cultures placed on collagen type IV or Matrigel®-treated culture surfaces with a temporal sequence of tube-like structure formation that occurs within 24 hours of plating[134,142-144]. It can be argued that this self-assembly of cells into tube-like structures does not recapitulate the process known as angiogenesis (i.e. formation of new vessels from pre-existing vessel) and recapitulates only one part of the vasculogenic process (i.e. formation of blood vessels from cellular components). The current studies are based on preliminary observations that freshly isolated adipose-derived SVF cell populations do not undergo tube-like structure formation in the first 24 hours after plating on Matrigel®. However, extending the assessment of the adipose SVF cell populations plated on Matrigel® for a 7-day period resulted in the observation of cell aggregation, tip cell formation, sprouting of vascular structures followed by branching and inosculation. Herein, we describe an *in vitro* assay that we propose captures each step of vasculogenesis and angiogenesis over a 7-day period via time-lapse microscopy utilizing rat epididymal fat or human lipoaspirate derived SVF as a cell source.

## Materials and Methods

*Animals and Ethics Statement*

All animal procedures were conducted in compliance with University of Louisville School of Medicine IACUC-approved protocols and NIH guidelines. Isoflurane gas was administered for anesthesia.

*SVF Isolation from Sprague Dawley Rats*

Rat epididymal fat pads were excised from 6 to 8-month-old Sprague Dawley rats at weights greater than 250g under sterile surgical procedure and isoflurane anesthesia. All procedures were reviewed and approved under the University of Louisville's Institutional Animal Care and Use Committee. Excised fat pads were placed in PBS containing 0.1% bovine serum albumin (Sigma Aldrich, St. Louis MO) and kept at 4°C for 15 min prior to digestion. Samples were washed with BSA-PBS and minced for 2 min until particulates could pass through a 50mL aspirating pipette. 2mg of Type I Collagenase (Worthington Biochemical Corporation, Lakewood NJ) was added per mL of fat, aliquoted at 20mL total volume in 50mL conical centrifuge tubes, and rotated in an Envirogenie Incubator (Scientific Industries, Bohemia, NY) at 35 rpm and 37°C for 35 min. Samples were pelleted via centrifugation at 350xg for 4 min at RT. Buoyant adipocytes were aspirated and discarded, and dense cellular pellets were suspended and washed one time in BSA-PBS. Samples were re-centrifuged for 4 min at 350xg. The SVF pellet was filtered through a 250μm mesh filter (Tissue Genesis Incorporated, Honolulu HA) and collected into DMEM containing endothelial cell growth supplement, 2mM L-glutamine, 10% fetal bovine serum, and 5mM Hepes buffer. Samples were kept at RT prior to plating.

*SVF Isolation from Human Lipoaspirate*

Human lipoaspirate was digested under sterile conditions following the same protocol as rat SVF isolation. Lipoaspirate was not minced however, and Worthington Collagenase Type I was added to obtain a final concentration of 6mg/mL collagenase to fat volume. The SVF pellet was resuspended in M199 media containing endothelial cell growth supplement, 10% fetal bovine serum, 2mM L-glutamine, 5mM Hepes buffer.

*Angiogenesis Assay and Image Capture*

Either 500μL of growth factor reduced Matrigel® (Corning, Corning NY), 5mg/mL bovine fibrin (Sigma, St. Louis MO), 3mg/mL rat tail collagen (Corning, Corning NY), 1% porcine gelatin (Sigma, St. Louis MO), or 2μg Laminin 332 (Abcam, Cambridge MA) was added to each well of a 48 well polystyrene cell culture plate (Corning, Corning NY) at 4°C. Fibrin was polymerized through thrombin activation at 2U/mg fibrinogen. Collagen was polymerized after the addition of 4N NaOH to a pH of 7.7 and incubation at 37°C. The Matrigel®, fibrin, and collagen hydrogels solidified after 15 min of incubation at 37°C. $1.6 \times 10^5$ SVF cells were subsequently plated per well and allowed to adhere to the ECM overnight in a tissue culture incubator (37°C, 5% $CO_2$). Media was changed the following day and the 48 well plates were loaded into a Cytation 5 cell imaging multi-mode reader (Biotek, Winooski VT) set to 37°C and 5% $CO_2$. A time lapse capture experiment was created in Gen 5 software utilizing a 4X objective capturing phase contrast images at 15 min intervals with an endpoint of 160h. Media was changed every other day. Specific inhibitors of angiogenesis were added at 25μM or 1μM at each media change over the 160h incubation time. Inhibitors included Imatinib mesylate (1μM) (Sigma Aldrich, St. Louis, MO), DAPT (25μM) (Abcam, Cambridge, UK), ZM 306416 (25μM)

(Selleckchem, Houston, TX), and ATN 161 (25μM) (Peptides International, Louisville, KY).

Image files were stitched together using ImageJ software. Individual still images were selected at remarkable time points to demonstrate events such as clustering (18h), tip cell formation (36h), stalk cell formation (60h) and inosculation (112h). SVF and huvec cells grown on Matrigel® to the 112h endpoint were fixed with 4% paraformaldehyde for 15 min at RT, permeabilized with 0.1% Triton X 100 for 15 min at RT and stained with griffonia simplicifolia 1 lectin conjugated to FITC (1:500) (Vector Biotechnologies, Burlingame, CA) and α-smooth muscle actin mouse monoclonal primary antibody (1:500) (Santa Cruz Biotechnology, Dallas, TX) overnight at 4°C to visualize endothelial and smooth muscle cells respectively.

*Event Counting and Statistical Analysis*

Cell clusters were automatically counted using Gen 5 software under cellular analysis tools with threshold intensities set at values less than 10,000, minimum object size set at 25μm and maximum object size set at 1mm. These counts along with manual counts of tip cells and stalk cells were taken using still frames at 18h, 36h, 60h, and 112h respectively of both control and treated groups. Graphs and statistics were run with GraphPad Prism v.7 Software (La Jolla, CA). P values were calculated via one-way ANOVAs with means and standard deviations plotted per group as compared to vehicle only (control group).

**Results**

SVF grown on fibrin, collagen, gelatin, and laminin extracellular matrices behave differently than SVF on Matrigel®. Cells form monolayers on the aforementioned ECM, whereas SVF grown on Matrigel® undergoes phenotypic change resembling vasculogenesis and angiogenesis after 112h (**Figure 1**). Subpopulations of SVF cells plated on Matrigel® begin to migrate and form clusters ranging in size and cell number after 18h of incubation (**Figure 2A, B**). These clustering events resemble angioblasts forming blood islands, the initial steps of vasculogenesis in the embryo. The next phenomenon occurs when tip cells subsequently migrate away from the cluster around 36 hours of incubation (**Figure 2C, D**). During angiogenesis, endothelial cells emerge from a preexisting vessel and remodel surrounding ECM via matrix metalloprotease secretion. Ultimately, these tip cells migrate away from the nascent vessel along with additional endothelial cells creating collateral vessels that will form lumens over time. Tip cells must have additional endothelial cells migrate behind them to properly signal growth and proliferation events away from the nascent vessel. These specific endothelial cells are termed stalk cells in angiogenesis.

Indeed, after tip cell migration, we see the development of stalk cells growing out of the cluster at 60h of incubation as demonstrated in **figure 2E**, **F**. Stalk cells signal adjacent tip cells through the NOTCH pathway to maintain tip phenotype as well as maintain stalk phenotype. Briefly, VEGF-A signaling through VEGFR-2 causes an upregulation of delta-like ligand 4 which subsequently binds Notch to facilitate receptor cleavage by γ-secretase. Soluble notch can then translocate to the nucleus and cause downstream transcriptional activation; including the up regulation of VEGFR-1, a receptor

with low signaling activity via the VEGF-A ligand. VEGFR-2 is downregulated while VEGFR-1 is upregulated on stalk cells, promoting the stalk cell phenotype.

After 60h of incubation and up to the endpoint of 112h we see the retention of stalk cells as well as tip cell migration and ultimately increased vessel density and complexity including branch-points and inosculation events as demonstrated in **figure 2G, H**. To validate that the neovasculature was comprised primarily of the endothelial cell population within SVF, cultures incubated to 112h were stained with griffonia simplicifolia 1, an isolectin that binds endothelial cell specific glycoproteins and widely used in the field as a rat endothelial cell marker. **Figure 3** demonstrates that both on gelatin and Matrigel® there is a predominance of endothelial cells, however, only on Matrigel® do GS1-positive tip cell and stalk cell phenotypes form.

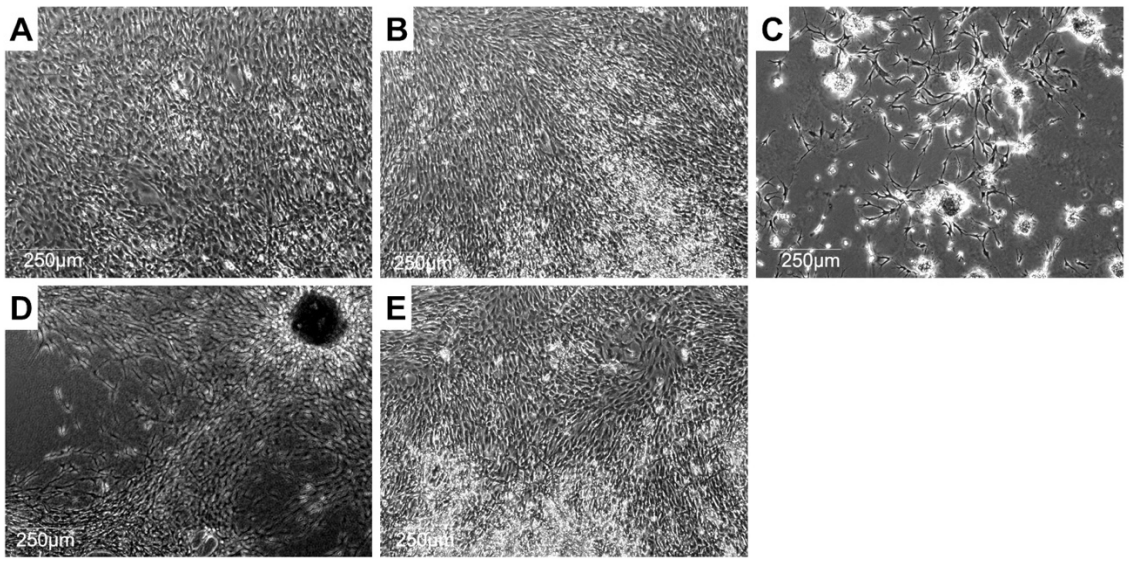


***Figure 1:*** *4X phase contrast images of SVF grown on 3 mg/mL collagen I (A), 1% gelatin (B),* Matrigel® *(C), 5 mg/mL fibrin (D), or 2 µg laminin 332 (E) after 112h of incubation. Monolayers of cells are formed on collagen I (A), gelatin (B) and laminin 332 (E) with cell clustering demonstrated on* Matrigel® *(C) and fibrin (D). SVF forms microvascular networks on* Matrigel® *(C).*

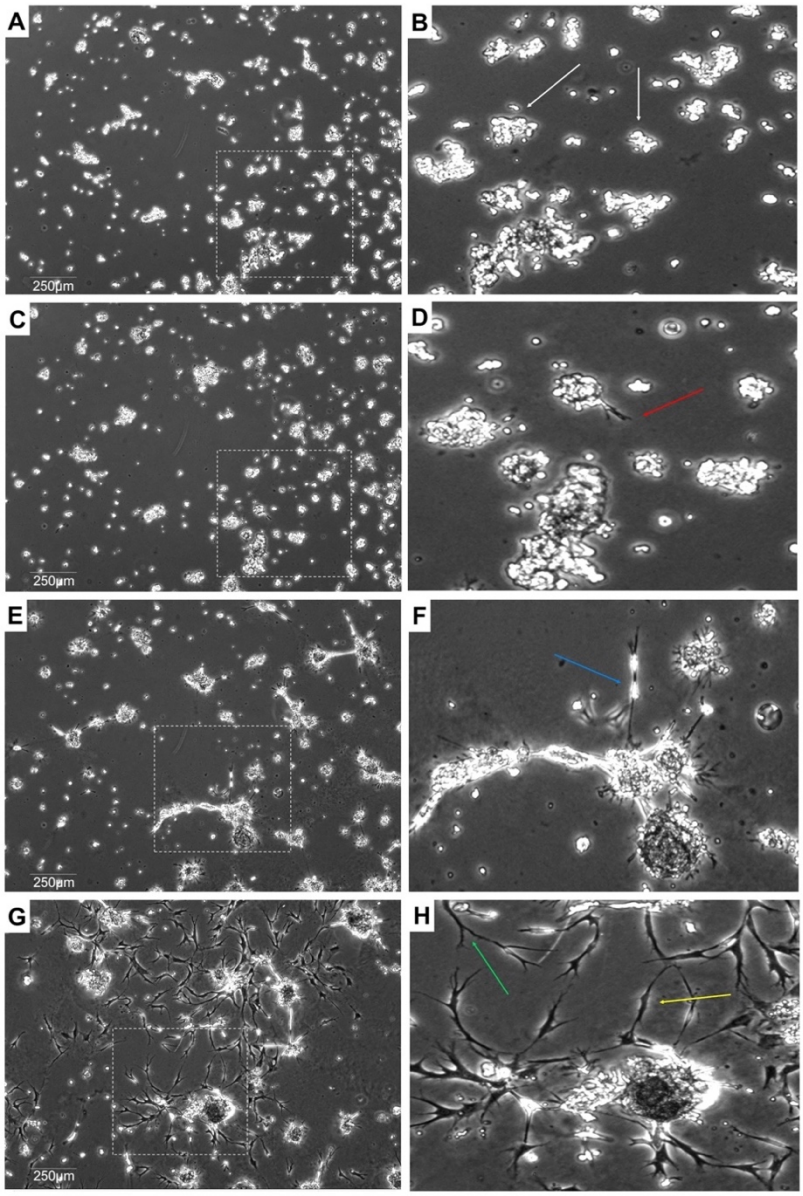


***Figure 2:*** *4X phase contrast images of SVF grown on* Matrigel® *at 18h (A, B), 36h (C, D), 60h (E, F) and 112h (G, H). Images B, D, F and H are 3X optical zooms of boxed sections of images A, C, E and G respectively. White arrows demonstrate initial cell clustering occurring at 18h. Tip cell formation occurs at 36h as marked by the red arrow. Stalk cell formation and elongation occurs at 60h as marked by the blue arrow. Branching (green arrow) and inosculation (yellow arrow) can be seen at 118h in vitro.*

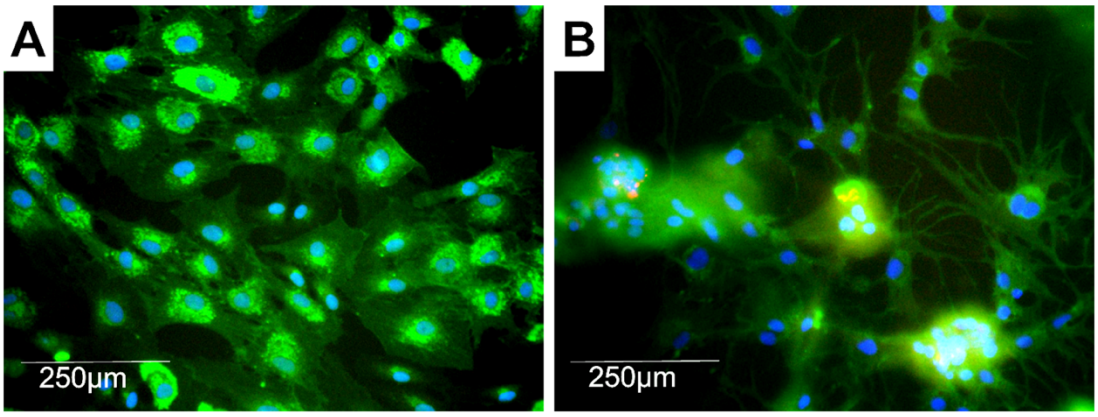


***Figure 3:*** *10X fluorescent images of SVF grown on 1% gelatin (A) or* Matrigel® *(B) for 112h. Blue: DAPI, Green: Griffonia simplicifolia 1 endothelial specific lectin-FITC, Red: α smooth muscle actin-rhodamine.*

To determine if SVF was undergoing vasculogenesis and angiogenesis specifically, the assay was repeated in the presence of the inhibitors DAPT, ZM 306416, Imatinib mesylate, and ATN-161. DAPT is an inhibitor of the γ-secretase that cleaves notch receptor to its soluble ligand preventing stalk cell phenotype. ZM 306416 is a small molecule inhibitor of VEGFR-1[145], again inhibiting stalk cell phenotype via the inhibition of VEGFR-1. Imatinib mesylate blocks platelet derived growth factor receptor-β (PDGFR-β)[146] which is found on mural cells and instrumental in the recruitment of perivascular support cells to developing endothelial tubes necessary for stabilization. ATN-161 is a small molecule inhibitor of the $\alpha_5\beta_1$ integrin[147], a membrane bound protein that binds ECM such as fibrin, fibronectin, and vitronectin (**Figure 4**). During the remarkable time points (18h, 36h, 60h and 112h) data on cluster number, cluster size, the percentage of clusters with tip cells, and the percentage of clusters with stalk cells were collected in the presence of each inhibitor and compared to DMSO (vehicle only) control via one-way ANOVA.

Cluster number was significantly reduced in the presence of 25μM DAPT as well as 1μM Imatinib mesylate at 36h as compared to DMSO controls ($p < 0.05$, $p < 0.005$ respectively, **Figure 5A**). It is possible that the biochemical pathways involved in stalk cell formation as well as mural cell migration may play a role in the recruitment of neighboring SVF cells during initial cell aggregation. In addition, a decreasing trend in overall cluster number over time is noted, which can be explained by neighboring clusters grouping together forming larger units, decreasing total counts. This phenomenon may be due to a variety of cell-cell signaling promoting cell migration and interaction leading to myofibroblastic contraction pulling groupings together. Indeed, myofibroblasts as well as other contractile cells have been found in adipose-derived SVF[148]. Cluster size does not

seem to change between inhibitor and non-inhibitor groups, however there is an increased trend in average size of clusters over 112h across all groups (**Figure 5 B**).

While tip cell phenotype initially begins around 16h of incubation, certain clusters retain tip cells even up until 112h of incubation. There is a significant reduction in tip cell expression in the presence of Imatinib mesylate at 18h of incubation ($p < 0.05$) with a non-significant decrease in tip cells in the presence of the other angiogenic inhibitors. Again, at 60h of incubation there is a significant decrease in tip cells in the presence of Imatinib mesylate ($p < 0.0005$).

As tip cells migrate stalk cells form to stabilize and facilitate tip cell migration away from clusters, up until tip cells inosculate with other microvessels, forming a neovascular network. These events occur at 112h, where control groups begin to decrease tip cell expression because of inosculation events, forming continuous vessel networks. However, cells treated with DAPT have statistically higher amounts of tip cells as compared to DMSO ($p < 0.05$). This retention of tip cells may be attributable to the loss of stalk cell production via NOTCH pathway inhibition. Tip cells still can form and begin initial migration away from clusters but cannot migrate more than a cell length away due to the lack of stalk cell production. Tip cell percentage at 112h in the presence of Imatinib mesylate is also significantly lower than the vehicle only group ($p < 0.05$, **Figure 5C**). These data are corroborated with stalk cell counts at the significant time points. Indeed, while tip cell percentage remains high in the presence of DAPT, and ZM 306416, stalk cell percentages decrease significantly in the presence of ZM 306416 and Imatinib mesylate at 60h of incubation (**Figure 5D**).

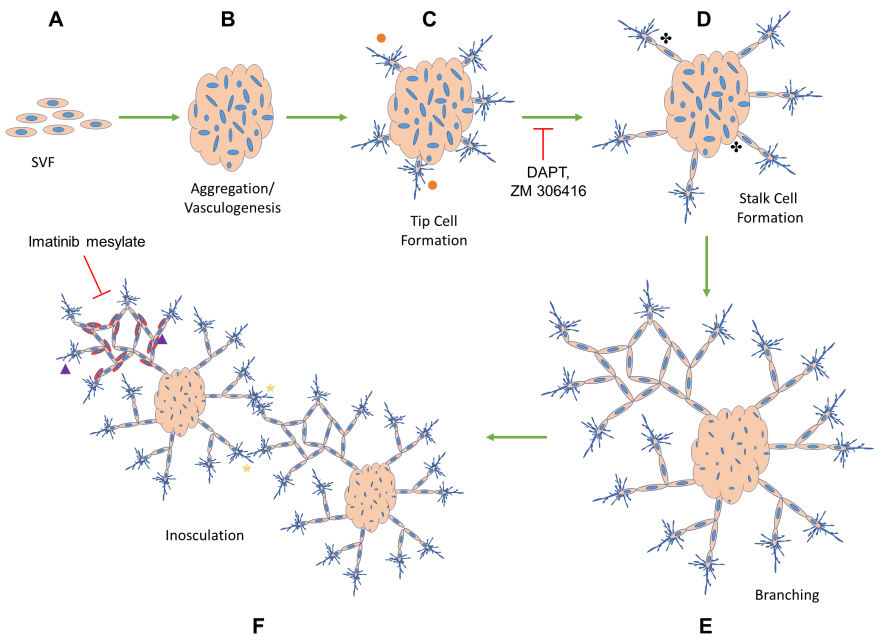


***Figure 4:*** *Schematic of SVF microvascular assembly on* Matrigel® *in vitro. Digested SVF cells (A) self-assemble into a cluster of cells by 18h (B). By 36 hours, endothelial cells sprout out of the cluster with dendritic-like extensions (tip cells: orange ●) (C). DAPT, an inhibitor of the γ- secretase that cleaves notch to its soluble ligand, blocks tip cell signaling to stalk cells, inhibiting stalk cell formation. Stalk cell formation occurs when notch signaling leads to a higher expression of VEGR-1 on the adjacent cell. ZM 306416 blocks VEGFR-1 and thus stalk cell phenotype. In the absence of inhibitors, stalk cells (black ✤) migrate away from clusters behind tip cells by 60h (D). Microvascular networks continue to grow after 112h and demonstrate increased complexity (E). Networks from adjacent clusters inosculate with one another (yellow *) and recruit perivascular support cells to endothelial tubes (purple ▲) (F). PDGFR-B is found on perivascular support cells and activated by endothelial PDGF-β, which signals pericyte recruitment and tube stabilization. Imatinib mesylate inhibits PDGFR-B.*

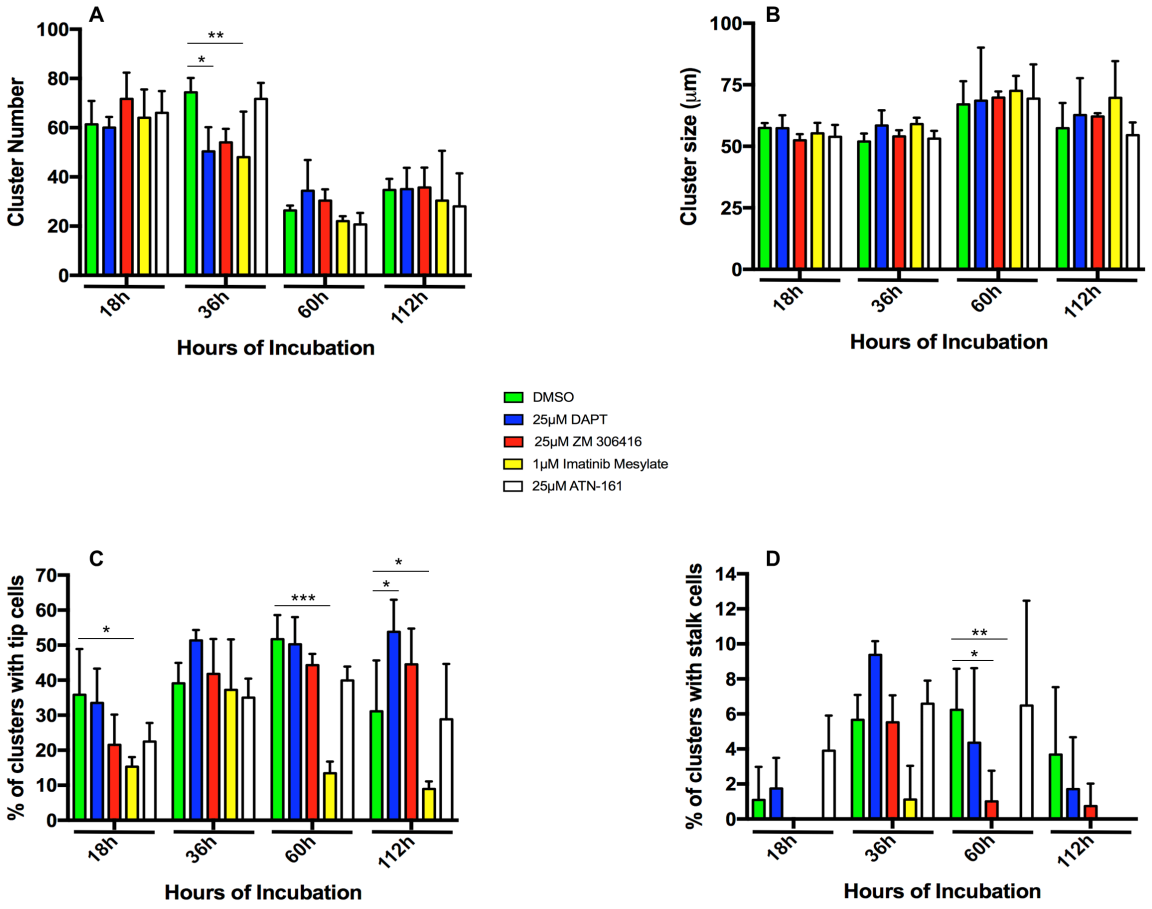


***Figure 5:*** *Number of SVF cell clusters (grouping of two or more cells over 25 μm in total size) at 18h, 36h, 60h and 112h of incubation in the presence of inhibitors on Matrigel® (A). Cluster size (μm) at 18h, 36h, 60h and 112h of incubation in the presence of inhibitors (B). Percentage of clusters containing tip cells at 18h, 36h, 60h and 112h of incubation in the presence of inhibitors (C). Percentage of clusters containing stalk cells at 18h, 36h, 60h and 112h of incubation in the presence of inhibitors (D). Angiogenic inhibitors (in DMSO) were added at days 0, 2, 4, and 6.* $p < 0.05$ *, $p < 0.005$ **, $p < 0.0005$ ***.

**Discussion**

The formation of blood vessels *in vivo* occurs due to the processes of vasculogenesis during development, and angiogenesis during development, pathologic, and physiologic conditions. The study of vasculogenesis and angiogenesis have been aided by *in vitro* models that have utilized the ability to culture expand endothelial cells and establish conditions that support the development of endothelial tube like-structures in 2D culture[134,149,150]. However, an *in vitro* model that recapitulates all vasculogenic and angiogenic processes has not been established.

The formation of tube-like structures by endothelial cells plated onto extracellular matrix has often been described as a model of angiogenesis *in vitro* but arguably this is not accurate since only one of the processes necessary for angiogenesis occurs – tube formation. The results presented support the conclusion that adipose derived stromal vascular fraction cell populations plated onto Matrigel®, immediately after isolation, exhibit both vasculogenic and angiogenic elements of microvessel formation.

The self-assembly of cells into microvessels requires the appropriate cells to communicate with one another via paracrine and mechanical factors to promote proliferation, migration and inosculation, ultimately forming functional microcirculation from individualized cellular components[151]. Recapitulating this process *in vitro* requires the presence of each cell type that makes up functional microcirculation, including but not limited to endothelial cells, smooth muscle cells, pericytes and tissue resident immune cells[152]. Adipose-derived SVF populations undergo vasculogenesis and angiogenesis as demonstrated by events such as cell clustering, followed by tip cell formation, stalk cell

formation, branching and ultimately complex network formation including the inosculation of adjacent vessel projections.

These events can be validated by well-known inhibitors of angiogenesis, some commonly used in the clinic as anti-angiogenic tumor pharmacotherapies. In the literature as well as in our assay, DAPT, an inhibitor of the γ-secretase that cleaves NOTCH to its soluble ligand, prevents endothelial stalk cell formation and subsequent tip cell migration[40,41]. ZM 306416, a small molecule competitive inhibitor of VEGFR-1 inhibits stalk cell phenotype. Additionally, Imatinib mesylate, an inhibitor of PDGFR-B; a receptor found on mural and perivascular support cells, prevents their recruitment to new endothelial tubes via PDGF-β ligand chemotaxis. This PDGF axis is instrumental in the mobilization and recruitment of stabilizing cells during angiogenesis, which ultimately leads to retention of non-leaky, functional neovasculature[50]. These inhibitors validate the vasculogenic and angiogenic processes occurring in this assay. However, the assay provides the opportunity to validate and test a variety of pro or anti-angiogenic pharmacotherapies.

Indeed, endothelial cell and mural cell self-assembly and proliferation is required to form functional microvasculature, however, extracellular matrix (ECM) components are necessary to stimulate cell growth and maturation[153,154]. Fully mature vascular networks restructure surrounding ECM, via matrix metalloproteases, to create a distinct basement membrane composed predominantly of type IV collagen and laminins 121 and 332; allowing for appropriate adventitial cell signaling, structural integrity, and decreased permeability[155-157]. Matrigel®, a complex mixture of extracellular matrix molecules created from Engelbreth-Holm-Swarm Mouse Tumor, is an ECM derivative that contains

basement membrane proteins necessary to stimulate endothelial cells to migrate, proliferate and create tube-like structure morphologies. As such, many *in vitro* angiogenesis assays use Matrigel® as the dominant ECM prior to cell plating. It is important to note that the initial vascuolgenic and angiogenic events occur within the first 24 hours of cell plating on substrates such as Matrigel® for pure endothelial cell populations[158]. This assay establishes a methodology to evaluate and classify the vasculogenic/angiogenic capability of patient specific SVF prior to clinical usage.

Although the current study represents a solely *in vitro* evaluation of vasculogenic and angiogenic processes by adipose-derived SVF cell populations, the discussion of how these results may relate to *in vivo* vasculogenesis and angiogenesis is warranted. Adipose-derived SVF cell populations are under extensive study for use in clinical applications where tissue revascularization is desired[159]. The direct injection of adipose derived SVF cells into ischemic tissue has been hypothesized to support the formation of new blood vessels in the target tissue. Most studies suggest the action of the SVF is to stimulate new blood vessel formation by angiogenic mechanisms, that is by the formation of new vessels from pre-existing vessels. Thus, the SVF cell population is providing a source of paracrine factors. Pre-clinical studies provide an alternative explanation for increased vessel density of SVF treated ischemic tissue. Using cell markers to evaluate the fate of injected adipose-derived SVF, the cells exhibit the ability to self-assemble into new vessels. The new vessels formed include arterioles, venules and capillaries and the cell tracking technology indicates these new vessels originate from the injected SVF cell population[92]. However, it remains unknown whether the injected SVF exhibit cell aggregation as observed in the current *in vitro* system. We believe that SVF harbors the appropriate milieu of cells to re-

form multi-cellular vascular components, including endothelial cells, smooth muscle cells, pericytes, adipose derived stem cells as well as additional immune and stromal cells. The development of this SVF-based automated assay of vasculogenesis may permit the assessment of patient specific SVF cell populations to analyze vasculogenic and angiogenic potential prior to surgical implantation.

## SVF cultured in 3D Fibrin and Collagen I; SVF Forms Robust Microvascular Networks in Fibrin, Not Collagen I

### Introduction

It is imperative to utilize biomaterials that can translate clinically when creating *in vitro* tissue engineered constructs. For example, adipose-derived SVF, when digested to recover microvessels, has shown potent angiogenesis in 3D collagen I *in vitro* and inosculates with host microvasculature *in vivo* upon implantation[67,84,95]. However, little is known about longer digests of SVF, leading to the recovery of discrete individualized cells and subsequent culturing in 3D matrices *in vitro*. Previously, we demonstrated that SVF forms microvascular networks on 2D Matrigel® undergoing known angiogenic mechanisms of cell clustering, tip cell formation, stalk cell formation, sprouting migration, pericyte recruitment, and endothelial to endothelial inosculation, which can be mitigated with inhibitors of the NOTCH pathway as well as the PDGF-B/PDGFR axis. However, it was noted, while SVF formed tubular microvessel-like structures on 2D Matrigel®, a non-translatable ECM mixture, it coalesced into monolayers on 2D fibrin and 2D collagen I instead[160].

It is known that cellular behavior, including focal adhesion production, phenotypic orientation, and migration are differentially activated when cells are embedded within 3D matrices versus cultured on top of 2D substrates; which can be due to a variety of both soluble factors and mechanical stimuli between cells and ECM[69,73]. As such, it seemed necessary to study SVF behavior when embedded in clinically utilized biomaterials such as fibrin and collagen I in order to create truly 3D implantable microvasculature.

Interestingly, freshly isolated, filtered SVF forms robust microvascular networks in 3D fibrin but not 3D collagen I over a period of 7 days. The aforementioned phenomena, while highly dependent on cell type and microenvironment, can possibly be explained through integrin binding and activation at higher densities in 3D cultures versus 2D cultures.

Endogenous extracellular matrix interacts with all cells via ligand binding at integrin receptors. Integrins are transmembrane receptors necessary for cell-extracellular matrix adhesion. They are made up of two subunits labelled alpha and beta which can be differentially spliced to create multiple receptors with varying ligand bindings and affinities. There are roughly 24 conformations of receptors that can bind to ECM proteins including collagens, laminins, fibronectin, vitronectin, fibrinogen, ICAMs and VCAMS to name a few. Specifically, of interest are the $\alpha_1\beta_1$ and $\alpha_2\beta_1$ integrins which bind to extracellular collagen I and the $\alpha_5\beta_1$ and $\alpha_V\beta_3$ integrins which bind to fibrin. Integrins are much more than just mediators of cell attachment to the surrounding ECM, they also operate as signal transducers through the membrane and can modulate pathways including phosphorylation and activation of multiple receptor tyrosine kinases that can subsequently activate downstream cell proliferation, differentiation, survival, and apoptosis[161,162].

In early experiments we embedded SVF cells (isolated from a 35min digest using collagenase) in 3D fibrin or 3D collagen I and noticed robust microvascular formation in fibrin but not collagen I through 7 days culture. Thusly, it was hypothesized that SVF microvascular formation within a 3D substrate may be accelerated through vasculogenesis, tubulogenesis, and angiogenesis if the integrins $\alpha_5\beta_1$ and $\alpha_V\beta_3$ were activated or hyperactivated via fibrin binding.

Initial studies by Soldi and colleagues demonstrated enhanced phosphorylation of VEGFR2 when endothelial cells were plated onto ECM such as vitronectin and fibrinogen, however, cells in suspension not plated with vitronectin or fibrinogen demonstrated reduced VEGFR2 phosphorylation in response to VEGF. In addition, in the presence of the anti-integrin $\alpha_V\beta_3$ antibody, endothelial cells had inhibited phosphorylation of VEGFR2 but not inhibited cell adhesion[163]. These studies singled out the integrin $\alpha_V\beta_3$ as the regulator of VEGFR2 signaling. The discoverers of the antibody against $\alpha_V\beta_3$ were Drake, Cheresh, and Little in 1995, where they noted that the antagonist LM609 inhibited the formation of early quail embryo blood vessels via disruption of lumen formation as well as fragmentation of 'normal' vascular patterning as described by fragmented aortae and thin, poorly formed, lateral anastomotic vessels[164].

$\alpha_V\beta_3$ integrin also forms complexes with PDGFRβ on perivascular cells[165]. In additional studies by Ruoslahti and colleagues, CHO cells were engineered to overexpress integrin subunits $\beta_3$ or $\beta_1$. Interestingly, there was increased activation of both VEGFR2 and PDGFRβ only in the cells overexpressing integrin subunit $\beta_3$. Additionally, mutants of $\beta_3$ with truncated cytoplasmic domains replaced by $\beta_1$ cytoplasmic domains were still able to phosphorylate both VEGFR2 and PDGFRβ, suggesting that it is the activated extracellular domain of integrin subunit $\beta_3$ that is responsible for phosphorylation of VEGFR2 and PDGFRβ. In addition, the extracellular domain of integrin subunit $\beta_3$ as well as the subunit $\alpha_V$ are necessary to phosphorylate VEGFR2, while only the extracellular domain of the integrin subunit $\beta_3$ is necessary to activate PDGFRβ[166].

Integrin $\alpha_V\beta_3$ participates in both 'outside in' and 'inside out' signaling. In other words, signals can be transduced via 1) ligand binding to extracellular domains, or 2)

cytosolic kinases phosphorylating cytoplasmic domains[167,168]. As previously mentioned, 'outside in' signaling via endothelial cell adhesion to vitronectin and fibrin through integrin $\alpha_V\beta_3$, leads to phosphorylation of tyrosine residues Y747 and Y759 on the subunit $\beta_3$. 'Inside out' signaling effectively refers to activation of VEGFR2 via VEGF binding, which recruits cSrc to the cytoplasmic domain of integrin subunit $\beta_3$, again phosphorylating tyrosine residues Y747 an Y759 demonstrating redundancy and cross-talk between VEGFR2-ligand complex activation of integrin $\alpha_V\beta_3$, and integrin $\alpha_V\beta_3$-ligand complex activation of VEGFR2[169].

Many have studied tissue engineering of microvessels in both 3D fibrin and 3D collagen I using a variety of endothelial cell sources for neovascularization[128,170,171]. However, herein we describe robust neovascularization of 3D tissue constructs, utilizing adipose-derived SVF cultured in 3D fibrin and 3D collagen I over 7 days. SVF forms robust microvascular networks via known angiogenic mechanisms in fibrin in a VEGF and an integrin $\alpha_V\beta_3$ dependent manner.

## Materials and Methods

*Animals and Ethics Statement*

All animal procedures were conducted in compliance with University of Louisville School of Medicine IACUC-approved protocols and NIH guidelines. Isoflurane gas was administered for anesthesia.

*SVF Isolation from Sprague Dawley Rats*

Rat epididymal fat pads were excised from 6 to 8-month-old Sprague Dawley rats at weights greater than 250g under sterile surgical procedure and isoflurane anesthesia. All procedures were reviewed and approved under the University of Louisville's Institutional Animal Care and Use Committee. Excised fat pads were placed in PBS containing 0.1% bovine serum albumin (Sigma Aldrich, St. Louis, MO) and kept at 4°C for 15 min prior to digestion. Samples were washed with BSA-PBS and minced for 2 min until particulates could pass through a 50mL aspirating pipette. 2mg of Type I Collagenase (Worthington Biochemical Corporation, Lakewood, NJ) was added per mL of fat, aliquoted at 20mL total volume in 50mL conical centrifuge tubes, and rotated in an Envirogenie Incubator (Scientific Industries, Bohemia, NY) at 35 rpm and 37°C for 35 min. Samples were pelleted via centrifugation at 350xg for 4 min at RT. Buoyant adipocytes were aspirated and discarded, and dense cellular pellets were suspended and washed one time in BSA-PBS. Samples were re-centrifuged for 4 min at 350xg. The SVF pellet was filtered through a 250μm mesh filter (Tissue Genesis Incorporated, Honolulu, HA) and collected into DMEM containing endothelial cell growth supplement, 2mM L-glutamine, 10% fetal bovine serum, and 5mM Hepes buffer. Samples were kept at RT prior to plating.

*Creation of 3D Fibrin and 3D Collagen I SVF Laden Cultures*

Freshly isolated SVF was mixed in 10mg/mL bovine fibrinogen (Sigma Aldrich, St. Louis, MO) dissolved in 50% normal saline and 50% rat complete media (1:1 vol:vol) at $8x10^5$ cells per 500μL. 2U of bovine thrombin (Sigma Aldrich, St. Louis, MO) was added per mg fibrinogen to the solution. Collagen I gels were created at 4°C using purified rat tail collagen I (Millipore, Temecula, CA) diluted to 3mg/mL in 4X DMEM base media and Millipore water. Activation of polymerization was achieved by adding 7μL 4N NaOH to reach a pH of 7.5 at RT. Aliquots of 500μL were plated in 48 well polystyrene tissue culture treated plates (Corning, Corning, NY) and allowed to polymerize to a gel for 30 min at 37°C in a tissue culture incubator. 500μL of rat complete media was added and replaced every other day on top of the polymerized gels for a culture length of 7 days.

*Inhibitors in Culture*

Inhibitors were added at each culture change to the media to reach the final concentrations as follows: DAPT (γ secretase inhibitor: 25μM) (Abcam, Cambridge, UK) ZM306416 (VEGFR1 inhibitor: 25μM) (Selleckchem, Houston, TX), Imatinib mesylate (PDGFR-β inhibitor: 1μM) (Sigma Aldrich, St. Louis, MO), LM609 (anti integrin $\alpha_V\beta_3$ monoclonal antibody: 10μg/mL) (Millipore, Temecula, CA), and human recombinant Flk1 (soluble VEGFR2: 500ng/mL) (Abcam, San Diego, CA).

*Imaging network formation and cell populations in 3D cultures*

SVF in 3D fibrin or 3D collagen I at 7 days were fixed with 4% paraformaldehyde for 15 min at RT, permeabilized with 0.1% Triton X 100 for 15 min at RT and stained with griffonia simplicifolia 1 lectin conjugated to FITC (1:500) (Vector Biotechnologies, Burlingame, CA) and α-smooth muscle actin mouse monoclonal primary antibody (1:500)

(Santa Cruz Biotechnology, Dallas, TX) overnight at 4°C to visualize endothelial and smooth muscle cells respectively. Additionally, some samples were also stained overnight at 4°C with rabbit monoclonal primary antibodies against nerve-glial antigen 2 (1:500), N-cadherin (1:500), or PDGF-Rβ (1:500) (Santa Cruz Biotechnology, Dallas, TX) with subsequent goat anti rabbit Alexafluor 594 secondary antibody (1:1000) (Thermofisher, Rockford, IL) for 2 hours at RT to demonstrate pericyte cellular migration and association with GS1 positive endothelial cell networks. 3D rendered images were captured using an Olympus confocal microscope capturing Z-stacks at every 3μm tissue depth. OIF image files were stitched into 3D composite images using AMIRA 6.0 software (FEI Visualization Sciences Group). Composite, colored images were created using Image J software (NIH).

*Image Analysis*

3D rendered images were analyzed using AMIRA 6.0 software. Microvessel tubes were skeletonized in order to measure number of segments indicating branching complexity, total vessel volume, and total vessel length. A segment is indicated as the longest measurable endothelial tube before it branches to give off multiple extensions. All image manipulation was conducted utilizing instructions from the AMIRA 6.0 user manual.

*Statistical Analysis*

Graphs and statistics were run with GraphPad Prism v.7 Software (La Jolla, CA). P values were calculated via one-way ANOVAs using Dunnet's multiple comparison tests with means and standard deviations plotted per group as compared to vehicle only (control group). Paired t tests were calculated comparing collagen I and fibrin events including

segment number, total vessel volume, total vessel length, and RNA expression level of integrin subunit $\alpha_V$.

*Gene Expression*

3D embedded SVF was acquired at day 7 of culture and processed for mRNA isolation. Briefly, gels were homogenized at 1:1 vol:vol of gel to trizol (ThermoFisher, Waltham, MA) and subsequently processed using RNeasy kits (Qiagen, Hilden, Germany) according to the provided manufacturer's protocol. cDNA was produced from mRNA using Agilent Affinity Script QPCR cDNA synthesis kit (Agilent, Santa Clara, CA) and again processed via included protocol. cDNA was analyzed via RT-PCR using primers designed against the rat integrin subunit $\alpha_V$ from DNA sequences provided by PubMed libraries. The forward primer: 'CGA CCT TGC CGT TTT GGC TGC AGT T' and the reverse primer: 'GGC CCA ACG TCT TCT TCG GTC TCA GG' were added to obtain a final concentration of 5μM along with Applied Biosystems SYBR Select Master Mix (ThermoFisher) and run in the Qiagen Rotor Gene 6000 set to a 95°C hold cycle for 10 min, cycling repeats at 95°C, 59°C, and 72°C 40 times for 30 seconds and a melt and cooldown cycle for 95°C for 10 min and 4°C for 1 hr. PCR product was quantified via 2% agarose, TBE gel electrophoresis using a Bio-rad ChemiDoc imaging system (BioRad, Hercules, CA).

**Results**

Adipose-derived SVF forms robust microvascular networks in 3D fibrin (10mg/mL) but not 3D collagen I (3mg/mL) within 7 days of culture (**Figure 6**). Endothelial cells coalesce into highly branched networks as indicated by GS1-FITC$^{+}$ staining. In addition, cells expressing alpha smooth muscle actin associate with endothelial networks as demonstrated by αSMA-rhodamine$^{+}$ cells adjacent to endothelial cells; suggesting further maturation into multicellular microvessels more closely resembling native arterioles (**Figure 6A, Figure 7**). These events do not take place in collagen I at 3mg/mL (**Figure 6B**). Rather, SVF cells embedded in collagen I are rounded and bunched throughout 7 days of culture without significant migration, elongation, or branching with no resemblance to endogenous microvascular architecture.

Additionally, due to the diverse population of cell types within SVF, it is noted that cells resembling pericytes also migrate and associate to newly formed endothelial networks in 3D fibrin cultures. This phenomenon is demonstrated through the expression of nerve glial antigen 2, N-cadherin, and PDGFR-β positive cells associating with endothelial cells (**Figures 8, 9, 10**). Interestingly, at 7 days, N-cadherin and PDGFR-β localization seem to be highly peri-nuclear, suggesting production of high quantities of these proteins in the rough endoplasmic reticulum or modification in the golgi before shuttling to the cell surface.

Microvascular networks also remodel surrounding fibrin ECM and produce basement membrane proteins including fibronectin and laminin 332 by day 7 (**Figure 11 B, C**).

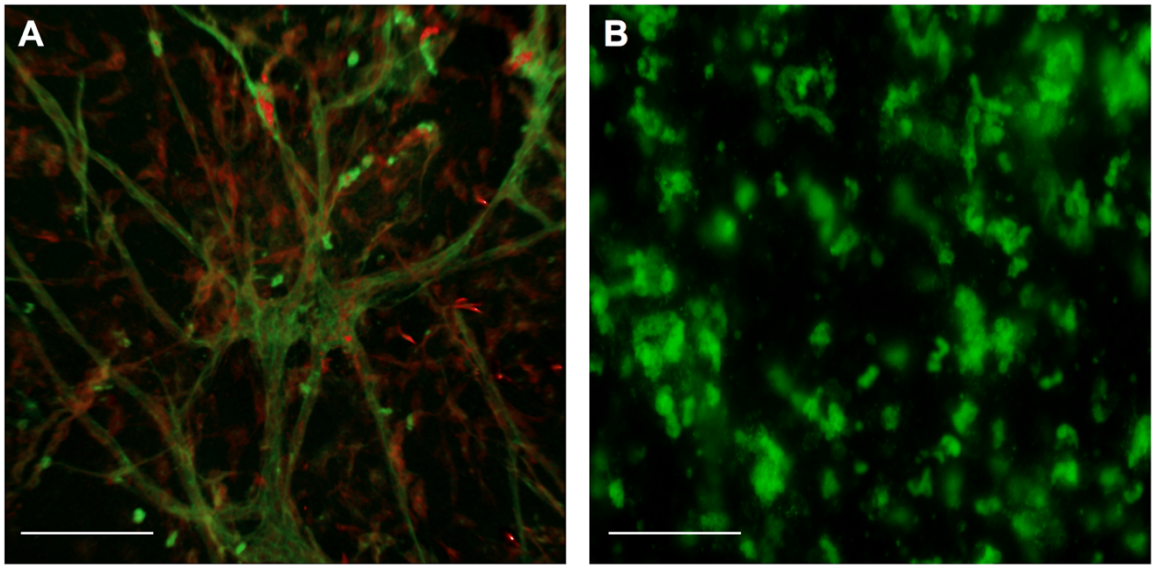


***Figure 6***: *Rat SVF forms microvascular networks in Fibrin but not Collagen I. $4x10^5$ Rat SVF cells cultured in 250μL fibrin (10mg/mL) at 7 days. Endothelial cells are represented by GS1-FITC$^+$ (green) and alpha smooth muscle actin producing cells by αSMA-Rhodamine$^+$ (red) (A). Endothelial cells are rounded and do not resemble organization into microvessel structures in collagen I (3mg/mL), in addition, there are very few alpha smooth muscle actin producing cells (B). Scale bar =200μm.*

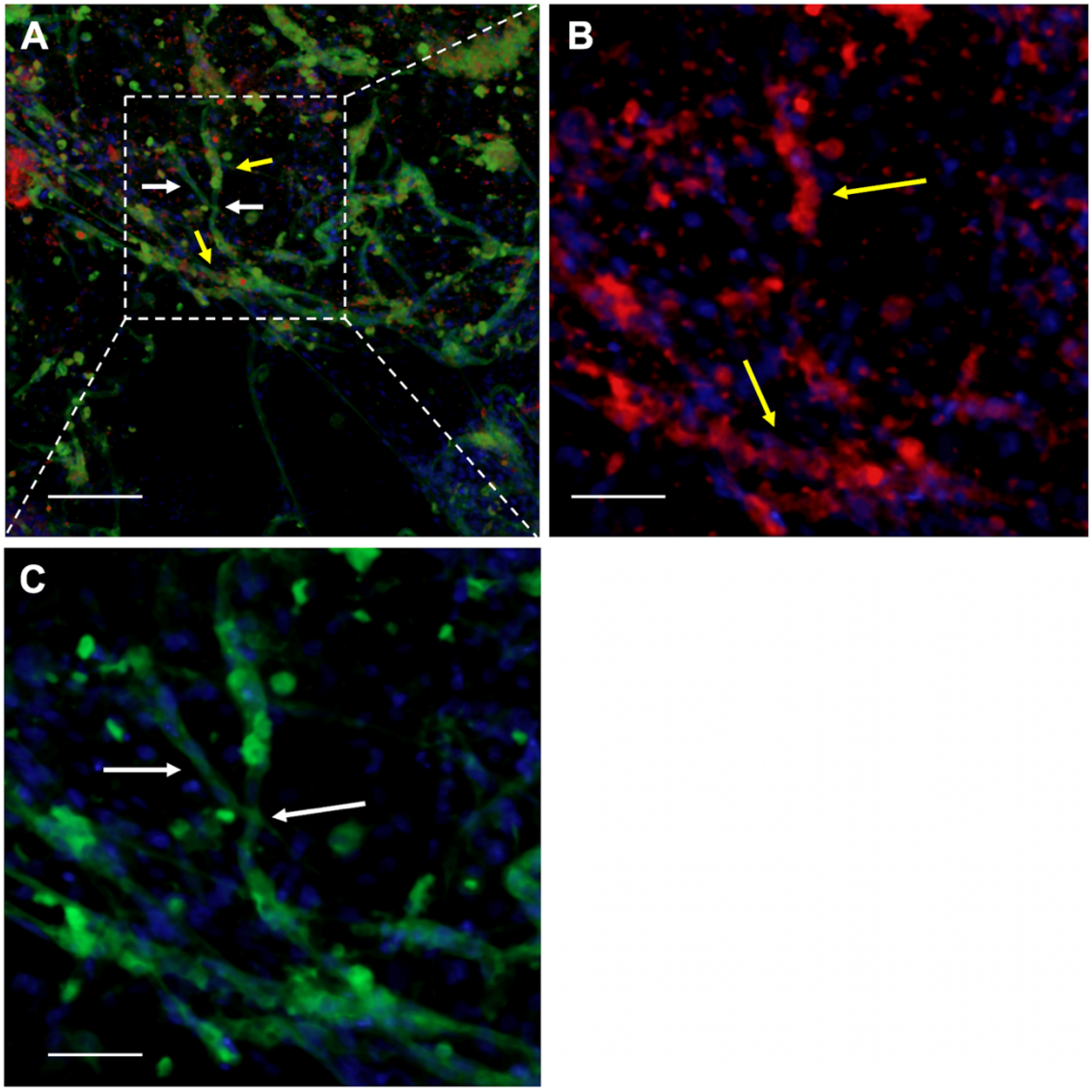


***Figure 7**: αSMA-Rhodamine$^{+}$ perivascular cells associate with GS1-FITC$^{+}$ endothelial networks in 3D fibrin (10mg/mL) in vitro (A) Scale bar = 200μm. αSMA-Rhodamine$^{+}$ perivascular cells only (B) Scale bar = 50μm. GS1-FITC$^{+}$ endothelial networks only (C) Scale bar = 50μm. Blue: DAPI$^{+}$ nuclei. White arrows indicate endothelial cells without surrounding cells. Yellow arrows indicate areas of perivascular cells surrounding endothelial cells.*

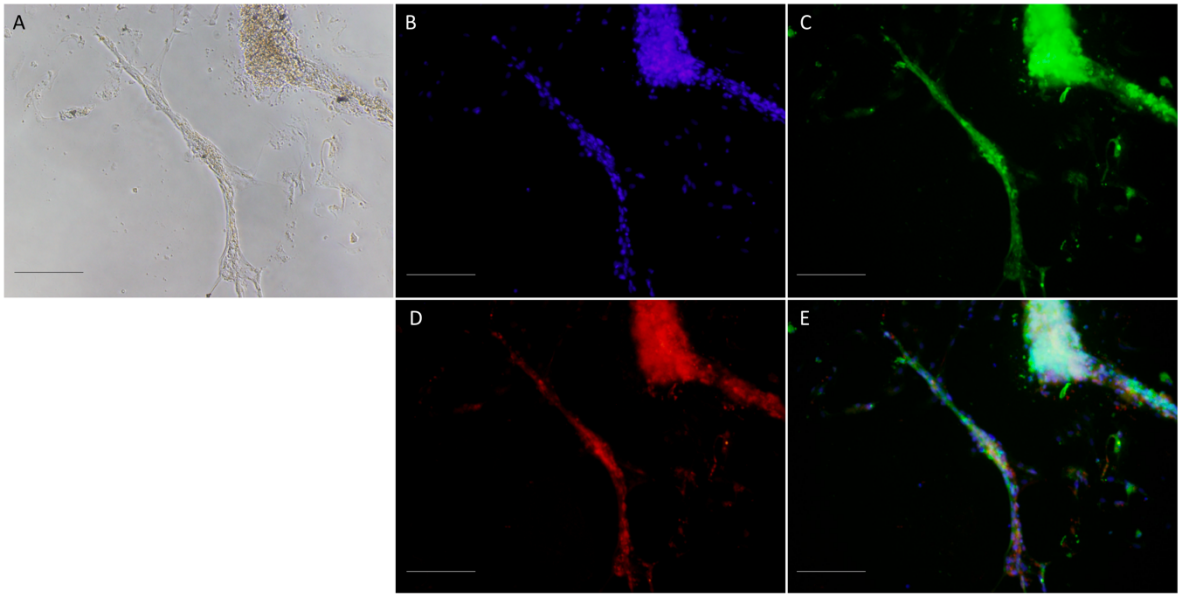


***Figure 8**: Rat SVF cultured in fibrin (10mg/mL) at 7 days demonstrating NG2$^+$ cells associating with endothelial networks. Phase contrast of microvessel morphology (A). DAPI$^+$ nuclear staining (B). Endothelial GS1-FITC$^+$ cells (C). NG2-Alexa 594$^+$ cells (D). Composite merge of channels (E). Scale bar = 200 μm.*

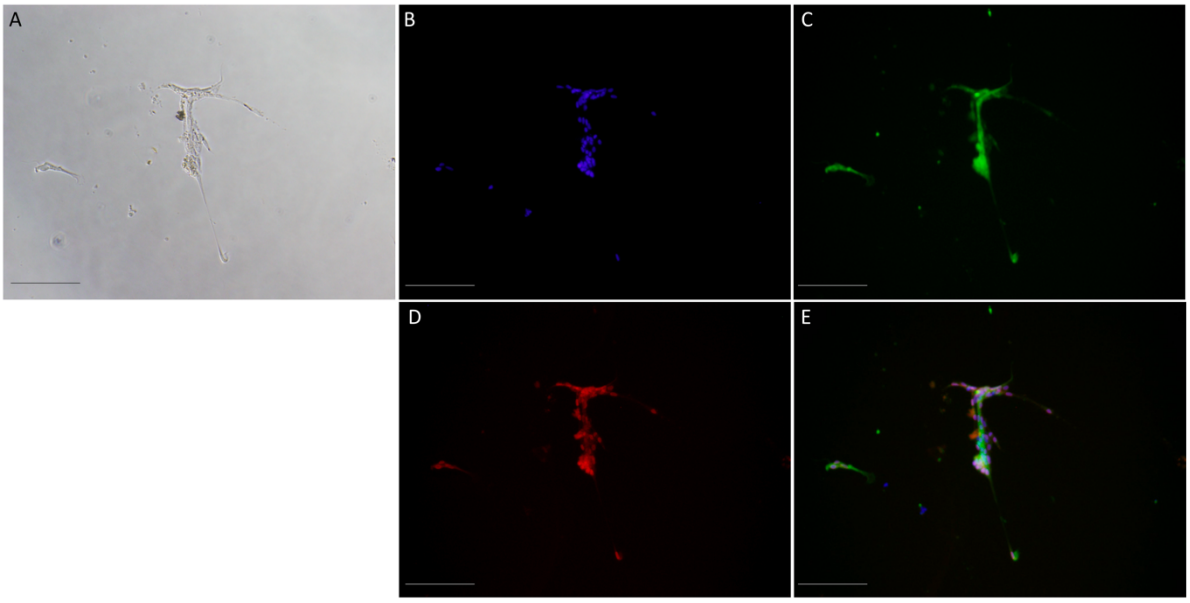


***Figure 9****: Rat SVF cultured in fibrin (10mg/mL) at 7 days demonstrating N-cadherin$^{+}$ cells associating with endothelial networks. Phase contrast of microvessel morphology (A). DAPI$^{+}$ nuclear staining (B). Endothelial GS1-FITC$^{+}$ cells (C). N-cadherin-Alexa 594$^{+}$ cells (D). Composite merge of channels (E). Scale bar = 200 μm.*

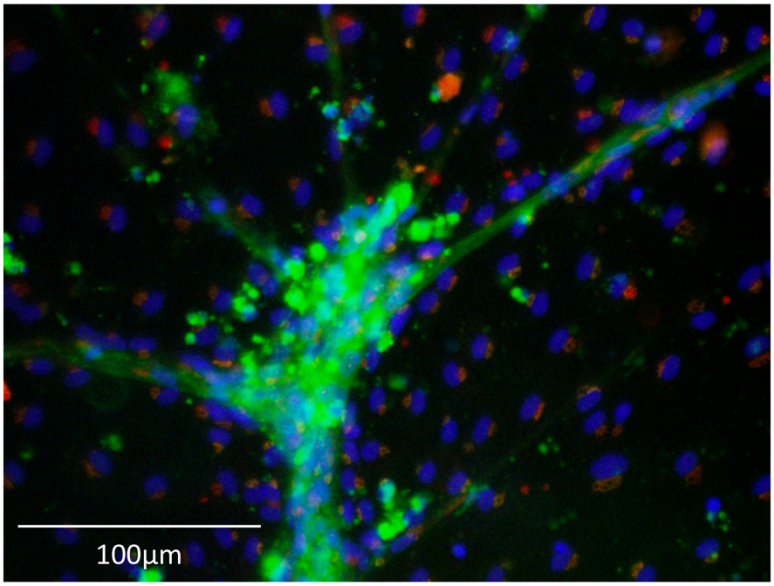


***Figure 10**: Rat SVF cultured in fibrin (10mg/mL) at 7 days demonstrating PDGFR-$\beta^+$ cells associating with endothelial networks. Composite image of DAPI$^+$ nuclear staining (blue). Endothelial GS1-FITC$^+$ cells (green). PDGFR-$\beta^+$ cells (red).*

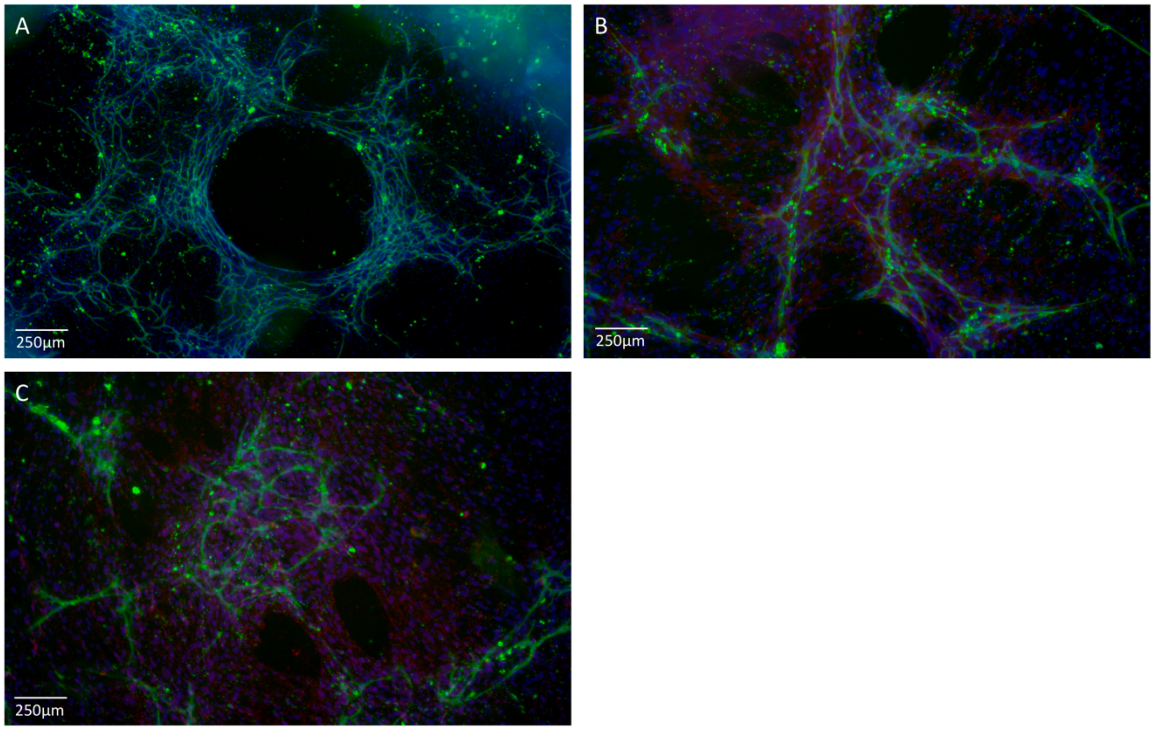


***Figure 11**: Rat SVF cultured in fibrin (10mg/mL) at 7 days demonstrating basement membrane protein production around endothelial networks. GS1-FITC$^{+}$ staining (green) and DAPI$^{+}$ nuclear staining (blue) (A). GS1-FITC$^{+}$ staining (green), DAPI$^{+}$ nuclear staining (blue), and fibronectin-Alexa594$^{+}$ staining (red) (B). GS1-FITC$^{+}$ staining (green), DAPI$^{+}$ nuclear staining (blue), and laminin332-Alexa594$^{+}$ staining (red) (C).*

To understand if SVF microvascular network formation in 3D fibrin occurs through similar angiogeneic mechanisms as seen in our previously published 2D SVF- Matrigel® assay[160], inhibitors were added to 3D cultures at days 0, 2, 4 and 6. These inhibitors included DAPT a γ secretase inhibitor affecting the NOTCH pathway that decreases differentiation of endothelial stalk cell phenotypes during angiogenesis; ZM 306416 a VEGFR-1 inhibitor also disrupting tip cell and stalk cell differentiation and tip cell migration; Imatinib mesylate a competitive inhibitor of PDGFR-$\beta$ disrupting perivascular cell recruitment and stabilization of endothelial networks; LM 609 a monoclonal antibody blocking ligand binding to integrin $\alpha_V\beta_3$ potentially disrupting VEGF-induced angiogenesis; and recombinant human VEGFR-2 (Flk1) a soluble VEGFR-2 that competes for VEGF-A ligand extracellularly.

3D confocal images of SVF grown in 3D fibrin for 7 days were skeletonized using AMIRA software to assess vessel complexity and density as measured by segment number, total vessel volume, and total vessel length. Samples with inhibitor were normalized to DMSO vehicle controls. In the presence of DAPT, samples demonstrated statistically significant increases in segment number ($p < 0.05$), total vessel volume ($p < 0.005$), and total vessel length as compared to DMSO ($p < 0.05$) (**Figures 12, 13**). This may be due to dysregulation of tip and stalk cell ratios. Indeed, in a diabetic mouse model of angiogenesis, reduced endothelial sprouting and migration were noted by Cao and colleagues, however, in the presence of PDGF, VEGF, and DAPT, vessel density increased 150%[172]. We see similar phenomena in our *in vitro* assay with as much as 2-fold total vessel volume increases and 1.5-fold segment number and total vessel length increases (**Figure 13**). These increases in vessel segment number, volume, and length, however, do

not indicate that these microvessels are fully functional. In order to assess functionality, engineered microvasculature must be implanted *in vivo*, inosculate with host microvessels to establish flow, and demonstrate retention overtime post pruning.

In the presence of ZM 306416, a VEGFR1 inhibitor, there are statistically significant decreases in vessel segment number ($p < 0.0005$), vessel volume ($p < 0.05$), and total vessel length ($p < 0.0001$) (**Figure 12, 13**). When treated with Imatinib mesylate, there are also statistically significant decreases in segment number ($p < 0.005$) and total vessel length ($p < 0.0005$) (**Figure 12, 13**). The integrin $\alpha_V\beta_3$ inhibitor LM609 at 10μg/mL also reduces SVF microvessel formation and complexity in 3D fibrin. There is a statistically significant decrease in segment number ($p < 0.0005$), total vessel volume ($p < 0.05$), and total vessel length ($p < 0.0001$) as compared to DMSO control. Finally, in the presence of recombinant Flk1 at 500ng/mL, there are also significant decreases in segment number ($p < 0.005$), total vessel volume ($p < 0.05$), and total vessel length ($p < 0.0005$) (**Figure 12, 13**).

To assess if fibrin or collagen differentially alter expression of integrin $\alpha_V\beta_3$ in SVF derived microvessels, RNA was isolated from 3D cultures after 7 days. Unfortunately, only the sequence of the $\alpha_V$ subunit was known for rats through database searching, and as such, primers were designed against that subunit. Interestingly, after 7 days, there was no significant difference between the expression profile of $\alpha_V$ as normalized to the housekeeping gene GAPDH between fibrin and collagen I cultures (**Figure 14**).

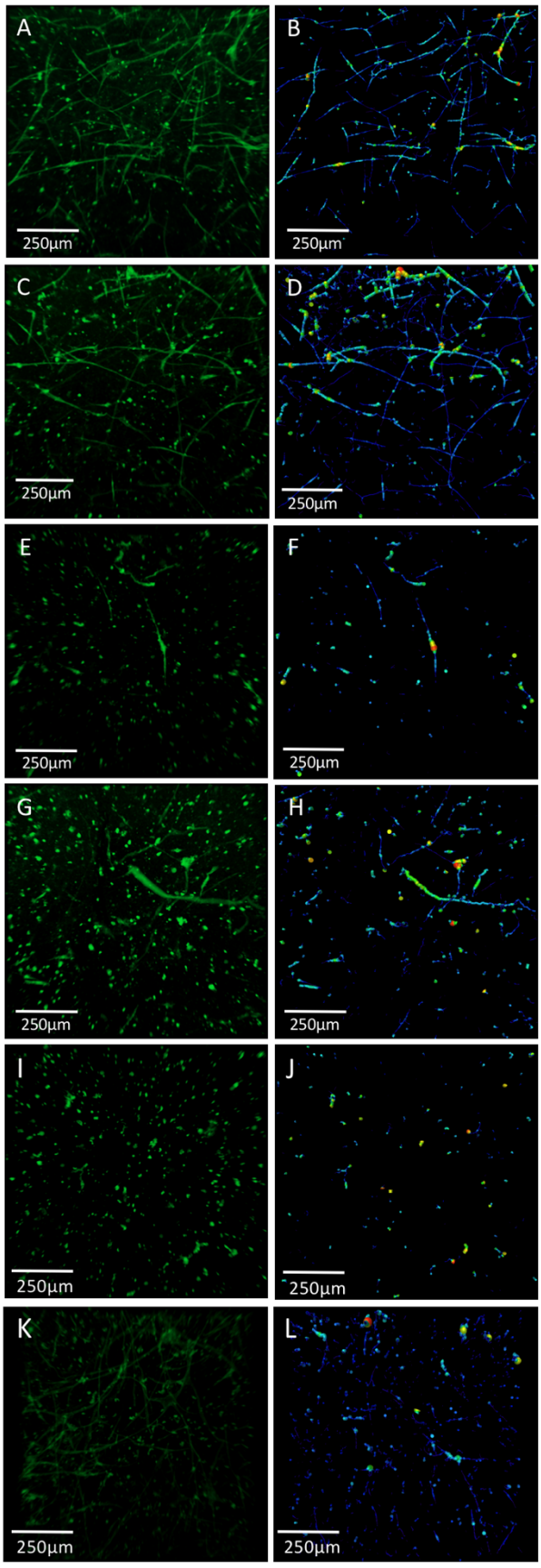


***Figure 12**: 3D rendered confocal z-stacks of rSVF in 10mg/mL Fibrin, day 7. Endothelial cells stained with GS1-FITC (Green) with samples: DMSO vehicle only (A, B), 25µM DAPT (C, D), 25µM ZM 306416 (E, F), 1µM Imatinib mesylate (G, H), 10µg/mL anti-$\alpha_V\beta_3$ mAb (I, J), and 500ng/mL soluble human recombinant Flk1 (K, L). Inhibitors were added to culture at days 0, 2, 4, and 6 during media changes. Images B, D, F, H, J, L are skeletonized renderings of vascular structures using AMIRA software to calculate segment number, total volume, and total length of vessels in vitro. Change in vessel color from blue to green to yellow to orange represents increasing diameter of tube structure in skeletonized images.*

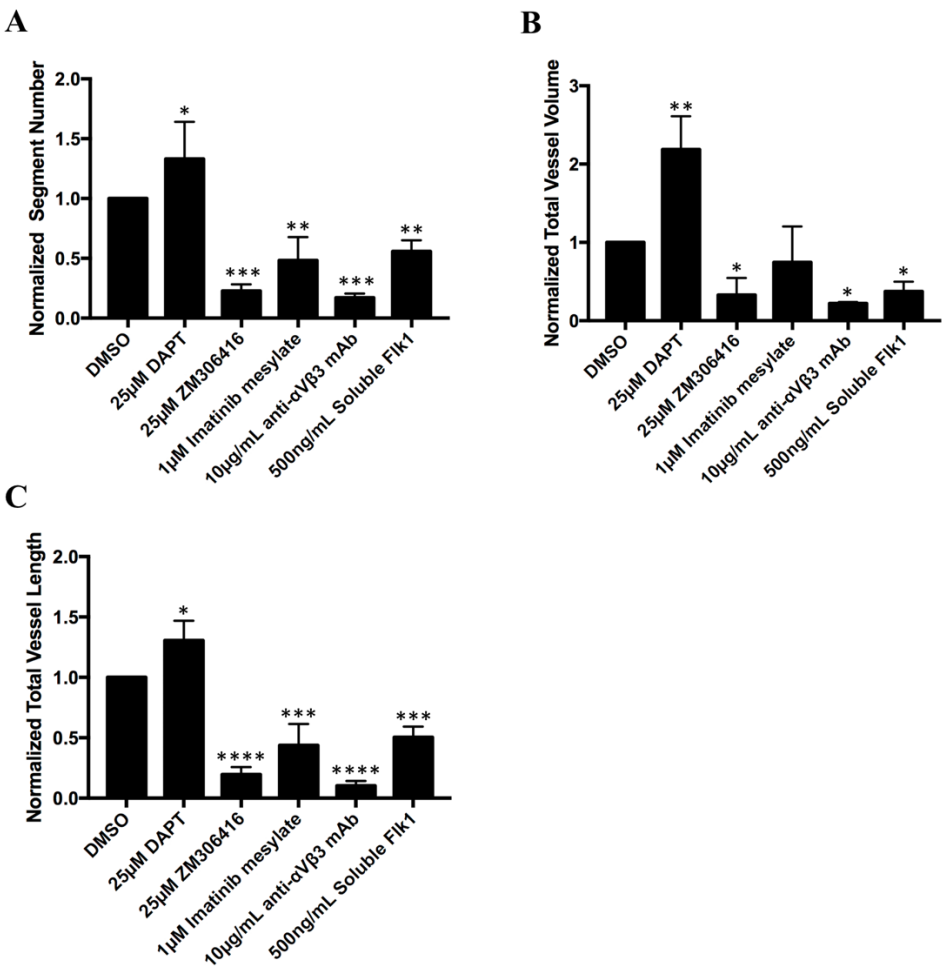


***Figure 13***: *A. Number of vessel segments normalized to vehicle control with significant increase in segment number in the presence of DAPT and significant decrease in segment number in the presence of ZM 306416, Imatinib mesylate, anti-αVβ3 mAb, and soluble Flk1. B. Total volume of vessel structures normalized to vehicle control with significant increase in total vessel volume in the presence of DAPT and significant decrease in total vessel volume in the presence of ZM 306416, anti-αVβ3 mAb, and soluble Flk1. C. Total vessel length normalized to vehicle control with significant increase in total vessel length in the presence of DAPT and significant decrease in total vessel length in the presence of ZM 306416, Imatinib mesylate, anti-αVβ3 mAb, and soluble Flk1. $p < 0.05$ (*), $p < 0.005$ (**), $p < 0.0005$ (***), $p < 0.0001$ (****).*

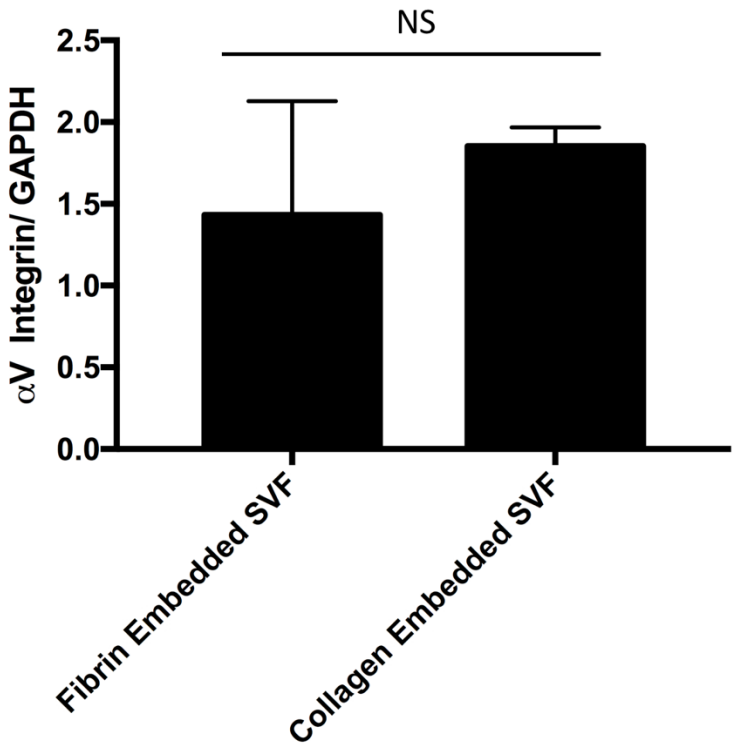


***Figure 14**: Gene expression of integrin $\alpha_V$ subunit normalized to GAPDH expression. RNA was isolated from rSVF cells ($4x10^5$cells/250$\mu$L gel) embedded in either 10mg/mL fibrin or 3mg/mL collagen I, cultured over 7 days. RNA was converted to cDNA and amplification with primers to the housekeeping gene GAPDH as well as the integrin $\alpha_V$ subunit was performed via PCR. There is no significant difference in expression of integrin $\alpha_V$ subunit normalized to GAPDH between SVF grown in fibrin and collagen I.*

**Discussion**

To create microvasculature from adipose-derived SVF, clinically available and translatable reagents have been a focus of studies to provide a 3D structure and support angiogenesis *in vitro*. If achieved, this would allow for the construction of implantable, discreet, pre-vascularized tissue units for *in vivo* purposes. Nicosia and colleagues were able to create an *in vitro* aortic ring model to stimulate and study angiogenesis in 3D, however, this model does not translate to the production of prevascularized 3D tissue for clinical applications[144]. 3D fibrin at 10mg/mL stimulates rapid formation of microvessels derived from embedded, freshly isolated SVF cell populations, while 3mg/mL collagen I does not over a period of 7 days. As such, it was hypothesized that preferential integrin activation by fibrin stimulates angiogenesis in our 3D culture system.

Many different types of integrins are ubiquitously expressed in adult tissues, however, fibrin-activated integrin $\alpha_V\beta_3$ is most abundantly expressed on endothelial cells participating in angiogenesis during tissue remodeling, growth, and pathogenesis, but not expressed in normal quiescent endothelial cells[173]. More specifically, the $\beta_3$ subunit expression decreases as early as the first weeks of life during remodeling of cardiac blood vessels as seen in mice[174]. However, in knockout studies, mice lacking $\beta_3$ not only have increased hemorrhagic events in utero, but also, capillaries in the heart fail to mature and create lumens via vacuolar formation, presenting similarly to immature non-functional endothelium. Indeed, a molecular complex and activation is needed between both VEGFR2 and integrin $\alpha_V\beta_3$ during angiogenesis[169,175-177]. Integrin $\beta_3$ subunit expression is necessary to stimulate endothelial morphogenesis, and also, it is required for the

recruitment of bone marrow derived cells to sites of angiogeneic remodeling via signaling release events from the bone marrow space[178].

As stated prior, integrin $\alpha_V\beta_3$ and others are activated by extracellular matrix proteins containing the RGD motif such as vitronectin, fibrinogen, and fibrin. The receptor itself is highly internalized through known clathrin-dependent endocytosis. Some have studied the production of internalizing-RGD proteins (iRGD) or RGD-targeted nanoparticles to image highly angiogenic tumor vascular structure [179,180]. In addition, inhibitors of integrin $\alpha_V\beta_3$ are produced endogenously to mitigate hyper-angiogenesis as seen in solid tumor growth. Some of these inhibitors are soluble protein fragments that mimic and compete with insoluble endogenous ECM for integrin binding. For example, angiostatin is a plasmin fragment that binds to $\alpha_V\beta_3$[181], canstatin is a type IV collagen fragment binding to $\alpha_V\beta_3$ and $\alpha_V\beta_5$[182], endostatin is a collagen XVIII fragment that binds to $\alpha_V\beta_3$, $\alpha_V\beta_5$, and $\alpha_5\beta_1$[183], and tumstatin is a type IV collagen fragment that binds to $\alpha_V\beta_3$ and $\alpha_5\beta_1$[184].

Synthetic inhibitors have also been tested as means to interrupt integrin $\alpha V\beta 3$-dependent angiogenesis in solid tumors. Of note is Cilengitide, an RGD peptide, which has undergone Phase III clinical testing for patients with glioblastoma multiforme, demonstrating durable remissions and increased survival for some patients[185]. In addition, the anti- $\alpha_V\beta_3$ antibody LM609 demonstrating inhibition of angiogenesis in a chick embryo model was also humanized and is being developed by Astra-Zeneca as etarazizumab (Abegrin) with early phase I studies demonstrating tolerability in patients with solid tumors as well[186].

In our assay, SVF forms robust microvascular networks in 3D fibrin in an integrin $\alpha_V\beta_3$-dependent manner. In the presence of LM609, there was significant decreases in vessel segment number, total vessel volume, and total vessel length. In addition, SVF-formed microvessels in fibrin require known angiogenic signaling pathways to function for network formation. In the presence of VEGFR1 inhibitor, PDGFR-$\beta$ inhibitor, as well as soluble VEGFR-2, there is decreased microvessel segment numbers, total vessel volumes, and total vessel lengths as compared to controls. Additionally, microvessels formed within 3D fibrin *in vitro* not only undergo endothelial tubulogenesis, but also recruit perivascular support cells in the form of $NG2^+$/PDGFR-$\beta^+$ pericytes and alpha smooth muscle actin producing cells, suggesting continual maturation mimicking endogenous functional microvasculature.

While not all mechanisms are fully understood, it is possible that in addition to integrin $\alpha_V\beta_3$ activation and VEGFR2 signaling, biomechanical factors such as tensile strength, fibril alignment and orientation, and deformability of 10mg/mL fibrin gels allows for increased cellular migration and proliferation as compared to 3mg/mL collagen type I constructs. Additional studies are needed to elucidate specific mechanisms involved in SVF vasculogenesis and angiogenesis in 3D fibrin, in addition to known integrin signaling pathways.

# CHAPTER III

# BIOPRINTING SVF-DERIVED MICROVASCULATURE AND ELECTROSPINNING SVF-DERIVED MACROVASCULATURE

## The Formation of SVF-Laden Spheroids Utilizing a 3D Bioprinter and Superhydrophobic Surfaces

### Introduction

Currently, clinical therapies utilizing SVF and other stem cell sources for transplantation often administer cells through means of direct injection, where cells are re-suspended into a sterile solution and delivered via syringe to sites of interest[20-22,104,120,187-190]. Unfortunately, with these procedures, many cells do not retain at the site of injection and rather migrate, enter circulation, or undergo apoptosis due to poor integration with diseased tissue[191,192]. To mitigate the problems seen with cell suspensions, many have studied *in vitro* cell assembly into aggregates, whereby cells are either encapsulated in biomaterials such as extracellular matrix or self-aggregate into cell clusters via specific culture methods[193-196]. As an example, SVF as a clinically utilized cell source has been encapsulated into hydrogels which include 3D collagen I and alginate for *in vivo*

applications[67,81,197-202]. Most encapsulation methods are simple 3D culture systems creating known geometries afforded by commercially available well-based polystyrene plates. However, of late, systems producing a spheroid format have shed new light on encapsulation of cells, reducing necrotic zones *in vitro,* and allowing discrete tissue units to be delivered *in vivo*.

Cell only spheroids, surface cell sodded spheroids, and cells encapsulated within hydrogel spheroids are the primary methods for creation of new format tissue units in a spheroid geometry. Specifically, cell only spheroids are created through self-aggregation in which cells communicate with one another forming tight adhesion junctions during the process of hanging within a droplet of media. However, this production process takes several days and is highly dependent upon rates of claudin and occludin association between cells which can vary drastically between cell types[203,204]. Surface sodding premade spheroids is also highly dependent upon cells' adhesive properties, which can limit biomaterial used, and in some cases, limit cellular integration, migration, and proliferation into the entire spheroid, possibly due to cells' inability to digest and remodel the biomaterial during migration. The final type of cell spheroid production is through encapsulation of cells within a biomaterial that can undergo phase change from liquid into gel form, embedding cells throughout the entire spheroid unit. Cell embedding has the advantages of equal distribution of cells within the entire spheroid, the ability to dose the amount of cells per spheroid creating advantageous ECM to cell ratios, and the ability to be produced in less than one day[201,205-209].

Previously, there have been some limitations with ECM spheroid productions specifically utilizing collagen I or fibrin. These ECM proteins while adhesive and allowing

for signal transduction, migration, proliferation, differentiation and remodeling by cells, do not retain shape unless crosslinked within a mold. Thus, it was imperative to develop new techniques allowing natural polymerization of cell laden hydrogels into replicable, precise tissue spheroids.

Extrusion printing is a customizable and well-established method of manufacturing specific 3D architectures, commonly utilizing non-biologics such as plastics and glass. As a subset method of 3D printing, extrusion bioprinting affords the use of biologically applicable hydrogels without the need of curative agents or other potential toxins as seen in manufacturing methods such as sterolithography. Many have utilized 3D axis, direct write CAD/CAM based 3D printers to extrude biomaterials with or without cells present[210,211]. As such, we found it necessary to approach similar systems in order to create SVF laden collagen I and fibrin spheroids for potential *in vivo* applications.

In order to produce replicable, exact shapes, simple extrusion of non-polymerized ECM such as collagen I would have to utilize plastic molds or shape holders due to the biomaterial not retaining certain architectures even post polymerization; introducing issues such as manual handling and removal which may damage or alter scaffolds and provide unnecessary variability. Such methods would limit clinical translatability of tissue engineered products. In addition, *in vivo* applications may require certain irregular shapes or patient specific cell doses that would force additional manipulation of 3D bioprinted, molded scaffolds. Instead, herein we describe a technique to automate and 3D print collagen I and fibrin containing SVF in spheroid format utilizing superhydrophobic surfaces, hydrophilic spotting, and extrusion bioprinting. Collagen and fibrin cell

containing spheroids may address aforementioned issues with fluid-suspended cellular injections and their limited retention at pathologic sites.

## Materials and Methods

*Fabrication of a Superhydrophobic Surface*

A superhydrophobic surface was produced on polystyrene 48-multiwell plates (Corning, Corning, NY) and/or 35mm Petri dishes using a two-step aerosol application of NeverWet™ (Rust Oleum, Vernon Hills, IL). The application of a binder to the surface as a base coat was sprayed onto non-treated plates and allowed to dry at RT for 1h. Secondly, a top sheet composed of polydimethylsiloxane modified with hexamethyldisilazane was added to form a superhydrophobic layer. The entire superhydrophobic layer was measured as 0.007mm. The plates were allowed to air dry for at least 1 more hr before the addition of hydrophilic spots. NeverWet™ has a reported contact angle of 165° which meets the criteria of hydrophobicity (contact angles > 150°). The contact angle of both water and unpolymerized collagen I (3mg/mL) was measured using side view photography and angle measurement tools in ImageJ (NIH, Bethesda, MD).

*Creation of Hydrophilic Spots*

Hydrophilic spots onto the superhydrophobic surface were created using a direct write 3D biporinter (Bio-Asssembly Tool (BAT) 3D Printer; nScrypt, Inc., Orlando, FL) to extrude Pluronic F-127 (Sigma Aldrich, St. Louis, MO). For each hydrophilic spot, the BAT extruded a target volume of 2μL of 3.8% (wt/wt) Pluronic F-127 in 1X phosphate-buffered saline (PBS). Using time-pressure extrusion, this required 2.5psi with an exposure time of 100ms through a 25G needle in order to create the extrusion force necessary to meet the target volume. The spots were then allowed to air dry for 30min before use.

*Animals and Ethics Statement*

All animal procedures were conducted in compliance with University of Louisville School of Medicine IACUC-approved protocols and NIH guidelines. Isoflurane gas was administered for anesthesia.

*SVF Isolation from Sprague Dawley Rats*

Rat epididymal fat pads were excised from 6 to 8-month-old Sprague Dawley rats at weights greater than 250g under sterile surgical procedure and isoflurane anesthesia. All procedures were reviewed and approved under the University of Louisville's Institutional Animal Care and Use Committee. Excised fat pads were placed in PBS containing 0.1% bovine serum albumin (Sigma Aldrich, St. Louis MO) and kept at 4°C for 15 min prior to digestion. Samples were washed with BSA-PBS and minced for 2 min until particulates could pass through a 50mL aspirating pipette. 2mg of Type I Collagenase (Worthington Biochemical Corporation, Lakewood NJ) was added per mL of fat, aliquoted at 20mL total volume in 50mL conical centrifuge tubes, and rotated in an Envirogenie Incubator (Scientific Industries, Bohemia, NY) at 35 rpm and 37°C for 35 min. Samples were pelleted via centrifugation at 350xg for 4 min at RT. Buoyant adipocytes were aspirated and discarded, and dense cellular pellets were suspended and washed one time in BSA-PBS. Samples were re-centrifuged for 4 min at 350xg. The SVF pellet was filtered through a 250μm mesh filter (Tissue Genesis Incorporated, Honolulu HA) and collected into DMEM containing endothelial cell growth supplement, 2mM L-glutamine, 10% fetal bovine serum, and 5mM Hepes buffer. Samples were kept at RT prior to bioprinting.

*SVF Cell-laden Collagen, Fibrin Spheroid Fabrication*

Freshly isolated SVF was suspended in unpolymerized rat tail collagen I (Millipore, Temecula, CA) mixed with 1X Dulbecco's modified Eagle's medium (DMEM) (Sigma Aldrich, St. Louis, MO) titered to a final pH of 7.4 utilizing 4N NaOH to create a 3mg/mL collagen I solution containing 1.6 x $10^6$ SVF cells/mL. The mixture was kept at 4°C prior to printing. The SVF-collagen I solution was transferred to a 3mL printing syringe (EFD, Nordson, Westlake, OH) and loaded into a time/pressure-based 3D Bioprinter (Biological Architecture Tool (BAT) nScrypt, Inc., Orlando, FL) where the mixture was continually cooled to 4°C using a refrigerant copper coil system encompassing printing syringes. The initial printing conditions were based on our previously published data for continuous cylinder printing[81,211-213]. SVF in bovine fibrinogen (10mg/mL) (Sigma Aldrich, St. Louis, MO) dissolved in 50% normal saline and 50% rat complete media and was printed using similar extrusion parameters as collagen I. Post printing, spheroids were incubated in a tissue culture incubator (37°C, 5% $CO_2$) for 10 min to allow hydrogel polymerization.

*Spheroid Culture Methods*

Spheroids were incubated in rat complete media composed of DMEM, 10% FBS, 5mM HEPES buffer, 2mM L-glutamine, endothelial growth supplement containing heparin, penicillin (45U/mL) and streptomycin (45μg/mL) in a spinner flask (125-mL MagnaFlex, Microcarrier Spinner Flask; Wheaton Industries, Millville, NJ). The spinner flask was placed onto a magnetic stirrer platform (MCS 104-L Biological Stirrer, Techne, Inc., Burlington, NJ) set to 40rpm over the entire culture period (14 days). For fibrin spheroids and spheroid contraction studies, individual spheroids were plated in separate wells of a 96-well ultra-low attachment plate (Corning, Corning, NY).

*Spheroid Size Measurements*

Images of spheroids were obtained through light microscopy using a 4X objective attached to an Olympus CKX41 light microscope (Olympus, Tokyo, Japan). Diameters were measured using ImageJ Software.

*Live/dead Assay*

SVF embedded in 3D collagen I spheroids were assessed for viability using the Live/Dead Viability/Toxicity Kit (Life Technologies, Inc., Carlsbad, CA). Briefly, spheroids were washed with PBS, incubated in 10μM calcein AM (live) and 10μM ethidium homodimer-1 (dead) at RT for 45 min. Samples were washed again and imaged using an Olympus IX71 epifluorescent microscope (Olympus, Tokyo, Japan). In order to quantify live and dead cells, standard curves were created using unembedded SVF cells at known amounts and counting live dead ratios with a NucleoCounter (ChemoMetec, Allerod, Denmark) for non-fluorescence, and a Cytation 5 Imaging Multi-Mode Reader (BioTek, Winooski, VT) for fluorescence. Utilizing the standard curve, cell viability in 3D spheroids was measured on days 0, 2, 6, 9, and 13. Distribution of cells within the spheroid was assessed via Hoechst 33258 bis-benzimide nuclear staining (Anaspec, CA) following 15min permeabilization with 0.1% Triton X-100 (Sigam Aldrich, St. Louis, MO).

*Confocal Microscopy*

For *in vitro* assessment of embedded SVF differentiation into microvessel structures, a MPE FluoView1000 confocal microscope was used along with a 10X water immersion objective to capture the entire spheroid in 1 frame (Olympus, Tokyo, Japan). Confocal image z-stacks were reconstructed into a 3D image using AMIRA 3D

visualization software (Thermo, Waltham, MA). Briefly, Spheroids at 11 days were fixed with 4% paraformaldehyde for 10min at RT, then permeabilized with 0.1% Triton X-100 (Sigma Aldrich, St. Louis, MO) for 15 min at RT. Following permeabilzation, spheroids were stained with Griffonia Simplicifolia-1 Isolectin 4 conjugated to FITC (GS1; Vector Laboratories, Burlingame, CA) at a dilution of 1:500. Additionally, mouse monoclonal α-smooth muscle actin primary antibody was added at 1:250 (Santa Cruz Biotechnology, Dallas, TX). Spheroids were incubated overnight at 4°C. The following day, spheroids were washed 3X in PBS, and incubated with RedDot nuclear stain (Biotium, Fremont, CA) and goat anti-mouse IgG Alexa Fluor 594 secondary antibody (Thermo Fisher, Waltham, MA) at 1:200 and 1:1000 dilutions respectively for 2hr at RT. Endothelial cells stained green and were positive with GS1-FITC, and αSMA containing cells stained red. All cell nuclei stained with RedDot were artificially colored blue.

*Statistical Analysis*

One-way ANOVA with Dunnett's multiple comparison was used to determine statistical significance between mean spheroid diameters calculated at day 2 and all other acquired time points. Graphs were created using GraphPad Prism v.7 software (GraphPad Software, Inc., La Jolla, CA).

## Results

*3D Biporinting Parameters*

The BAT was capable of both time and pressure regulated extrusion of all biomaterials including Pluronic® F-127, collagen I, and fibrinogen at various concentrations and viscosities relying on multiple pen extrusion tips. Contact angles of spheroids and superhydrophobic surfaces were recorded at 155° for water, and 156° for unpolymerized collagen I containing SVF (data not shown). Extrusion parameters were selected in order to produce spheroids of consistent size and shape at a rate of 10.3 spheroids/min. Specific parameters adjusted included syringe volume (3cc), syringe pressure (5 psi), pressure duration (100ms), and needle gauge (18G blunt) (**Table 1**). While multiple parameters were tested, higher pressures as well as larger needle gauges afforded more consistent results and were thusly selected. In order to maintain spheroid volumes at roughly 25μL, pressure duration was kept low (100ms). Syringe volumes were selected to accommodate batch volumes of > 100 spheroids per print. Collagen concentrations as well as fibrinogen concentrations were selected based off of previously published data demonstrating robust angiogenesis by microvessel fragments or SVF cells within these 3D culture systems.

*Spheroid Bioprinting*

In order to produce discreet spheroids of uniform size, it was necessary to extrude collagen I prior to its polymerization while still in liquid format. However, if extruded on normal untreated polystyrene, cohesive effects would not allow the maintenance of spheroid architectures and would flatten and spread prior to polymerization. Thus, it was imperative to design superhydrophobic surfaces to allow consistent spheroid production.

To immobilize spheroids when bioprinted onto superhydrophobic surfaces, hydrophilic spots were printed using Pluronic® F-127 (**Figure 15**). Pluronic was chosen due to its amphiphilic properties as well as phase change properties that would allow precise flat cylinders to immobilize collagen spheroids, and also, post collagen polymerization, for spheroids to be easily released by simple temperature decrease to 10°C. Spheroid position was retained post printing during motorized stage movements (X-Y axes) as well as during transfer of plates to a tissue culture incubator. Spheroids were easily removed upon pluronic phase change and maintained size and shape over these processes. Entire production time was roughly 30-35min before spheroid usage; equating to roughly 5 min per 48 spheroids produced, 20 min instrument preparation time, and 10 min of polymerization time post print.

*Spheroid Morphology and Cell Viability*

Using volumes of 2mL, approximately 100-150 spheroids were produced containing SVF at $4x10^5$ cells/250μL, or roughly $4x10^4$ cells/spheroid. Spheroids had a mean diameter of 3.54mm immediately post print with a standard deviation of 0.195mm. Cell viability of SVF embedded in spheroids in spinner culture, was assessed at 2 days and 6 days post print (**Figure 16**). Cells were distributed evenly throughout the entire hydrogel (**Figure 16a**) immediately post print and throughout the culture period. In addition, the majority of the cells remained viable as measured at 2 and 6 days in culture with some cells undergoing apoptosis as seen by positive ethidium homodimer staining. Polymerization times were sufficient to retain heterogeneity in cell distribution without notice of dense cell settling in specific locations of spheroids. Interestingly, at 6 days post culture, retained microvessels within collagen I demonstrated angiogenic events such as sprouting,

morphological characteristics seen by calcein AM live stains (**Figure 16f**). Angiogenic events were noticeable at earlier time points in 10mg/mL fibrin spheroids at day 4 by phase contrast microscopy (**Figure 17**).

SVF viability was quantified at days 0, 2, 6, 9, and 13 (**Figure 18**). Immediately post print, 68.24% ± 3.59% of cells were viable, 5.96% lower than non-printed, pipetted controls, and 27.8% lower than initial media-suspended cell counts via NucleoCounter, suggesting that collagen I and its pH change may alter cell viability post encapsulation, however, pressures afforded due to extrusion printing do not significantly affect cell viability during spheroid production (**Figure 19**).

Over 14 days in culture, collagen and fibrin spheroids undergo contraction with a concomitant decrease in diameter (**Figure 18, 20**). However, contraction rates are not uniform during the 14-day culture period. Specifically, from days 2 to 3, collagen spheroids decreased on average 0.0083 ± 0.0875mm/day all the way to 0.3675 ± 0.1359mm/day from days 6 to 7. However, contraction rates reduced from days 9 to 13 (0.042 ± 0.0463mm) suggesting that cells are possibly remodeling or digesting the matrix as they migrate and proliferate at the highest rates around 7 days in spinner culture. Average spheroid diameters were significantly different between days 2 and each subsequent day in spinner culture ($p < 0.0001$) (**Figure 20**).

As spheroids contract, light microscopy is not sufficient to analyze embedded cellular morphology due to the extreme density of cells and collagen I, not affording sufficient light passage. As such, we analyzed cellular morphology looking specifically for microvessel formation and *in vitro* maturation via confocal microscopy of spheroids at day 14 to render a z-stack 3D image. To analyze neovascularization morphology,

endothelial cells were stained with GS1-FITC, and α-smooth muscle actin positive (perivascular support cells/mural cells) were stained with an Alexa Fluor 594 conjugated primary antibody against cytosolic αSMA (**Figure 21**). Endothelial cells form networks mimicking endogenous microvasculature with areas of αSMA positive cells surrounding endothelial tubes. However, in 3mg/mL collagen I spheroids, microvessel density is less than that in 10mg/mL fibrin spheroids. These data are similar to our previously published data with SVF in 3D collagen I and 3D fibrin *in vitro*.

| *Printing Parameter* | *Selected Value* | *Range Evaluated* |
|---|---|---|
| [a]Syringe pressure | 5 psi | 3-6 psi |
| [b]Pressure duration | 100 ms | 100-300 ms |
| [c]BAT cartridge size | 3 cc | 3 cc |
| [d]Needle gauge | 18 G, blunt | 18-25 G, blunt |
| [e]Collagen I concentration | 3 mg/mL | 3 mg/mL |

***Table 1****: Conditions to Print 3D Spheroids Using the Bioassembly Tool Bioprinter.* *[a]Pressure effects were evaluated during 100ms of duration.* *[b]Time of pressure extrusion was evaluated at a constant 5 psi.* *[c]The nScrypt Bioassembly Tool utilizes EFD cartridges in a precision fluid dispensing system (Nordson Corporation, Westlake, OH).* *[d]Nordson EFD extrusion tops.* *[e]Rat tail-derived collagen I.*

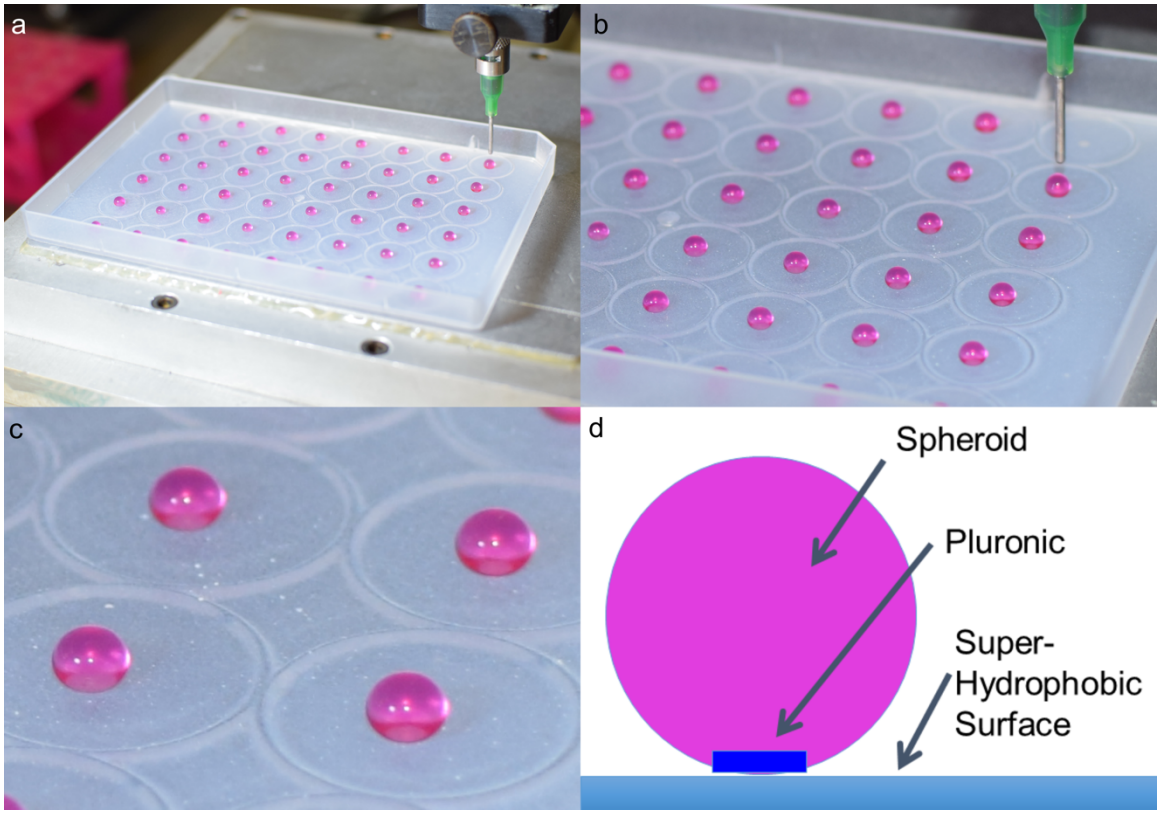


***Figure 15***: *Photographs of SVF-laden 3mg/mL collagen spheroids immediately post bioprinting (a-c). Diagram demonstrating biphilic surface properties allowing for spheroid formation of aqueous substances using hydrophobic coatings and hydrophilic immobilization spots (Pluronic® F-127) (d).*

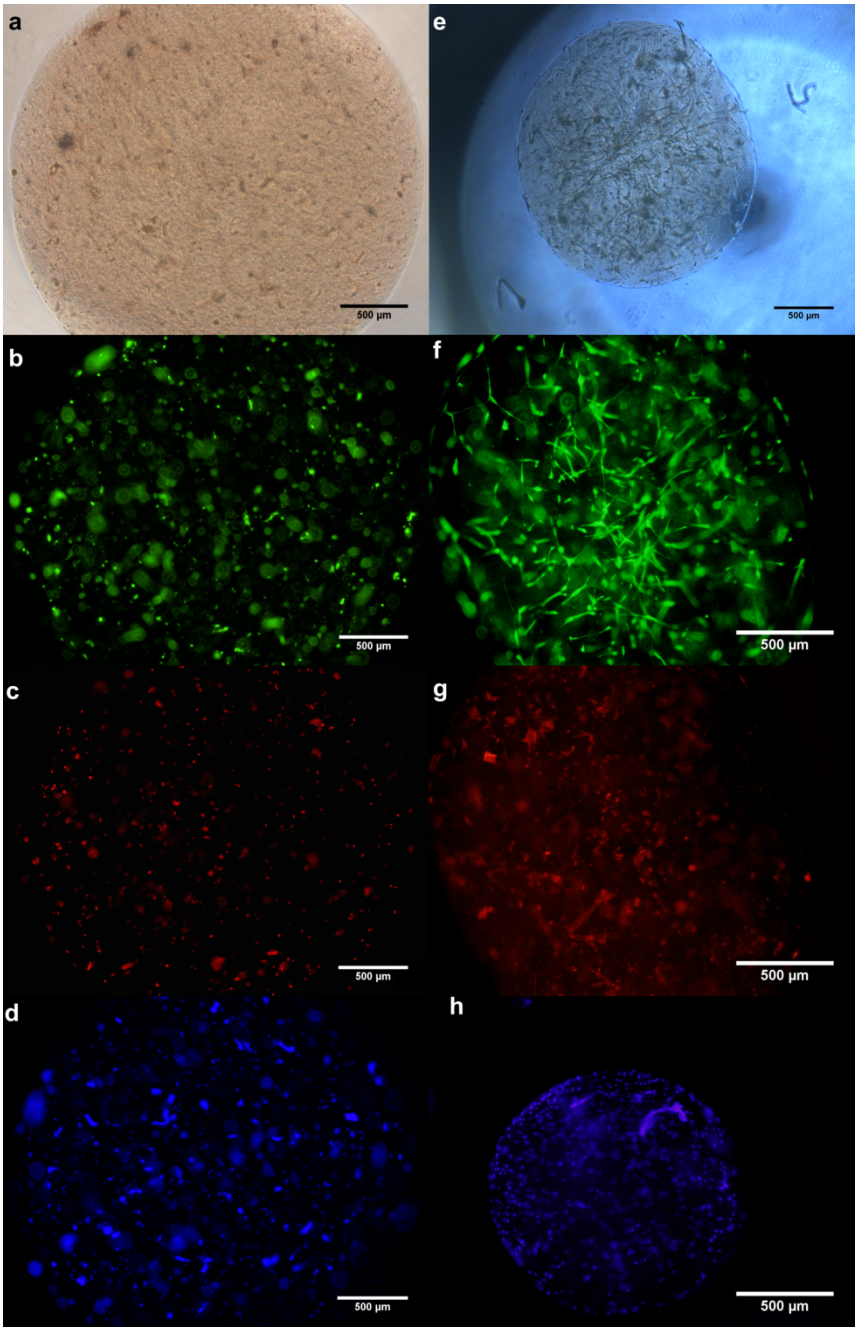


***Figure 16**: SVF encapsulated in 3mg/mL collagen I spheroids, Live/Dead Analysis. Phase contrast microscopy of SVF laden collagen I spheroids at day 2 (a) and day 6 (e). Calcein AM live stain at day 2 (b) and day 6 (f). Ethidium homodimer-1 dead cell stain at day 2 (c) and day 6 (g). Hoeschst 33258 bis-benzimide nuclear stain at day 2 (d) and day 6 (h).*

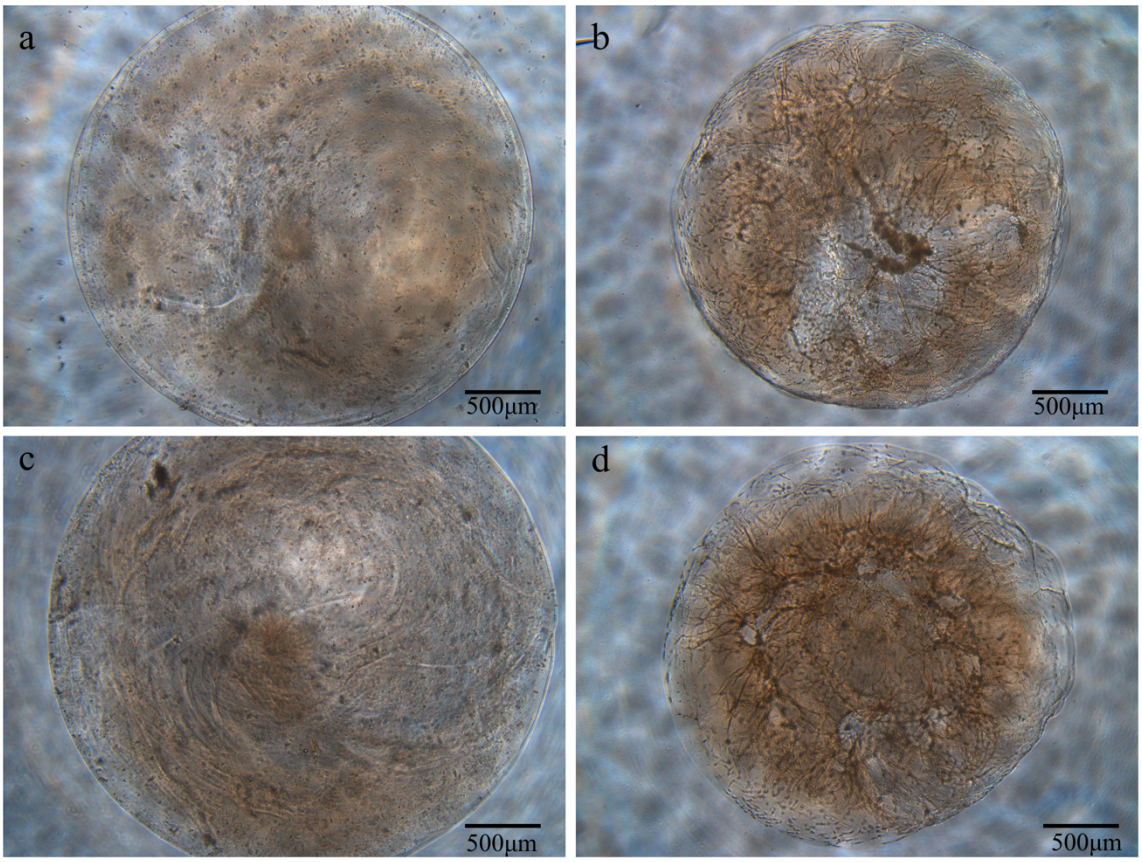


***Figure 17**: SVF-laden 10mg/mL fibrin spheroids at day 1 (a, c) and day 4 (b, d) in culture. Microvascular network phenotypes are present in day 4 culture spheroids. Similar morphologic events do not occur in collagen I until day 6 with SVF-derived microvessel fragments present.*

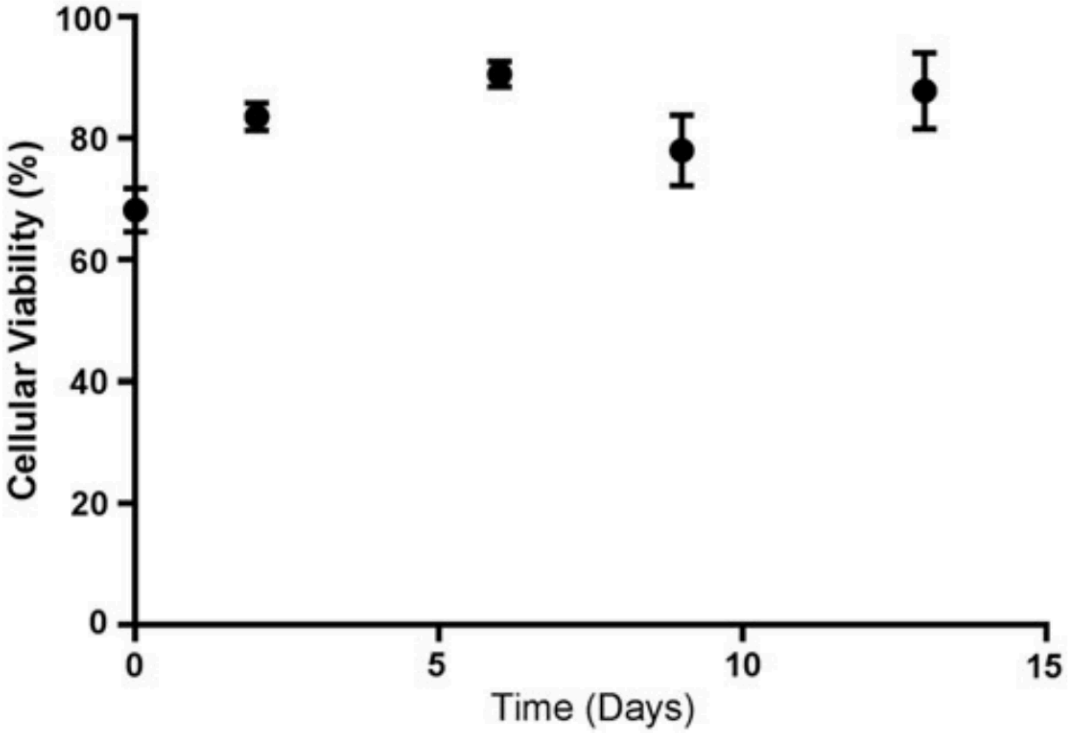


***Figure 18***: *SVF viability in 3mg/mL collagen I spheroids at days 0, 2, 6, 9, and 13. There is no significant change in viability over the 2-week culture period of embedded cells. There is a trend towards increased viability over time.*

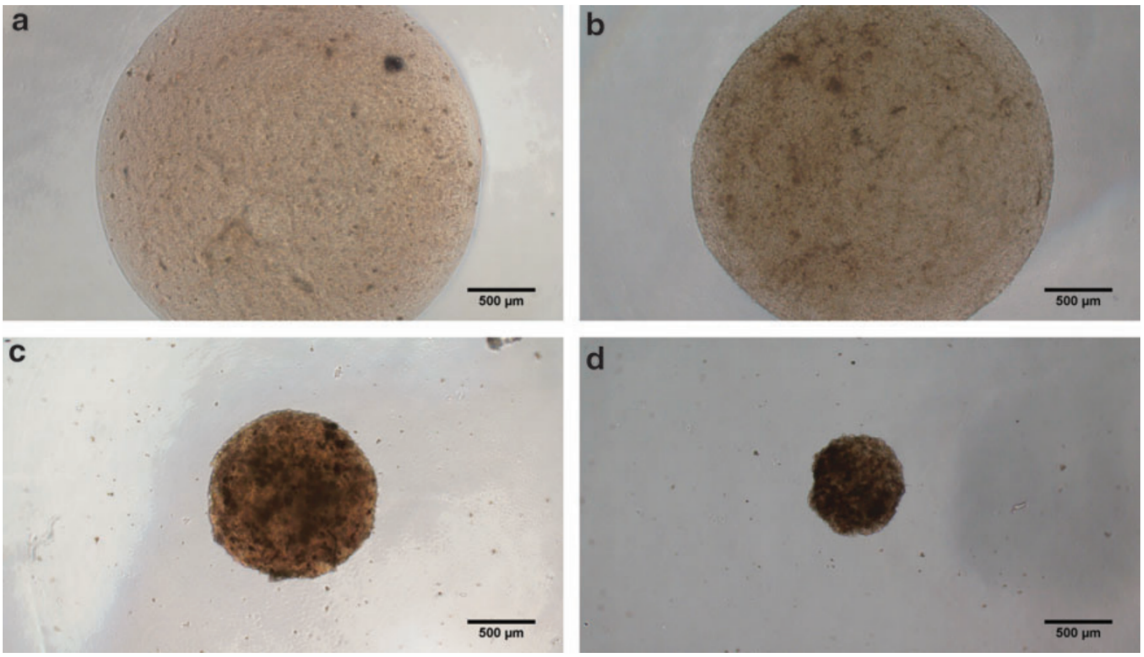


***Figure 19***: *3mg/mL Collagen I spheroids containing SVF undergoing contraction on days 2 (a), 6 (b), 9 (c), and 13 (d) in spinner culture. There is significant remodeling of collagen by SVF cells which causes spheroids to contract, increase in density, and decrease in diameter.*

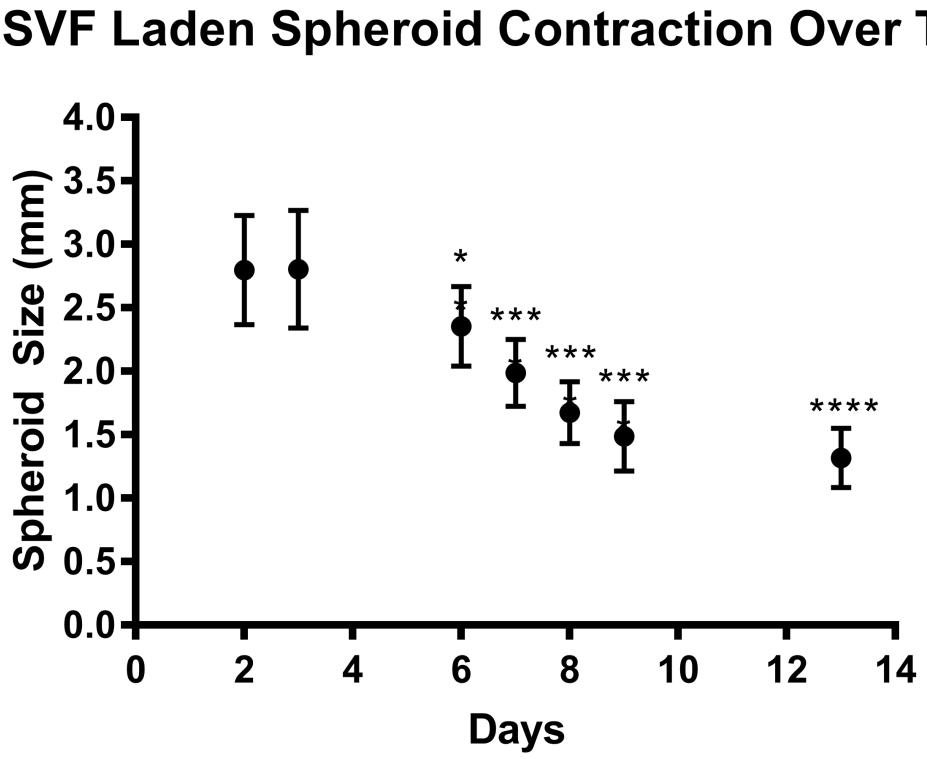


***Figure 20***: *3mg/mL collagen I spheroids containing SVF decrease in diameter significantly between days 2 and all other subsequent days in spinner culture. (n = 12, * p < 0.05, *** p < 0.001, **** p< 0.0001).*

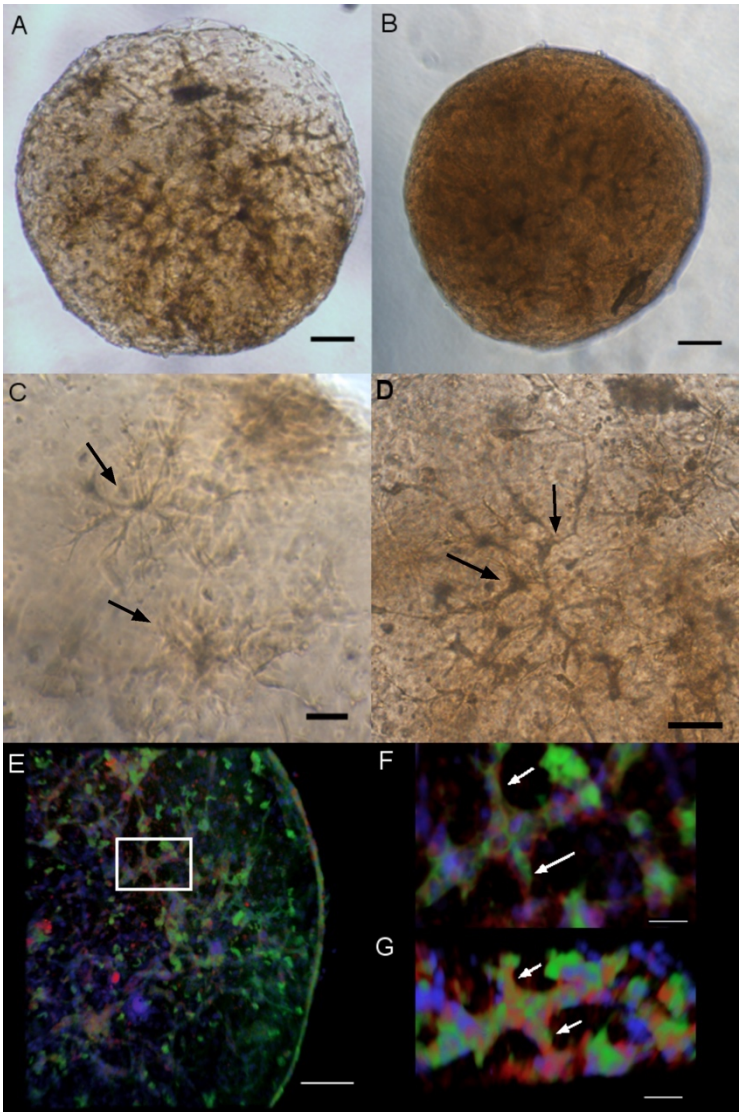


***Figure 21**: SVF containing microvessel fragments undergoes angiogenesis when embedded and cultured over 14 days in bioprinted 3mg/mL collagen I spheroids. Phase contract microscopy following 11 days in culture (A) scale bar = 100μm. Phase contrast image demonstrating increased density and contraction of the same spheroid at 12 days in culture (B) scale bar = 100μm. Phase contrast image demonstrating angiogenic sprouting as indicated by arrows in 8 days culture (C) and 11 days culture (D) scale bar = 50μm. Confocal z-stack image demonstrating microvessel structures within collagen I spheroids are made up of endothelial cells (GS1-FITC$^{+}$, green) and αSMA containing cells (αSMA-Alexa Fluor 594$^{+}$, red) and have branching morphology (arrows) after 14 days in culture (E, F, G) scale bar = 100μm (E), scale bar = 50μm (F, G).*

**Discussion**

Many clinical trials are currently studying the use of stem and other regenerative cells for delivery to pathological tissues with the hopes of therapeutic tissue remodeling through exogenous cell proliferation and/or release of paracrine factors stimulating endogenous cell proliferation and/or function. While therapies have seen functional benefits such as increases in ejection fraction for example, many have demonstrated limited cell retention at sites of implantation rendering unremarkable therapeutic effect[20-22]. As such, additional methods for discrete *in vitro* tissue formation have been studied, whereby cells are cultured to promote self-aggregation, or hydrogels are utilized to create 3D systems that can provide a stimulating microenvironment for embedded cells in order to mature into tissue units[88,214]. Most 3D systems utilize a mixture of cells with a scaffold or substrate that provides sites for cell adhesion and migration, as well as three-dimensionality, more closely mimicking endogenous tissue histological layouts. Our lab and others have studied extensively the creation of tissue engineered microvessels utilizing adipose-derived SVF cell populations embedded in 3D collagen I and fibrin[67,95,215].

To create dosable, discrete, viable, tissue units with limited handling and manipulation, however, it was imperative to develop a new model of production. Previously we were able to bioprint SVF in materials such as alginate into a spheroid format utilizing direct-write 3D bioprinting and automation through CAD/CAM systems[209,212]. Unfortunately, while SVF cells remained viable in alginate, they did not undergo typical morphogenic alteration forming microvessels through vasculogenesis and angiogenesis as seen in our other culture systems utilizing collagen I and fibrin.

Most *in vitro* tissue engineering utilizing collagen I and similar ECMs require crosslinking of liquid collagen to form gel collagen which occurs after pH change in a mold such as a tissue culture plate. This however introduces problems when trying to remove 3D constructs from plates for *in vivo* implantations. Handling inevitably produces variations and damage to 3D ECM during the removal process due to high adherence between ECM and polystyrene. As such, we found it necessary to reassess bioprinting spheroids onto superhydrophobic surfaces which would mitigate adhesion problems, as well as allow for rapid production of spheroid architectures through automated methods.

Initial printing on non-treated, polystyrene tissue culture plates of both collagen I and fibrin resulted in flattening of SVF/hydrogel solutions prior to their polymerization, creating non-implantable 3D tissue sheets. Additionally, after superhydrophobic coating and during subsequent extrusion based bioprinting, liquid droplets of collagen I containing SVF would not release from pen tips onto the superhydrophobic surface. To overcome this lack of adherence, a disk of Pluronic® F-127, a triblock co-polymer with amphiphilic moieties was printed onto the superhydrophobic surface which allowed for collagen I liquid droplet removal post extrusion from the pen tip, as well as spheroid architecture to form due to pluronic disk diameters of 500μm or less.

Extrusion based bioprinting using our afformentioned parameters allowed tailoring of spheroid sizes and volumes based on applied syringe pressures. Spheroids could be produced ranging in size from 1mm to 3.5mm in order to prevent core necrosis due to lack of nutrient diffusion. SVF cells embedded in fibrin as well as SVF cells + SVF-derived microvessel fragements embedded in collagen I all underwent angiogenesis over the culture period of 14 days without noticeable necrotic cores or increased apoptosis. Fibrin

spheroids would demonstrate microvessel morphologies faster in culture than collagen I spheroids. These events can be described as phenotypic orientation of endothelial cells as well as perivascular cells into branching structures. However, in order to assess microvessel function, further studies are needed after spheroid implantation *in vivo* to analyze if microvessel-spheroid-tissue units innosculate with host vasculature and provide blood flow to areas of interest.

Automation through direct-write computer-assisted design and manufacture allows the opportunity to create discrete spheroids containing cells in a very precise and controlled manner with high throughput, and tailor ability relevant to a clinical point-of-care setting. Creating spheroid architectures allows cells to grow in 3D culture without adhering to plates and receive nutrients without undergoing apoptosis. In addition, known spheroids can be dosed with specific amounts of cells and spheroids themselves can be delivered to pathological tissues via large gauge syringes in known quantities. With regards to our studies with SVF, cells embedded within collagen I spheroids or fibrin spheroids still undergo angiogenesis and may be a way to deliver discrete microvascularized tissue units to patients in the future.

**The Creation of Blood Vessel Mimics Utilizing Electrospinning and Cell Sodding Technologies.**

## Introduction

Atherosclerosis is a primary cause of acute myocardial infarction in which coronary artery lumenal occlusion and cessation of blood flow occurs due to build-up of plaques in vessel walls. Commonly, patients undergo either percutaneous angioplasty or surgical bypass to reestablish blood flow to injured myocardium. Surgical bypass grafts are usually harvested from the saphenous vein or from the internal mammary artery. However, in patients with comorbidities or patients undergoing multiple bypasses, available endogenous conduit vessels may be limited. As such, many have researched the production of artificial blood vessel mimics (BVMs) through multiple technologies as potential options for surgical bypass vessels[79,216-220].

Already of clinical utilization are materials such as dacron or expanded polytetrafluoroethylene (ePTFE), also known as Gore-Tex® for large vessel bypasses. These materials are successful for large vessels but unsuccessful for small diameter vessels (< 6 mm) due to their high rate of thrombogenicity at small diameters and limited endothelialization past a distance of 2 cm distally from native vessel anastomosis[221]. Reported patency rates are only 40% post six months surgery and 25% post 3 years[222]. Additionally, these materials are non-degradable and allow for limited cellular ingrowth. As such, there is a need for new techniques to tissue engineer biodegradable vessels that can provide mechanical stability, tissue morphology including ECM mimicry, and appropriate porosity for cellular integration.

Electrospinning is a process in which fibers ranging in sizes from 50 to 500 nm are produced via Taylor cone jetting across a high voltage potential[223]. Specifically, a voltage is applied to a liquefied, viscoelastic, polymer solution changing its charge, providing movement to a grounded object such as a collection mandrel when the charge force overcomes the solution's surface tension. The liquefied polymer, as it moves through the air in a whipping fashion, evaporates the solvent and fibers are left for deposition onto a collection surface producing a randomly-oriented fibrous mat or tube. Fiber morphology can be changed by altering electrospinning parameters such as solution viscosity, electrical conductivity, polymer molecular weight, flow rate of solution, spinning distance, applied voltage, and humidity and temperature[224]. Altering parameters allows high variation in electrospun products for the production of micro-scale textures and pores resembling endogenous ECM, allowing cellular infiltration either *in vivo* or *in vitro*[225].

Common polymers used in electrospinning include polycaprolactone (PCL), poly (L-lactide-co-ε-caprolactone) (PLCL), poly-lactic acid (PLA), polyurethane (PU), L-lactide-co-trimethylene carb, and polypropylene[21,226-233]. Many publications describe PCL based-blood vessels that demonstrate good mechanical properties such as longitudinal stress and strain to rupture requiring high pressures, as well as strong suture strength and burst pressure[226]. In addition, electropsun PCL can be tailored to a wide variety of fiber thickness which may play an additional role in cellular migration and adherence. From a clinically translatable standpoint, PCL demonstrates biodegradability over a period of 6 months *in vivo* and is already FDA approved for the use in medical devices[234]. In addition, PCL can be mixed and electrospun with ECM proteins such as collagen or fibrinogen that can allow for additional adhesion ligands for cells post implantation[76,223,235]. Currently,

electrospun PCL has been utilized as artificial bone graft scaffolding for bony reconstruction, conduits for bioengineered arteries and veins, as well as neuronal guides during nerve approximation allowing axonal growth and guidance[236-238]. As such, we decided to focus on the use of PCL polymer to create our blood vessel mimics for *in vitro* studies.

Of the critical requirements for cellularization of biomaterials, porosity, specifically size and 3D architecture of individual pores within a biomaterial plays a key role to enhance or decrease cellular infiltration both post implantation or through *in vitro* methods such as pressure sodding with cells[239-241]. With regards to electrospun scaffolds, many evaluate and report in terms of bulk porosity meaning the total volume of porous space within the scaffold. However, while those measurements are important, at the cellular level, it is believed that individual pore sizes are the most immediate determinant of cellular migration, adherence, and infiltration.

Pore sizes are primarily measured through image processing methods in which electrospun scaffolds are imaged in 2D using multiple microscopy techniques, and from those images pore sizes are extrapolated[242-245]. This introduces some difficulty however because of the high irregularity in random pore shapes and sizes as well as the inability to approximate overlapping fibers in 3D space utilizing only 2D images. Indeed, multiple layers of highly randomized fibers are produced during electrospinning and one construct may be significantly different than another construct if just one spinning parameter is changed. Alternate imaging modalities create 3D image data via confocal microscopy or micro CT imaging which are arguably more accurate than 2D image analysis, however, require longer process times and expensive equipment[239,240,244,246-249].

The final method to calculate pore size is through mercury porosimetry in which total volume measurement is produced, yet, pore sizes can be calculated using the Washburn equation[242,250-253]. Specifically, one has to make the assumption that the material being analyzed is in a format resembling bundles of cylindrical tubes, which as mentioned prior is not an appropriate representation of electrospun scaffolds. In addition, since porosimetry is a measure of pressure of fluids going through a given material, while pore size can be calculated, it is only represented as the narrowest points within a given pore.

Herein, we describe the creation of blood vessel mimics using PCL or PCL-collagen I mixtures which can have resistance built in modelling the venturi bypass graft from arterial to venous intraluminal pressures[254,255]. In addition, we demonstrate a novel method for image analysis to gather pore size data for electrospun scaffolds utilizing widely available ImageJ software and built in functions. We evaluated BVMs with varying pore sizes to analyze SVF cellular infiltration in conduits exposed to physiological flow rates and pressures in an *in vitro* bioreactor over a period of two weeks. In addition, non-cellularized, PCL electrospun material was implanted within epididymal adipose tissue *in vivo* to analyze cellular infiltration within pore sizes ranging from 1 μm to 8 μm. *In vitro* BVMs demonstrated similar SVF cell retention at low pore sizes (1 μm, 2 μm, 5 μm) but not high pore sizes (8+ μm). *In vivo*, electrospun material demonstrates insignificant differences in cellular infiltration in materials of ranging pore sizes at an epididymal implant location.

## Materials and Methods

*Electrospinning*

PCL was dissolved using a 5:1 v/v chloroform: methanol solvent mixture at 8%, 13%, and 18% as a weight/volume percentage. In order to achieve smaller pore sizes, 4% PCL was dissolved in hexafluoro-2-isopropanol. Dissolution was carried out in 20 mL glass scintillation vials on an orbital shaker overnight. Dissolved PCL was then loaded into a syringe with a pump and electrospun according to the following parameters:

| *Solvent* | *Hexafluoro-2-isopropanol* | *5:1 Chloroform:Methanol* |
|---|---|---|
| *Flowrate* | 4 mL/hr | 8 mL/hr |
| *Slide Speed* | 4 | 4 |
| *Rotor Speed* | 400 rpm | 400 rpm |
| *Voltage* | 22.5 kV | 25 kV |
| *Collector Distance* | 25 cm | 25 cm |
| *Mandrel Size* | 10 mm, 4 mm | 10 mm, 4 mm |
| *Needle type* | 3.8 cm 18G blunt tip | 3.8 cm in 18G blunt tip |

In order to produce electrospun scaffolds of a more biologically active composition, we chose to electrospin 3:1 v/v PCL:Collagen I at equivalent pore sizes to the PCL only counterparts. Briefly, PCL and collagen were dissolved individually into HFP at 4%, 10%, and 13% as a weight/volume percentage. The 18% solution was attempted but unable to form stable Taylor Cone and thus unable to be electrospun. Dissolution was carried out in 20 mL glass scintillation vials on an orbital shaker overnight. The next day, PCL and

Collagen I solutions of the same concentration were mixed together in a 3:1 PCL:Collagen I ratio volume:volume. The mixture was vortexed for 1 minute and allowed to de-bubble by gently mixing for at least 1 hour on the orbital shaker before being loaded into a syringe with a pump and electrospun according to the following parameters:

| *Solvent* | *Hexafluoro-2-isopropanol* |
|---|---|
| *Flowrate* | 4 mL/hr |
| *Slide Speed* | 4 |
| *Rotor Speed* | 400 rpm |
| *Voltage* | 22.5 kV (4%), 25 kV (10%), 27.5-30 kV (13%) |
| *Collector Distance* | 25 cm |
| *Mandrel Size* | 10 mm |
| *Needle type* | 3.8 cm 18G blunt tip |

All electrospun scaffolds were measured such that dispensing volumes of PCL or PCL/Col created scaffolds of 500 μm thickness. After electrospinning, scaffolds were dried in a desiccator for at least 12 hours and stored as needed in the desiccator.

*Scanning Electron Micrograph Imaging and ImageJ Pore Size Calculation*

Dried scaffold samples were sputter coated with gold and then imaged using a JSM-820 SEM (Jeol). Sample micrographs were opened in ImageJ and then thresholded to exclude everything except for the top layer of fibers on the scaffold as determined by image focus. The thresholded images were processed using ImageJ's analyze function in terms of centroid x/y location in addition to major and minor axis lengths in order to calculate pore sizes. Minor axis lengths shorter than the average fiber width of 10 randomly selected

fibers were added as an exclusion criterion due to threshold pixilation within single fibers (termed "railroading"). This size-based thresholding allowed for the removal of pixels and pixel groups within a fiber that fell below the grayscale threshold and would otherwise have been counted as false positive pores. The size-based threshold needed to be done manually as an automated method determining fiber size would include these pixel groups that would cause single fiber sections to be split into two much thinner fibers, thereby skewing fiber size results and thus pore size results.

*Animals and Ethics Statement*

All animal procedures were conducted in compliance with University of Louisville School of Medicine IACUC-approved protocols and NIH guidelines. Isoflurane gas was administered for anesthesia.

*SVF Isolation from Sprague Dawley Rats*

Rat epididymal fat pads were excised from 6 to 8-month-old Sprague Dawley rats at weights greater than 250g under sterile surgical procedure and isoflurane anesthesia. All procedures were reviewed and approved under the University of Louisville's Institutional Animal Care and Use Committee. Excised fat pads were placed in PBS containing 0.1% bovine serum albumin (Sigma Aldrich, St. Louis, MO) and kept at 4°C for 15 min prior to digestion. Samples were washed with BSA-PBS and minced for 2 min until particulates could pass through a 50mL aspirating pipette. 2mg of Type I Collagenase (Worthington Biochemical Corporation, Lakewood, NJ) was added per mL of fat, aliquoted at 20mL total volume in 50mL conical centrifuge tubes, and rotated in an Envirogenie Incubator (Scientific Industries, Bohemia, NY) at 35 rpm and 37°C for 35 min. Samples were pelleted via centrifugation at 350xg for 4 min at RT. Buoyant adipocytes were aspirated

and discarded, and dense cellular pellets were suspended and washed one time in BSA-PBS. Samples were re-centrifuged for 4 min at 350xg. The SVF pellet was filtered through a 250μm mesh filter (Tissue Genesis Incorporated, Honolulu, HA) and collected into DMEM containing endothelial cell growth supplement, 2mM L-glutamine, 10% fetal bovine serum, and 5mM Hepes buffer. Samples were kept at RT prior to BVM sodding.

*SVF Cell Sodding Electrospun Tubes and Conditions of the Pulsatile Flow Bioreactor*

Electrospun 4 mm diameter tubes were cut to lengths of 10 cm and pre-wet for 30 min in Rat complete media at RT. Luer locks were sewed onto both endings and a 18G 8cm blunt end needle attached to a 10 mL syringe was loaded with 5 mL rat complete media containing 2.512 x $10^6$ rSVF cells. This value was calculated based off of previously published data demonstrating success in patients when BVM grafts were sodded with 2 x $10^5$ cells/$cm^2$ [81]. Pressure sodding without exceeding 5PSI forces the liquid media through the pores of the electrospun material while the cells themselves are trapped and retained within the pores. Cells were pressure sodded in a vertical fashion slowly dispensing the 5mL mixture without exceeding pressures of 1 PSI.

Sodded grafts were immediately sewn into a bioreactor chamber which features a luminal inlet, a luminal outlet, and an extra-luminal outlet for dispersion of air or excess chamber volumes. Sodded electrospun tubes were surrounded by rat complete media that was changed every other day. Tygon tubing connecting a reservoir tank of 500mL of media was used as the solution to pass luminally mimicking blood flow utilizing a flow rate-controlled peristaltic pump (Watson-Marlow, Wilmington, MA). Flow was slowly raised to a final value of 22mL/min by day 5 in culture. These flow rates were calculated to provide shear forces of 52 dynes/$cm^2$ resembling endogenous physiological flow pressures

seen in similar diameter arteries/arterioles *in vivo*. BVMs were cultured for 14 days prior to explant for further analysis.

*Electrospun Mat Implants in Rat Epididymal Fat*

From the 10 mm mandrel PCL electrospun tubes, 6mm flat disks were cut and sterilized via ethylene dioxide gas for implantation. 6-month-old male Sprague dawley rats were anesthetized using isofluorane at 5%wt/vol. A midline incision was made, and PCL disks were implanted into the epididymal fat pads held in place with 5-0 prolene. Incisions were approximated and closed, and animals were allowed to recover for 30 days. Animals were anesthestized and sacrificed upon explant where the tissue was removed, formalin fixed overnight and prepared for paraffin blocking, hematoxylin and eosin staining, and GS1 immunohistochemistry (n = 8 animals).

*Histology and Immunohistochemistry*

Following 14 days of bioreactor conditioning, as well as following 30 days of PCL disk implants, tissue samples were blocked in paraffin after 3% formalin fixation and sectioned in 6 μm slices. Hematoxylin and eosin (H&E) were used to examine basic histological tissue structure and cellular infiltration. Immunoperoxidase staining using antibodies against Griffonia simplicifolia 1 determined presence of endothelial cells in *in vivo* explants. Explanted samples were characterized on an objective scale of 1 to 5 via blinded methods to analyze presence of inflammatory cells within the biomaterial (inflammation), the presence and formation of a fibrous capsule surrounding the biomaterial, vessel presence at the interface of biomaterial and host tissue, patent microvessel infiltration into the biomaterial, parenchymal and stromal cell incorporation, fibrosis (granulomatous tissue formation), and necrosis.

*Statistical Analysis*

Calculated pore sizes were averaged and plotted using GraphPad Prism v.7 Software (GraphPad Prism, Inc., La Jolla, CA) and analyzed for statistical significance between groups using ordinary one-way ANOVA and Tukey's multiple comparisons test. Statistical analysis of implants of PCL and ePTFE were compared using two-way ANOVA with multiple comparisons.

## Results

*Creating an Electrospun BVM With Built-in Resistance*

Electrospun PCL tubes were created in the shape of the venturi possus bypass graft, using an 'hour glass shaped' mandrel, forming a built-in resistor such that when exposed to lumenal flow, pressure is lowered as fluid travels proximally to distally and out the venous outflow side. Material deposited evenly on the mandrel with a total wall thickness of 500 μm, and variation in diameter starting with inflow at 4 mm, resistor in the middle at 1mm, and outflow at 4 mm (**Figure 22**). Intraluminal pressures of un-sodded grafts were measured using a mockflow loop and flow meters attached at the inlet side or outlet side. A range of pressures were recorded as flow rates were varied such that at the highest flow rate of 72 mL/min, 60 mmHg pressure on inlet (arterial) side and 20 mmHg on outlet (venous) side were noted (**Figure 23**).

*Creating Electrospun BVMs with Varying Pore Sizes*

Variations in spinning parameters allowed for the creation of 4 different porosities utilizing PCL as the electrospun material. Specifically, when using chloroform and methanol as the solvents, with a flowrate of 8mL/hr and 25kV, mixing PCL to create 8% weight/volume gave an average luminal pore size of 1.9 μm, 13% gave an average luminal pore size of 2.9μm, and 18% gave an average luminal pore size of 5.1μm. Changing the solvent to hexafluoro-2-isopropanol and decreasing the flowrate to 4mL/hr as well as decreasing the voltage to 22.5kV afforded a 4% PCL mixture to create an average luminal pore size of 1.1 μm (**Figure 24**). These measurements were acquired utilizing 2D images captured via SEM (**Figure 25**). Thresholding using 2D SEM images and ImageJ software

allowed the precise measurement of individual pores after identifying railroading patterns (**Figure 26**) and removing false positives (**Figure 27**).

In addition, after testing multiple mixture ratios of PCL and Collagen I, it was possible to reproduce similar pore sizes with 3:1 vol:vol of PCL to bovine collagen I resembling 4%, and 8% PCL only electrospun tubes, i.e. average pore sizes ranging from 1.2 μm to 3.0 μm (**Figure 28**).

*Analyzing Cellular Infilitration Within In vivo Implants of Electrospun PCL*

Four varying porosities of electrospun PCL were implanted within rat epididymal fat tissue, explanted after 30 days, and analyzed on an objective scale of 1-5 for inflammatory response (relative amount of inflammatory cells present in biomaterial), the presence and thickness of a fibrous capsule surrounding the biomaterial, the amount of vascular structures surrounding the biomaterial, the amount of vascular structures penetrating through the biomaterial, overall parenchymal and stromal cellular incorporation into the biomaterial, the presence of fibrosis or granulation tissue within the biomaterial, and the presence of necrosis as compared to ePTFE control. There were no statistically significant differences in inflammation, capsule formation, vascularization at interface, fibrosis, and necrosis between the 4 varying porosities of PCL electrospun implants and the ePTFE control. However, there were statistically significant differences in vascular penetration of the biomaterial between ePTFE and 4% PCL ($p < 0.0001$), between ePTFE and 8% PCL ($p < 0.05$), between ePTFE and 13% PCL ($p < 0.0001$) and between ePTFE and 18% PCL ($p < 0.0001$) (**Figure 29**). A sample of explanted 4% PCL biomaterial and 18% PCL biomaterial are illustrated in **Figure 30** demonstrated peri-

implant vasculature as well as intra-implant penetrating vasculature as highlighted by arrows.

*Analyzing SVF-Sodded Electrospun PCL Tubes Post Two-Week Perfusion in a Bioreactor*

SVF sodded PCL constructs were stained with H&E to analyze cellular retention within the biomaterial at different porosities exposed to physiological flow pressures over a period of two weeks. SVF cells were retained within the pores of 4% PCL, 8% PCL, and 13% PCL immediately post sodding as seen via SEM images (**Figures 31 B, 32 B, 33 B, 34 B**). Post two weeks flow, and under H&E assessment, while all constructs had some cellularity, 18% PCL demonstrated the least amount of nucleated cells retained post bioreactor flow for 2 weeks (**Figure 34 E, F**).

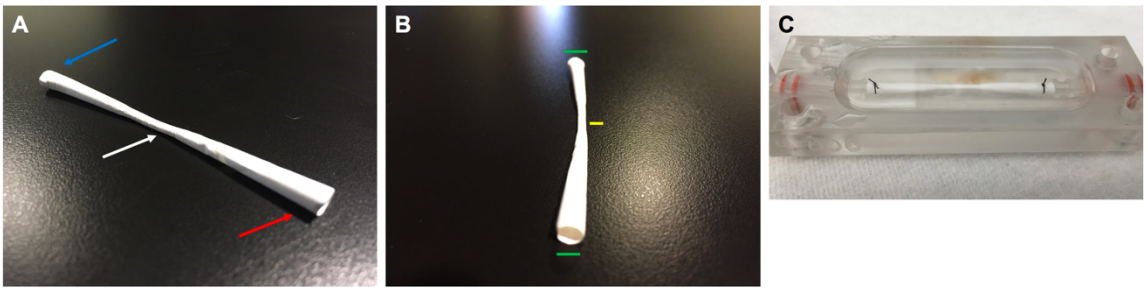


***Figure 22***: *PCL Electrospun Macrovessel Mimic (unsodded). (A) Red arrow: artery anastomotic site, white arrow: Venturi resistor, blue arrow: vein anastomotic site. (B) The electrospun graft has 4mm opening diameters (green lines) tapering down to a 1mm diameter at the Venturi resistor (yellow line). (C) Electrospun macrovessel mounted in a microcirculation chamber.*

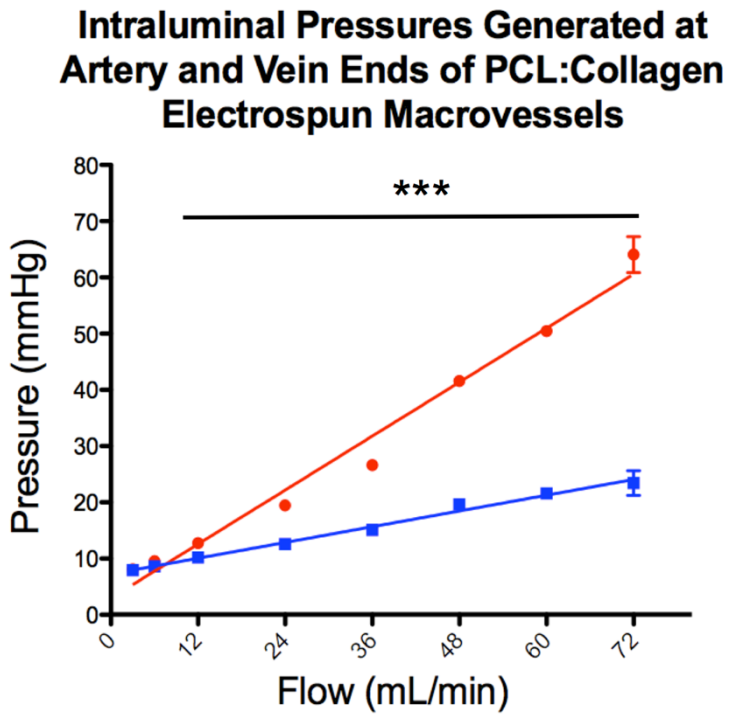


***Figure 23**: Intraluminal Pressures Generated Using a Mock Flow Loop and Microcirculation Chamber Housing PCL Electrospun Macrovessels. Red: Artery end values. Blue: Vein end values. (n = 2, *** $p < 0.001$).*

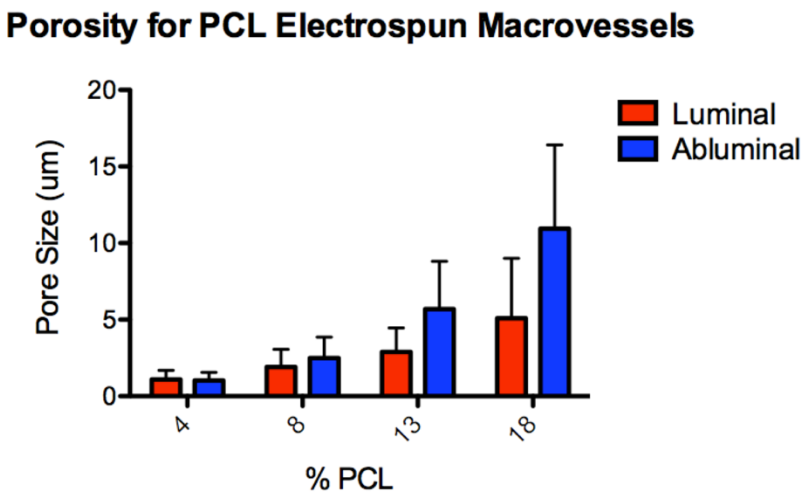


***Figure 24***: *Porosity of 4%, 8%, 13%, and 18% PCL Electrospun Macrovessels as Measured by 2D SEM. Measurements were taken on both the luminal side (red) and abluminal side (blue) of the material.*

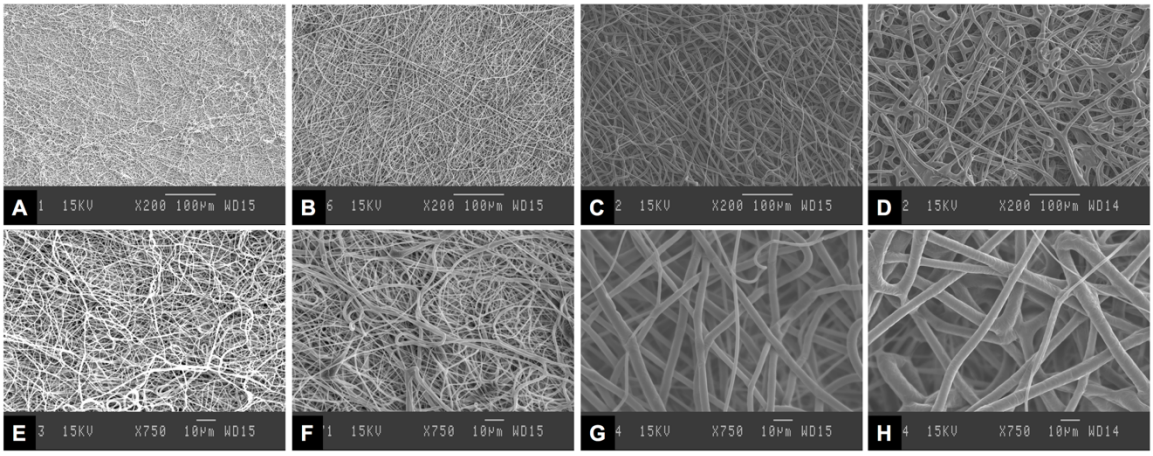


***Figure 25**: Scanning Electron Microscopy Images of PCL Electrospun Macrovessels Demonstating Different Porosities at Different Concentrations of PCL. 4% PCL 200X (A) 750X (E); 8% PCL 200X (B) 750X (F); 13% PCL 200X (C), 750X (G); 18% PCL 200X (D) 750X (H).*

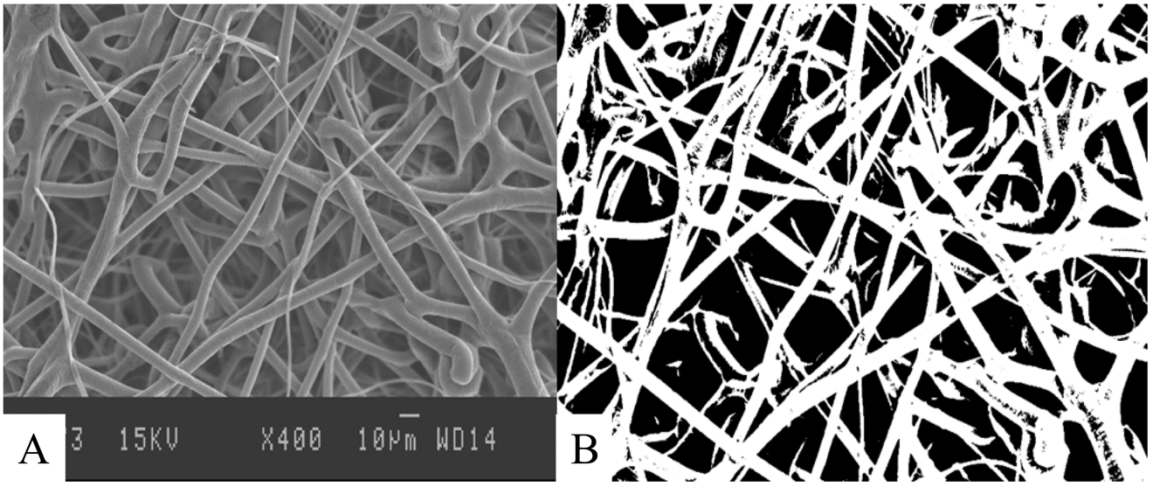


***Figure 26***: *Representative SEM Image and Thresholding Using ImageJ to Calculate Pore Sizes of Electrospun PCL. (A) 18% PCL SEM image 400X. (B) Image thresholded to isolate the top layer of the construct but still demonstrating railroading patterns in individual fibers based on contrast and pixel density.*

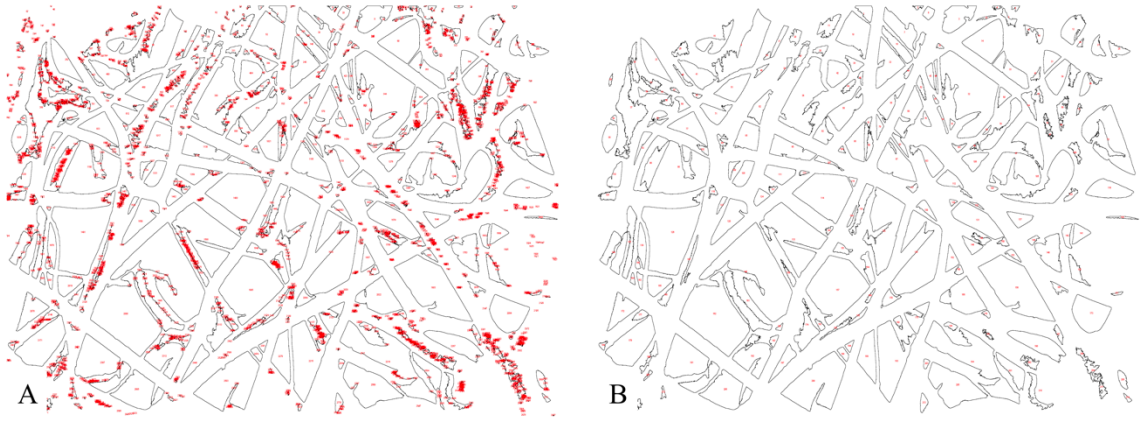


***Figure 27**: Calculated Pore Sizes Using ImageJ of Non-thresholded and Thresholded Images. (A) Aggregates of pixel-sized pores representing false positives (red) prior to any thresholding. (B) True pores labeled in red after pixel-size-based threshold exclusions applied in ImageJ.*

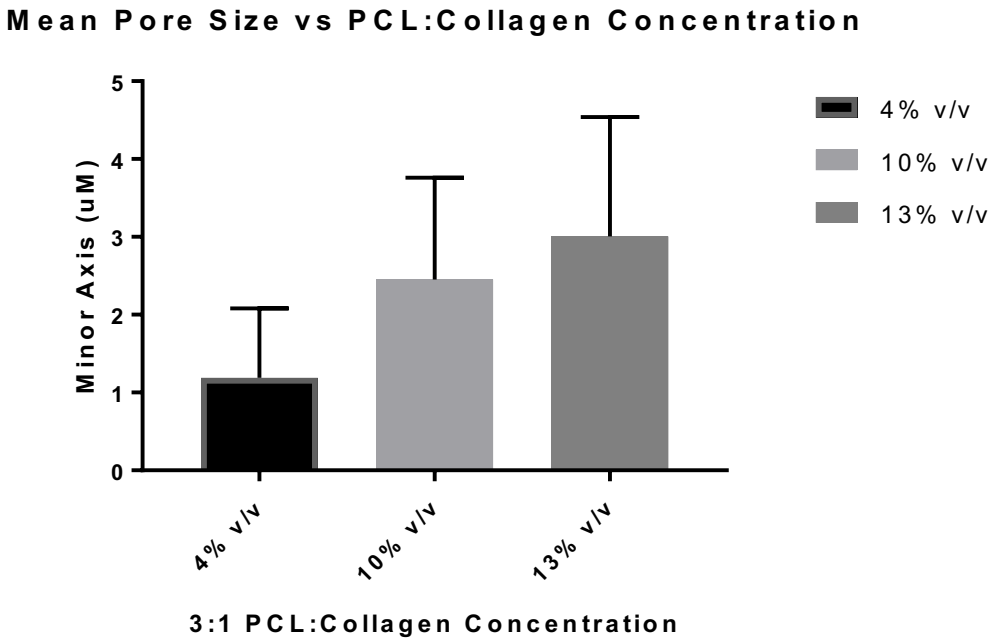


***Figure 28***: *Pore size of 3:1 Elextrospun PCL: Collagen I at 4% PCL, 10% PCL, and 13% PCL.*

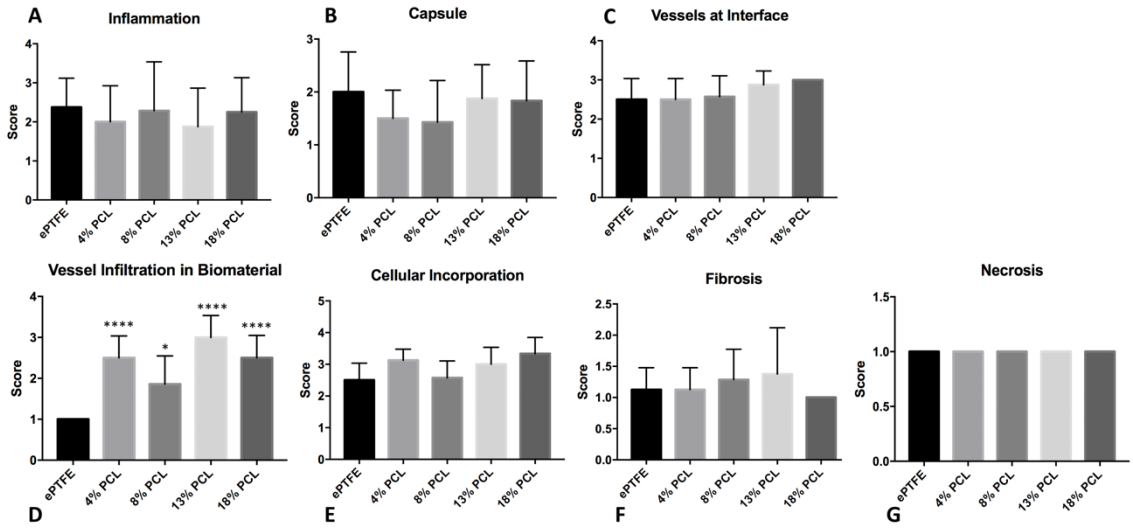


***Figure 29***: *H&E Determined Scores of Inflammation (A), Capsule Formation (B), Vessels at Interface (C), Vessel Infiltration (D), Cellular Incorporation (E), Fibrosis (F), and Necrosis (D) of Implanted Electrospun PCL in Rat Epididymal Fat Pads After 30 Days.* * $p < 0.05$, **** $p < 0.0001$.

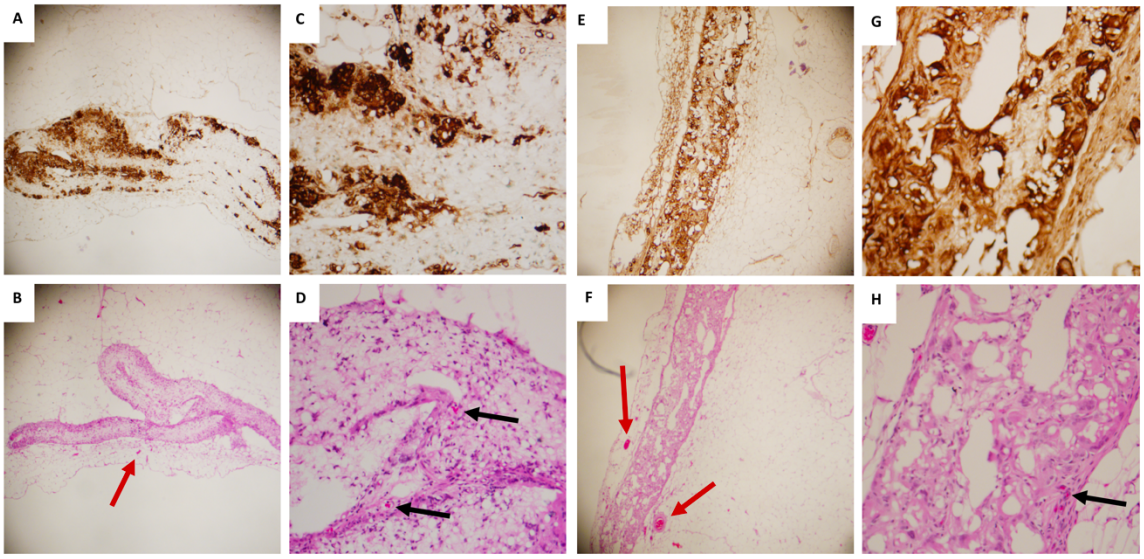


***Figure 30***: *H&E and GS1 Immunohistochemistry of Explanted 4% and 18 % Electrospun PCL after 30 Days in Rat Epididymal Fat. (A) 4% PCL stained with GS1 for endothelial cells, (B) H&E stain of 4% PCL, (C) 4X zoom of (A), (D) 4X zoom of (B), (E) 18% PCL stained with GS1, (F) H&E stain of 18% PCL, (G) 4X zoom of (E), (H) 4X zoom of (F.) Red arrows demonstrate vasculature surrounding the biomaterial, black arrows demonstrate microvessel penetration into the biomaterial.*

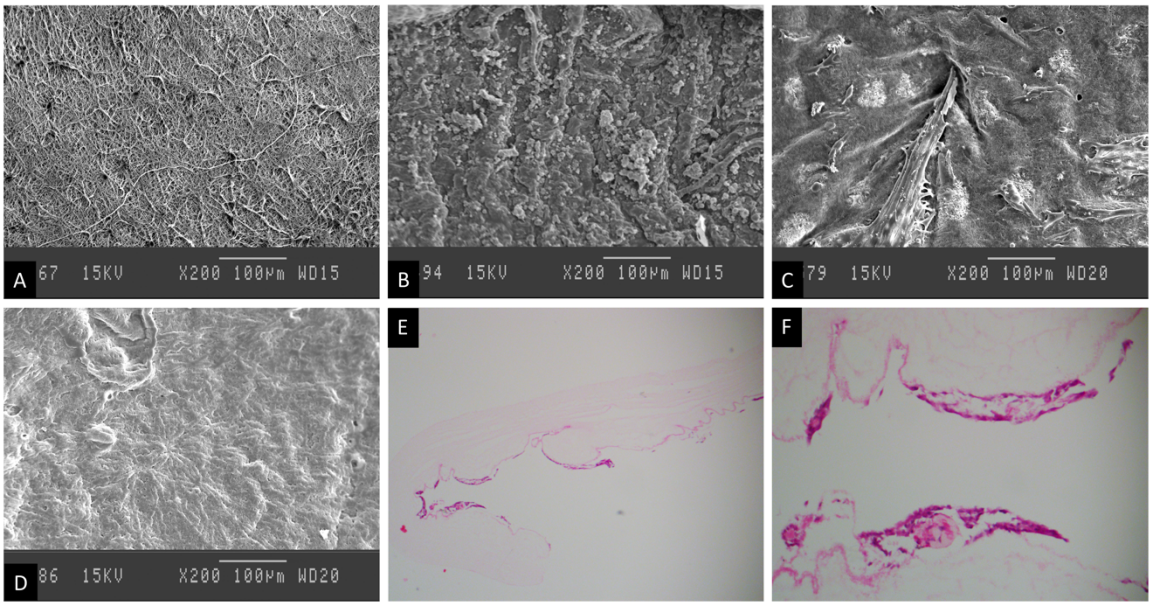


***Figure 31***: *SEM Images and H&E Stained 4% PCL Sodded with SVF Post 2 Weeks Flow in an In vitro Bioreactor. (A) SEM image of 4% PCL prior to cell sodding. (B) SEM image immediately after sodding with SVF cells at $2x10^5$ cells/$cm^2$, (C) SEM image of luminal side of 4% PCL post 2 weeks flow at 22mL/min, (D) SEM image of abluminal side of 4% PCL post 2 weeks flow at 22mL/min, (E) H&E stained 4% PCL BVM post 2 weeks flow, (F) 4X zoom of (E); most nucleated cells are sequestered in the first few layers of the luminal side of the biomaterial.*

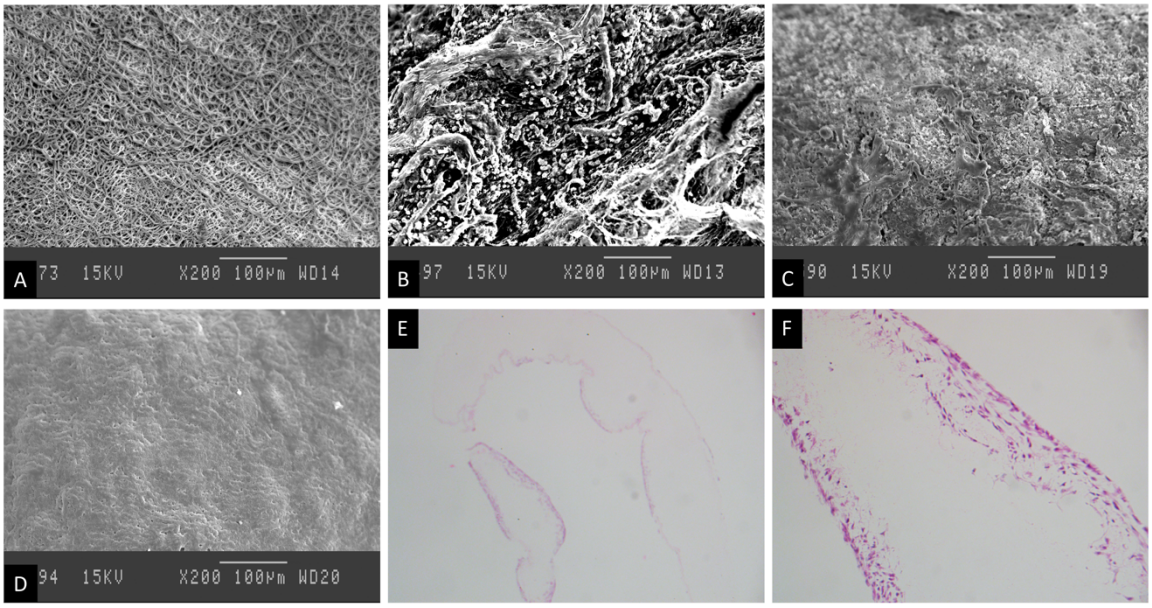


***Figure 32***: *SEM Images and H&E Stained 8% PCL Sodded with SVF Post 2 Weeks Flow in an In vitro Bioreactor. (A) SEM image of 8% PCL prior to cell sodding. (B) SEM image immediately after sodding with SVF cells at* $2x10^5$ *cells/cm*$^2$*, (C) SEM image of luminal side of 8% PCL post 2 weeks flow at 22mL/min, (D) SEM image of abluminal side of 8% PCL post 2 weeks flow at 22mL/min, (E) H&E stained 8% PCL BVM post 2 weeks flow, (F) 4X zoom of (E); most nucleated cells travel through the entire thickness of the biomaterial.*

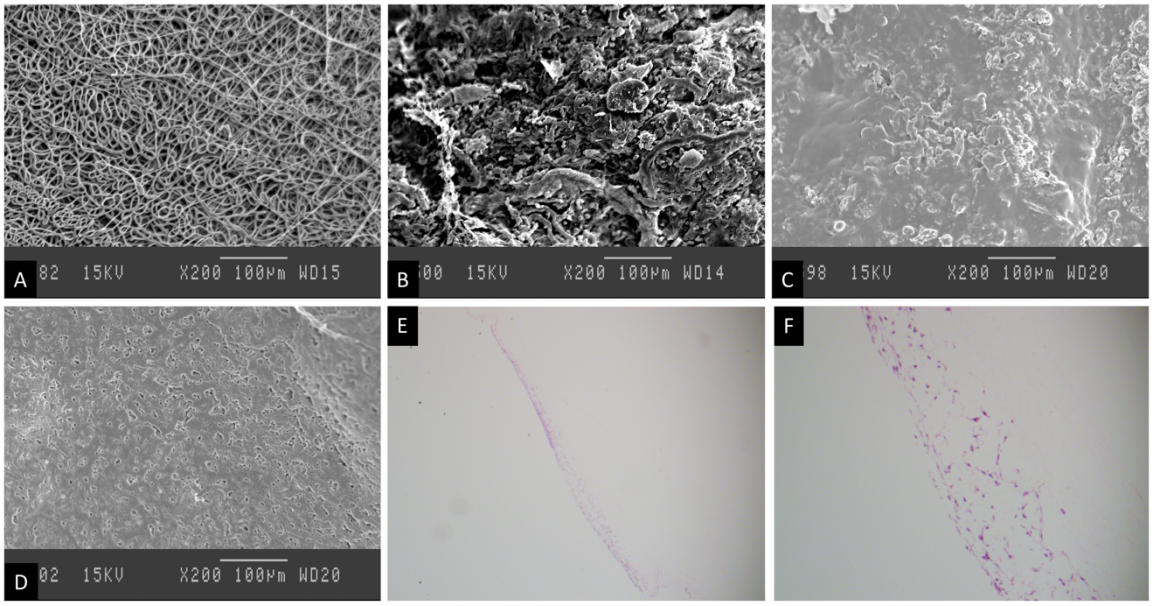


***Figure 33***: *SEM Images and H&E Stained 13% PCL Sodded with SVF Post 2 Weeks Flow in an In vitro Bioreactor. (A) SEM image of 13% PCL prior to cell sodding. (B) SEM image immediately after sodding with SVF cells at* $2x10^5$ *cells/cm*$^2$*, (C) SEM image of luminal side of 13% PCL post 2 weeks flow at 22mL/min, (D) SEM image of abluminal side of 13% PCL post 2 weeks flow at 22mL/min, (E) H&E stained 8% PCL BVM post 2 weeks flow, (F) 4X zoom of (E); most nucleated cells travel through the entire thickness of the biomaterial, however, less overall cells remain in biomaterial as compared to 8% PCL.*

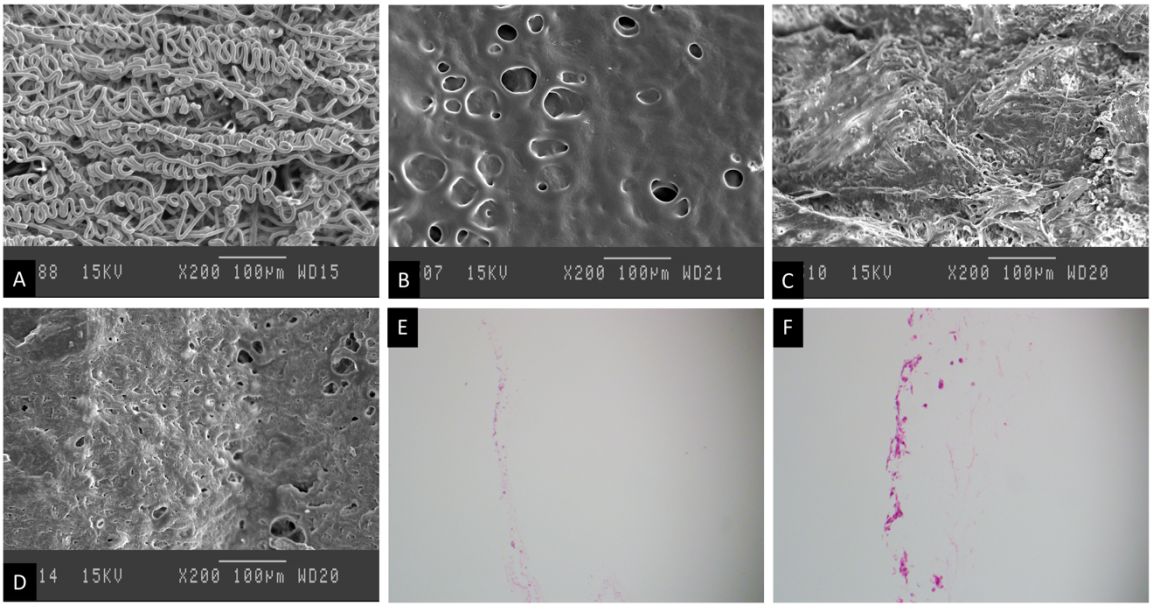


***Figure 34***: *SEM Images and H&E Stained 18% PCL Sodded with SVF Post 2 Weeks Flow in an In vitro Bioreactor. (A) SEM image of 18% PCL prior to cell sodding. (B) SEM image immediately after sodding with SVF cells at* $2x10^5$ *cells/cm*$^2$*, (C) SEM image of luminal side of 18% PCL post 2 weeks flow at 22mL/min, (D) SEM image of abluminal side of 18% PCL post 2 weeks flow at 22mL/min, (E) H&E stained 8% PCL BVM post 2 weeks flow, (F) 4X zoom of (E); most nucleated cells travel through the entire thickness of the biomaterial, however, less overall cells remain in biomaterial as compared to all other percentages tested of PCL.*

**Discussion**

Utilizing electrospinning to produce nanofibrous scaffolds for vascular tissue engineering is a promising technique that has advantages over other fabrication methods. Firstly, electrospun scaffolds can utilize FDA approved biomaterials that have biodegradable properties when implanted allowing tissue to encompass and replace the scaffold. Secondly, electrospinning affords the ability to create fibrous mats or tubes in which fibers can have tailored diameters of 50 to 500nm in thickness. Additionally, the randomly distributed nature of fiber deposition can mimic endogenous fibrillar ECM protein such as collagen I or reticular collagen III seen in specific tissue sites such as adventitia of larger arteries. These fiber orientations as such also create micropores within the material allowing for cellular penetration, migration, and infiltration creating micro-niches for cellular growth and retention.

These pores themselves can be altered by spinning parameters as well and are a function of fiber size and orientation. There are several thought processes in regard to cellular infiltration when it comes to electrospun materials. Many believe that the orientation of the fibers themselves dictate cellular adhesion geometry and cells tend to line fibers and attach, if the fiber orientation is unidirectional. Schoeneberger and colleagues studied the effects of highly aligned PCL electrospun mats versus randomly oriented fiber PCL mats on tendon fibroblast adhesion and macrophage MMP production[256]. They concluded that highly aligned electrospun scaffolds tend to downregulate the expression of MMPs by M2 macrophages which could limit additional inflammatory response post fibroblast attachment, providing a usable scaffold for tendon reconstruction in patients with highly inflammatory tissues such as tendonitis.

Additionally, Tan and colleagues studied endothelial cell attachment to aligned PCL/PEG electrospun scaffolds and concluded that their bilayer grafts promoted cell adhesion and ECM production when fibers were oriented in the same direction [257].

Others believe that pore size is more indicative of cellular infiltration into electropsun materials than fiber alignment. For example, Wang and colleagues prepared a hybrid method of electrospinning randomly oriented fibrous PCL and electrospraying poly(ethylene oxide) PEO to create large pores in engineered vascular grafts in which they noticed increased poor size correlated with increased NIH3T3 cell infiltration with 'dense and loose' layer alternation[258].

Our PCL and PCL: Collagen I electrospun grafts, while demonstrating random fiber deposition, were tailored to produce varying pore sizes in order to analyze sodded SVF cellular retention within electrospun BVMs mounted in microfluidic chambers exposed to physiological blood flow pressures; as well as implanted within adipose tissue to analyze *in vivo* cellular response and infiltration. We developed a novel technique to analyze pore sizes using widely available ImageJ software and specific thresholding parameters with 2D SEM images. We were able to accurately produce measurements of average pore size by image optimization removing dense pixel false positives and measuring minor axis length in dead spaces between fibers. Our electrospinning conditions were altered such that pore sizes ranging from 1 to 5+μm were achieved with varying the fewest parameters possible between PCL only scaffolds as well as PCL and collagen I mixed material scaffolds.

Interestingly, flow pressures producing 52dynes/cm$^2$ shear allowed cellular retention in all 4 varying porosities of PCL, however, at the largest pore size (5+μm) the number of nucleated cells retained were lower than that of the pore sizes ranging from 1 to

3μm. When embedded into tissue however, all constructs demonstrated similar response in terms of inflammatory cells present, fibrous capsule formation, peri-implant vascularization and limited necrosis and fibrosis. However, electropsun PCL at all porosities demonstrated higher presence of microvessel penetration into the biomaterial as compared to ePTFE control. This phenomenon may be attributable to malleability of material as well as fibrous layout and pore structure allowing for angiogenesis and endothelial migration through PCL as compared to ePTFE. While average pore sizes were determined, the random fiber deposition allowed for a wide variability in pore sizes at the extremes, which may allow microvessels of 10μm or larger in diameter the ability to penetrate through without the need of degrading or mobilizing PCL fibers. ePTFE does not afford similar pore sizes and may be a reason for limited microvessel migration through the material. Additional studies are necessary to elucidate techniques to create even greater ranges in pore size as well as techniques to introduce additional ECM protein into electrospinning. Increased cellular retention may occur not only as a condition of porosity but as a condition of cellular adherence through focal adhesion production and integrin binding to ECM proteins providing a wide range of materials to test affording both biodegradability and cellular adhesion and signaling activation.

# CHAPTER IV

# SUMMARY AND CONCLUSIONS

Stem and other cell therapeutics demonstrate promising potential for the stimulation and regeneration of pathological tissues. Ischemic cardiovascular disease is a leading cause of death in the western world and as such, many cellular-based therapies have been studied to accelerate myocardial return to function in conjunction with currently approved pharmacotherapies. While ischemic cardiomyopathies are composed of multicellular breakdown and dysfunction, the reestablishment of perfused tissue via macro and microcirculation is fundamental to mitigate continual tissue necrosis and scarring.

Our group and others have focused on stromal vascular fraction as the cell source to regenerate microcirculation both *in vitro* and *in vivo*. Stromal vascular fraction is a highly complex and dynamic group of cells that can be easily isolated from tissue sources. Over the past several decades many have isolated and characterized stromal vascular fraction from accessible subcutaneous adipose tissue depots in humans and other mammals via lipoaspiration or other minimally invasive surgical techniques. Many have even developed companies around proper harvesting and limited tissue manipulation through the production of automated systems that can accept lipoaspirate and produce injectable SVF for clinical treatments. SVF can undergo dynamic cellular re-assortment and phenotypic modification to produce microvessels with lumens in 3D systems.

Additionally, upon *in vivo* implantation, SVF forms robust microvascular networks that signal with host microvasculature to inosculate, receive circulating blood, and perfuse surrounding tissue. These exogenous 'tissue engineered' vessels remain within the host tissue and do not undergo extensive pruning or remission.

Due to these phenomena and others, many have studied specific cellular populations within SVF due to the heterogeneity of cells present, in order to analyze signaling events necessary for microvascular reformation. SVF contains endothelial cells, smooth muscle cells, pericytes and perivascular cells, fibroblasts and other stromal cells, adipose derived stem cells, mesenchymal stem cells, hematopoietic stem cells, and circulating immune cells depending on hemostasis of the adipose tissue at time of resection and digestion. These cell types can signal vasculogenic and angiogenic events such that individual endothelial cells regroup and reorganize into networks which ultimately undergo tubulogenesis both on specific 2D surfaces and within 3D matrices, in a culture system or upon implantation.

Endothelial tubes however are not descriptive of functional microvessels and rather, the multitude of cell types present allows continual maturation via pericyte recruitment and stabilization through known PDGF-B ligand secretion and signaling. We were able to analyze these mechanisms and others within angiogenic pathways via our novel 2D *in vitro* time-lapse assay whereby inhibitors were added to block known angiogenic signaling events. We believe that patient SVF can be analyzed prior to use in a clinical setting for 'vascular potential' which may mitigate cost and effectiveness of treatment if end goals are SVF incorporation and formation of new microvascular tissue.

Additionally, the delivery of discrete tissue units rather than liquid suspensions of cells may render larger therapeutic effects due to higher retention at injection sites as well as the creation of a microenvironment stable enough to allow embedded, exogenous SVF to mature into microvessels within host pathological tissue. For example, infarct zone post myocardial infarction if left untreated will form thick dense fibrous scar tissue that is not amenable to surrounding microvessel infiltration and reperfusion. As such, it is possible that delivery of larger tissue units of preformed microvessels will respond and integrate into pathologic tissue more so than cell-suspended solutions at infarct border zones. This theory has been studied by ourselves and others whereby SVF, whether in the form of a cardiac patch using Vicryl$^{TM}$ mesh support or embedded in 3D collagen I, provides functional benefits such as increased ejection fraction when implanted on the pericardial surface of infarcted heart tissue in rats[67,139,140]. However, the use of additional ECM and other scaffolds to develop *in vitro* cardiac patches of SVF microvessels has not been fully elucidated.

Using digestion protocols to create individual SVF cell suspension, when cultured in 3D fibrin versus 3D collagen I, freshly isolated SVF undergoes the initiation of tube-like "microvessel" formation *in vitro* in a time period of 4 days. To form microvessels *in vitro* in 3D Collagen I systems, microvessel fragments must be present as the initiator of angiogenesis and incubation can range from a minimum of 7 days to 14 days to notice phenotypic change. The role of fibrin specific integrins accelerate signaling between SVF endothelial cells and ECM stimulating angiogenic events such as tip cell and stalk cell formation, endothelial cell migration, and tubulogenesis all in a VEGF dependent manner.

In order to produce and deliver tissue units of SVF, we have developed a system using bioprinting methods to automate and dispense liquid droplets of collagen I or fibrin containing SVF, ultimately forming ECM spheroids full of SVF-derived microvessels. The use of automated systems allows for production of viable tissue in spheroid format, which is easily dosable and injectable through large gauge syringes. Tissues in spheroid format also allow for the production of large volumes with limited media in spinner flask culture. In addition, tissue is in sizes that allow for nutrient diffusion and permeabilization without production of necrotic cores or zones.

Lastly, we have created a new model to analyze the porosity of electrospun grafts which may have potential for artificial large vessel creation. SVF can be embedded within the pores of electropsun PCL and undergo exposure to physiological blood flow in *in vitro* bioreactors. Material devoid of cells also shows promising ability of cellular infiltration and local tissue microvessel penetration as compared to other materials such as ePTFE upon implantation *in vivo*.

SVF grown in 3D fibrin in spheroid format may provide clinically translatable tissue units for treatment of ischemic cardiomyopathies. Microvessels delivered may inosculate with host microvasculature at border zones of infarct and stimulate reperfusion at the microcirculatory level in the pathological tissue. Macrovessels of specific porosity may elucidate artificial blood vessel formats that can be beneficial to patients requiring CABG without native vessels that can be surgically transplanted. These therapies in the future may function alongside current standard care treatments to accelerate myocardial reperfusion post-surgery and mitigate tissue damage at the cellular level. Many additional experiments are necessary to understand both at the molecular level SVF cellular behavior

in 3D culture systems as well as at the bioengineering level to produce tissue constructs that are structurally relevant for surgical applications including both microvessel and macrovessel morphologies.

Future directions include large animal ischemic infarct models whereby SVF can be harvested and produced in fibrin spheroid format for injection at border zone areas. In addition, electrospun sodded macrovessels can be surgically implanted in multiple areas and anastomosed with host arteries to understand native tissue integration, and host response creating new arterial tissue.

# REFERENCES


1. Benjamin EJ, Blaha MJ, Chiuve SE, et al. Heart Disease and Stroke Statistics-2017 Update: A Report From the American Heart Association. *Circulation.* 2017;135(10):e146-e603.
2. Libby P, Ridker PM, Hansson GK. Progress and challenges in translating the biology of atherosclerosis. *Nature.* 2011;473(7347):317-325.
3. Tabas I, Williams KJ, Boren J. Subendothelial lipoprotein retention as the initiating process in atherosclerosis: update and therapeutic implications. *Circulation.* 2007;116(16):1832-1844.
4. Berliner JA, Navab M, Fogelman AM, et al. Atherosclerosis: basic mechanisms. Oxidation, inflammation, and genetics. *Circulation.* 1995;91(9):2488-2496.
5. Goldstein JL, Brown MS. A century of cholesterol and coronaries: from plaques to genes to statins. *Cell.* 2015;161(1):161-172.
6. Cannon PJ, Weiss MB, Sciacca RR. Myocardial blood flow in coronary artery disease: studies at rest and during stress with inert gas washout techniques. *Prog Cardiovasc Dis.* 1977;20(2):95-120.
7. Parodi O, De Maria R, Oltrona L, et al. Myocardial blood flow distribution in patients with ischemic heart disease or dilated cardiomyopathy undergoing heart transplantation. *Circulation.* 1993;88(2):509-522.

8. Olivetti G, Abbi R, Quaini F, et al. Apoptosis in the failing human heart. *N Engl J Med.* 1997;336(16):1131-1141.

9. Searle J, Kerr JF, Bishop CJ. Necrosis and apoptosis: distinct modes of cell death with fundamentally different significance. *Pathol Annu.* 1982;17 Pt 2:229-259.

10. Weber KT, Janicki JS, Campbell C, Replogle R. Pathophysiology of acute and chronic cardiac failure. *Am J Cardiol.* 1987;60(5):3C-9C.

11. Wong DT, Puri R, Richardson JD, Worthley MI, Worthley SG. Myocardial 'no-reflow'--diagnosis, pathophysiology and treatment. *Int J Cardiol.* 2013;167(5):1798-1806.

12. Gavin JB, Maxwell L, Edgar SG. Microvascular involvement in cardiac pathology. *J Mol Cell Cardiol.* 1998;30(12):2531-2540.

13. Diodato M, Chedrawy EG. Coronary artery bypass graft surgery: the past, present, and future of myocardial revascularisation. *Surg Res Pract.* 2014;2014:726158.

14. Favaloro RG. Saphenous vein autograft replacement of severe segmental coronary artery occlusion: operative technique. *Ann Thorac Surg.* 1968;5(4):334-339.

15. Favaloro RG, Effler DB, Groves LK, Fergusson DJ, Lozada JS. Double internal mammary artery-myocardial implantation. Clinical evaluation of results in 150 patients. *Circulation.* 1968;37(4):549-555.

16. Favaloro RG, Effler DB, Groves LK, Suarez EL. [Surgery for coronary arteriosclerosis. Clinical experience in 1,5000 operated patients]. *Prensa Med Argent.* 1968;55(22):1019-1026.

17. Kuhlmann U, Gruntzig A, Vetter W, Lutolf U, Meier B, Siegenthaler W. Percutaneous transluminal dilatation: a new treatment of renovascular hypertension? *Klin Wochenschr.* 1978;56(14):703-707.

18. Gruntzig A, Kuhlmann U, Vetter W, Lutolf U, Meier B, Siegenthaler W. Treatment of renovascular hypertension with percutaneous transluminal dilatation of a renal-artery stenosis. *Lancet.* 1978;1(8068):801-802.

19. Gruntzig A. Transluminal dilatation of coronary-artery stenosis. *Lancet.* 1978;1(8058):263.

20. Li Q, Guo Y, Ou Q, et al. Intracoronary administration of cardiac stem cells in mice: a new, improved technique for cell therapy in murine models. *Basic Res Cardiol.* 2011;106(5):849-864.

21. He JQ, Vu DM, Hunt G, Chugh A, Bhatnagar A, Bolli R. Human cardiac stem cells isolated from atrial appendages stably express c-kit. *PLoS One.* 2011;6(11):e27719.

22. Bolli R, Chugh AR, D'Amario D, et al. Cardiac stem cells in patients with ischaemic cardiomyopathy (SCIPIO): initial results of a randomised phase 1 trial. *Lancet.* 2011;378(9806):1847-1857.

23. Leblanc AJ, Nguyen QT, Touroo JS, et al. Adipose-derived cell construct stabilizes heart function and increases microvascular perfusion in an established infarct. *Stem Cells Transl Med.* 2013;2(11):896-905.

24. Panzhinskiy E, Zawada WM, Stenmark KR, Das M. Hypoxia induces unique proliferative response in adventitial fibroblasts by activating PDGFbeta receptor-JNK1 signalling. *Cardiovasc Res.* 2012;95(3):356-365.

25. Folkman J. Tumor angiogenesis: therapeutic implications. *N Engl J Med.* 1971;285(21):1182-1186.

26. Folkman J, Merler E, Abernathy C, Williams G. Isolation of a tumor factor responsible for angiogenesis. *J Exp Med.* 1971;133(2):275-288.

27. Folkman J, Haudenschild C. Angiogenesis in vitro. *Nature.* 1980;288(5791):551-556.

28. Walmsley M, Cleaver D, Patient R. Fibroblast growth factor controls the timing of Scl, Lmo2, and Runx1 expression during embryonic blood development. *Blood.* 2008;111(3):1157-1166.

29. Gospodarowicz D. Humoral control of cell proliferation: the role of fibroblast growth factor in regeneration, angiogenesis, wound healing, and neoplastic growth. *Prog Clin Biol Res.* 1976;9:1-19.

30. Montesano R, Vassalli JD, Baird A, Guillemin R, Orci L. Basic fibroblast growth factor induces angiogenesis in vitro. *Proc Natl Acad Sci U S A.* 1986;83(19):7297-7301.

31. Risau W, Sariola H, Zerwes HG, et al. Vasculogenesis and angiogenesis in embryonic-stem-cell-derived embryoid bodies. *Development.* 1988;102(3):471-478.

32. Wadzinski MG, Folkman J, Sasse J, Devey K, Ingber D, Klagsbrun M. Heparin-binding angiogenesis factors: detection by immunological methods. *Clin Physiol Biochem.* 1987;5(3-4):200-209.

33. Samathanam CA, Adesanya OO, Zhou J, Wang J, Bondy CA. Fibroblast growth factors 1 and 2 in the primate uterus. *Biol Reprod.* 1998;59(3):491-496.

34. Yu P, Wilhelm K, Dubrac A, et al. FGF-dependent metabolic control of vascular development. *Nature.* 2017;545(7653):224-228.

35. Guerrin M, Scotet E, Malecaze F, Houssaint E, Plouet J. Overexpression of vascular endothelial growth factor induces cell transformation in cooperation with fibroblast growth factor 2. *Oncogene.* 1997;14(4):463-471.

36. Flamme I, Breier G, Risau W. Vascular endothelial growth factor (VEGF) and VEGF receptor 2 (flk-1) are expressed during vasculogenesis and vascular differentiation in the quail embryo. *Dev Biol.* 1995;169(2):699-712.

37. Senger DR, Galli SJ, Dvorak AM, Perruzzi CA, Harvey VS, Dvorak HF. Tumor cells secrete a vascular permeability factor that promotes accumulation of ascites fluid. *Science.* 1983;219(4587):983-985.

38. Keck PJ, Hauser SD, Krivi G, et al. Vascular permeability factor, an endothelial cell mitogen related to PDGF. *Science.* 1989;246(4935):1309-1312.

39. Ellis LM. Bevacizumab. *Nat Rev Drug Discov.* 2005;Suppl:S8-9.

40. Blanco R, Gerhardt H. VEGF and Notch in tip and stalk cell selection. *Cold Spring Harb Perspect Med.* 2013;3(1):a006569.

41. Tung JJ, Tattersall IW, Kitajewski J. Tips, stalks, tubes: notch-mediated cell fate determination and mechanisms of tubulogenesis during angiogenesis. *Cold Spring Harb Perspect Med.* 2012;2(2):a006601.

42. Corson MA, James NL, Latta SE, Nerem RM, Berk BC, Harrison DG. Phosphorylation of endothelial nitric oxide synthase in response to fluid shear stress. *Circ Res.* 1996;79(5):984-991.

43. Govers R, Rabelink TJ. Cellular regulation of endothelial nitric oxide synthase. *Am J Physiol Renal Physiol.* 2001;280(2):F193-206.

44. Kinlay S, Behrendt D, Wainstein M, et al. Role of endothelin-1 in the active constriction of human atherosclerotic coronary arteries. *Circulation.* 2001;104(10):1114-1118.

45. Moncada S, Erusalimsky JD. Does nitric oxide modulate mitochondrial energy generation and apoptosis? *Nat Rev Mol Cell Biol.* 2002;3(3):214-220.

46. Rinaldo JE, Basford RE. Neutrophil-endothelial interactions: Modulation of neutrophil activation responses by endothelial cells. *Tissue Cell.* 1987;19(5):599-606.

47. Lindahl P, Hellstrom M, Kalen M, et al. Paracrine PDGF-B/PDGF-Rbeta signaling controls mesangial cell development in kidney glomeruli. *Development.* 1998;125(17):3313-3322.

48. Dumont DJ, Gradwohl G, Fong GH, et al. Dominant-negative and targeted null mutations in the endothelial receptor tyrosine kinase, tek, reveal a critical role in vasculogenesis of the embryo. *Genes Dev.* 1994;8(16):1897-1909.

49. Mizugishi K, Yamashita T, Olivera A, Miller GF, Spiegel S, Proia RL. Essential role for sphingosine kinases in neural and vascular development. *Mol Cell Biol.* 2005;25(24):11113-11121.

50. Gaengel K, Genove G, Armulik A, Betsholtz C. Endothelial-mural cell signaling in vascular development and angiogenesis. *Arterioscler Thromb Vasc Biol.* 2009;29(5):630-638.

51. Augst AD, Kong HJ, Mooney DJ. Alginate hydrogels as biomaterials. *Macromol Biosci.* 2006;6(8):623-633.

52. Ling Y, Rubin J, Deng Y, et al. A cell-laden microfluidic hydrogel. *Lab Chip.* 2007;7(6):756-762.

53. Bayless KJ, Davis GE. Sphingosine-1-phosphate markedly induces matrix metalloproteinase and integrin-dependent human endothelial cell invasion and lumen formation in three-dimensional collagen and fibrin matrices. *Biochem Biophys Res Commun.* 2003;312(4):903-913.

54. Nichol JW, Koshy ST, Bae H, Hwang CM, Yamanlar S, Khademhosseini A. Cell-laden microengineered gelatin methacrylate hydrogels. *Biomaterials.* 2010;31(21):5536-5544.

55. Hutson CB, Nichol JW, Aubin H, et al. Synthesis and characterization of tunable poly(ethylene glycol): gelatin methacrylate composite hydrogels. *Tissue Eng Part A.* 2011;17(13-14):1713-1723.

56. Price GM, Wong KH, Truslow JG, Leung AD, Acharya C, Tien J. Effect of mechanical factors on the function of engineered human blood microvessels in microfluidic collagen gels. *Biomaterials.* 2010;31(24):6182-6189.

57. Chrobak KM, Potter DR, Tien J. Formation of perfused, functional microvascular tubes in vitro. *Microvasc Res.* 2006;71(3):185-196.

58. Zheng Y, Chen J, Craven M, et al. In vitro microvessels for the study of angiogenesis and thrombosis. *Proc Natl Acad Sci U S A.* 2012;109(24):9342-9347.

59. Golden AP, Tien J. Fabrication of microfluidic hydrogels using molded gelatin as a sacrificial element. *Lab Chip.* 2007;7(6):720-725.

60. Rayner SG, Zheng Y. Engineered Microvessels for the Study of Human Disease. *J Biomech Eng.* 2016;138(11).

61. Hasenberg T, Muhleder S, Dotzler A, et al. Emulating human microcapillaries in a multi-organ-chip platform. *J Biotechnol.* 2015;216:1-10.

62. Shiu YT, Weiss JA, Hoying JB, Iwamoto MN, Joung IS, Quam CT. The role of mechanical stresses in angiogenesis. *Crit Rev Biomed Eng.* 2005;33(5):431-510.

63. Haas TL, Davis SJ, Madri JA. Three-dimensional type I collagen lattices induce coordinate expression of matrix metalloproteinases MT1-MMP and MMP-2 in microvascular endothelial cells. *J Biol Chem.* 1998;273(6):3604-3610.

64. Krishnan L, Underwood CJ, Maas S, et al. Effect of mechanical boundary conditions on orientation of angiogenic microvessels. *Cardiovasc Res.* 2008;78(2):324-332.

65. Jain RK. Molecular regulation of vessel maturation. *Nat Med.* 2003;9(6):685-693.

66. Madri JA, Williams SK. Capillary endothelial cell cultures: phenotypic modulation by matrix components. *J Cell Biol.* 1983;97(1):153-165.

67. Hoying JB, Boswell CA, Williams SK. Angiogenic potential of microvessel fragments established in three-dimensional collagen gels. *In Vitro Cell Dev Biol Anim.* 1996;32(7):409-419.

68. Ingber D. Integrins as mechanochemical transducers. *Curr Opin Cell Biol.* 1991;3(5):841-848.

69. Ingber D. Extracellular matrix and cell shape: potential control points for inhibition of angiogenesis. *J Cell Biochem.* 1991;47(3):236-241.

70. Ingber DE. Control of capillary growth and differentiation by extracellular matrix. Use of a tensegrity (tensional integrity) mechanism for signal processing. *Chest.* 1991;99(3 Suppl):34S-40S.

71. Gonen-Wadmany M, Gepstein L, Seliktar D. Controlling the cellular organization of tissue-engineered cardiac constructs. *Ann N Y Acad Sci.* 2004;1015:299-311.

72. Kolodney MS, Wysolmerski RB. Isometric contraction by fibroblasts and endothelial cells in tissue culture: a quantitative study. *J Cell Biol.* 1992;117(1):73-82.

73. Ingber DE. Mechanical signaling and the cellular response to extracellular matrix in angiogenesis and cardiovascular physiology. *Circ Res.* 2002;91(10):877-887.

74. Knox G, West JP. Dacron grafts in the treatment of arteriosclerotic occlusion of the superficial femoral artery; report of seven cases. *Ann Surg.* 1957;145(1):59-67.

75. Xu CY, Inai R, Kotaki M, Ramakrishna S. Aligned biodegradable nanofibrous structure: a potential scaffold for blood vessel engineering. *Biomaterials.* 2004;25(5):877-886.

76. Boland ED, Matthews JA, Pawlowski KJ, Simpson DG, Wnek GE, Bowlin GL. Electrospinning collagen and elastin: preliminary vascular tissue engineering. *Front Biosci.* 2004;9:1422-1432.

77. Ahn H, Ju YM, Takahashi H, et al. Engineered small diameter vascular grafts by combining cell sheet engineering and electrospinning technology. *Acta Biomater.* 2015;16:14-22.

78. Mo XM, Xu CY, Kotaki M, Ramakrishna S. Electrospun P(LLA-CL) nanofiber: a biomimetic extracellular matrix for smooth muscle cell and endothelial cell proliferation. *Biomaterials.* 2004;25(10):1883-1890.

79. Lee SJ, Yoo JJ, Lim GJ, Atala A, Stitzel J. In vitro evaluation of electrospun nanofiber scaffolds for vascular graft application. *J Biomed Mater Res A.* 2007;83(4):999-1008.

80. Williams SK, Kosnik PE, Kleinert LB, Vossman EM, Lye KD, Shine MH. Adipose stromal vascular fraction cells isolated using an automated point of care system improve the patency of expanded polytetrafluoroethylene vascular grafts. *Tissue Eng Part A.* 2013;19(11-12):1295-1302.

81. Touroo JS, Dale JR, Williams SK. Bioengineering human blood vessel mimics for medical device testing using serum-free conditions and scaffold variations. *Tissue Eng Part C Methods.* 2013;19(4):307-315.

82. Krishnan L, Touroo J, Reed R, Boland E, Hoying JB, Williams SK. Vascularization and cellular isolation potential of a novel electrospun cell delivery vehicle. *J Biomed Mater Res A.* 2014;102(7):2208-2219.

83. Rodbell M. Metabolism of Isolated Fat Cells. I. Effects of Hormones on Glucose Metabolism and Lipolysis. *J Biol Chem.* 1964;239:375-380.

84. Nunes SS, Maijub JG, Krishnan L, et al. Generation of a functional liver tissue mimic using adipose stromal vascular fraction cell-derived vasculatures. *Sci Rep.* 2013;3:2141.

85. Koh YJ, Koh BI, Kim H, et al. Stromal vascular fraction from adipose tissue forms profound vascular network through the dynamic reassembly of blood endothelial cells. *Arterioscler Thromb Vasc Biol.* 2011;31(5):1141-1150.

86. Williams SK, Wang TF, Castrillo R, Jarrell BE. Liposuction-derived human fat used for vascular graft sodding contains endothelial cells and not mesothelial cells as the major cell type. *J Vasc Surg.* 1994;19(5):916-923.

87. Dong Z, Peng Z, Chang Q, Lu F. The survival condition and immunoregulatory function of adipose stromal vascular fraction (SVF) in the early stage of nonvascularized adipose transplantation. *PLoS One.* 2013;8(11):e80364.

88. Klar AS, Guven S, Zimoch J, et al. Characterization of vasculogenic potential of human adipose-derived endothelial cells in a three-dimensional vascularized skin substitute. *Pediatr Surg Int.* 2016;32(1):17-27.

89. Mitchell JB, McIntosh K, Zvonic S, et al. Immunophenotype of human adipose-derived cells: temporal changes in stromal-associated and stem cell-associated markers. *Stem Cells.* 2006;24(2):376-385.

90. Ramakrishnan VM, Boyd NL. The Adipose Stromal Vascular Fraction as a Complex Cellular Source for Tissue Engineering Applications. *Tissue Eng Part B Rev.* 2017.

91. Monsuur HN, Weijers EM, Niessen FB, et al. Extensive Characterization and Comparison of Endothelial Cells Derived from Dermis and Adipose Tissue: Potential Use in Tissue Engineering. *PLoS One.* 2016;11(11):e0167056.

92. Chang CC, Krishnan L, Nunes SS, et al. Determinants of microvascular network topologies in implanted neovasculatures. *Arterioscler Thromb Vasc Biol.* 2012;32(1):5-14.

93. Merfeld-Clauss S, Lease BR, Lu H, March KL, Traktuev DO. Adipose stromal cells differentiation toward smooth muscle cell phenotype diminishes their vasculogenic activity due to induction of activin A secretion. *J Tissue Eng Regen Med.* 2017;11(11):3145-3156.

94. Tsuji W, Rubin JP, Marra KG. Adipose-derived stem cells: Implications in tissue regeneration. *World J Stem Cells.* 2014;6(3):312-321.

95. Shepherd BR, Chen HY, Smith CM, Gruionu G, Williams SK, Hoying JB. Rapid perfusion and network remodeling in a microvascular construct after implantation. *Arterioscler Thromb Vasc Biol.* 2004;24(5):898-904.

96. Williams SK, Morris ME, Kosnik PE, et al. Point-of-Care Adipose-Derived Stromal Vascular Fraction Cell Isolation and Expanded Polytetrafluoroethylene Graft Sodding. *Tissue Eng Part C Methods.* 2017;23(8):497-504.

97. Gadelorge M, Bourdens M, Espagnolle N, et al. Clinical-scale expansion of adipose-derived stromal cells starting from stromal vascular fraction in a single-use bioreactor: proof of concept for autologous applications. *J Tissue Eng Regen Med.* 2016.

98. Conde-Green A, Kotamarti VS, Sherman LS, et al. Shift toward Mechanical Isolation of Adipose-derived Stromal Vascular Fraction: Review of Upcoming Techniques. *Plast Reconstr Surg Glob Open.* 2016;4(9):e1017.

99. SundarRaj S, Deshmukh A, Priya N, Krishnan VS, Cherat M, Majumdar AS. Development of a System and Method for Automated Isolation of Stromal Vascular Fraction from Adipose Tissue Lipoaspirate. *Stem Cells Int.* 2015;2015:109353.

100. Nazari-Shafti TZ, Bruno IG, Martinez RF, Coleman ME, Alt EU, McClure SR. High yield recovery of equine mesenchymal stem cells from umbilical cord matrix/Wharton's jelly using a semi-automated process. *Methods Mol Biol.* 2015;1235:131-146.

101. Doi K, Tanaka S, Iida H, et al. Stromal vascular fraction isolated from lipo-aspirates using an automated processing system: bench and bed analysis. *J Tissue Eng Regen Med.* 2013;7(11):864-870.

102. Hanke A, Prantl L, Wenzel C, et al. Semi-automated extraction and characterization of Stromal Vascular Fraction using a new medical device. *Clin Hemorheol Microcirc.* 2016;64(3):403-412.

103. Jang Y, Koh YG, Choi YJ, et al. Characterization of adipose tissue-derived stromal vascular fraction for clinical application to cartilage regeneration. *In Vitro Cell Dev Biol Anim.* 2015;51(2):142-150.

104. Bansal H, Comella K, Leon J, et al. Intra-articular injection in the knee of adipose derived stromal cells (stromal vascular fraction) and platelet rich plasma for osteoarthritis. *J Transl Med.* 2017;15(1):141.

105. Filardo G, Perdisa F, Roffi A, Marcacci M, Kon E. Stem cells in articular cartilage regeneration. *J Orthop Surg Res.* 2016;11:42.

106. Almubarak S, Nethercott H, Freeberg M, et al. Tissue engineering strategies for promoting vascularized bone regeneration. *Bone.* 2016;83:197-209.

107. Nguyen PD, Tran TD, Nguyen HT, et al. Comparative Clinical Observation of Arthroscopic Microfracture in the Presence and Absence of a Stromal Vascular Fraction Injection for Osteoarthritis. *Stem Cells Transl Med.* 2017;6(1):187-195.

108. Zuk PA, Zhu M, Mizuno H, et al. Multilineage cells from human adipose tissue: implications for cell-based therapies. *Tissue Eng.* 2001;7(2):211-228.

109. Matsumoto D, Sato K, Gonda K, et al. Cell-assisted lipotransfer: supportive use of human adipose-derived cells for soft tissue augmentation with lipoinjection. *Tissue Eng.* 2006;12(12):3375-3382.

110. Yoshimura K, Sato K, Aoi N, Kurita M, Hirohi T, Harii K. Cell-assisted lipotransfer for cosmetic breast augmentation: supportive use of adipose-derived stem/stromal cells. *Aesthetic Plast Surg.* 2008;32(1):48-55; discussion 56-47.

111. Yoshimura K, Asano Y, Aoi N, et al. Progenitor-enriched adipose tissue transplantation as rescue for breast implant complications. *Breast J.* 2010;16(2):169-175.

112. Yoshimura K, Sato K, Aoi N, et al. Cell-assisted lipotransfer for facial lipoatrophy: efficacy of clinical use of adipose-derived stem cells. *Dermatol Surg.* 2008;34(9):1178-1185.

113. Mesimaki K, Lindroos B, Tornwall J, et al. Novel maxillary reconstruction with ectopic bone formation by GMP adipose stem cells. *Int J Oral Maxillofac Surg.* 2009;38(3):201-209.

114. Lendeckel S, Jodicke A, Christophis P, et al. Autologous stem cells (adipose) and fibrin glue used to treat widespread traumatic calvarial defects: case report. *J Craniomaxillofac Surg.* 2004;32(6):370-373.

115. Rigotti G, Marchi A, Galie M, et al. Clinical treatment of radiotherapy tissue damage by lipoaspirate transplant: a healing process mediated by adipose-derived adult stem cells. *Plast Reconstr Surg.* 2007;119(5):1409-1422; discussion 1423-1404.

116. Garcia-Olmo D, Garcia-Arranz M, Garcia LG, et al. Autologous stem cell transplantation for treatment of rectovaginal fistula in perianal Crohn's disease: a new cell-based therapy. *Int J Colorectal Dis.* 2003;18(5):451-454.

117. Garcia-Olmo D, Garcia-Arranz M, Herreros D. Expanded adipose-derived stem cells for the treatment of complex perianal fistula including Crohn's disease. *Expert Opin Biol Ther.* 2008;8(9):1417-1423.

118. Garcia-Olmo D, Garcia-Arranz M, Herreros D, Pascual I, Peiro C, Rodriguez-Montes JA. A phase I clinical trial of the treatment of Crohn's fistula by adipose mesenchymal stem cell transplantation. *Dis Colon Rectum.* 2005;48(7):1416-1423.

119. Garcia-Olmo D, Herreros D, Pascual I, et al. Expanded adipose-derived stem cells for the treatment of complex perianal fistula: a phase II clinical trial. *Dis Colon Rectum.* 2009;52(1):79-86.

120. Garcia-Olmo D, Herreros D, Pascual M, et al. Treatment of enterocutaneous fistula in Crohn's Disease with adipose-derived stem cells: a comparison of protocols with and without cell expansion. *Int J Colorectal Dis.* 2009;24(1):27-30.

121. Taxonera C, Schwartz DA, Garcia-Olmo D. Emerging treatments for complex perianal fistula in Crohn's disease. *World J Gastroenterol.* 2009;15(34):4263-4272.

122. Constantin G, Marconi S, Rossi B, et al. Adipose-derived mesenchymal stem cells ameliorate chronic experimental autoimmune encephalomyelitis. *Stem Cells.* 2009;27(10):2624-2635.

123. Yoon PW, Bastian B, Anderson RN, et al. Potentially preventable deaths from the five leading causes of death--United States, 2008-2010. *MMWR Morb Mortal Wkly Rep.* 2014;63(17):369-374.

124. Valarmathi MT, Fuseler JW, Davis JM, Price RL. A Novel Human Tissue-Engineered 3-D Functional Vascularized Cardiac Muscle Construct. *Front Cell Dev Biol.* 2017;5:2.

125. Bogorad MI, DeStefano J, Wong AD, Searson PC. Tissue-engineered 3D microvessel and capillary network models for the study of vascular phenomena. *Microcirculation.* 2017.

126. Kc P, Shah M, Liao J, Zhang G. Prevascularization of Decellularized Porcine Myocardial Slice for Cardiac Tissue Engineering. *ACS Appl Mater Interfaces.* 2017;9(3):2196-2204.

127. Riemenschneider SB, Mattia DJ, Wendel JS, et al. Inosculation and perfusion of pre-vascularized tissue patches containing aligned human microvessels after myocardial infarction. *Biomaterials.* 2016;97:51-61.

128. Laschke MW, Menger MD. Prevascularization in tissue engineering: Current concepts and future directions. *Biotechnol Adv.* 2016;34(2):112-121.

129. Laschke MW, Menger MD. Adipose tissue-derived microvascular fragments: natural vascularization units for regenerative medicine. *Trends Biotechnol.* 2015;33(8):442-448.

130. Sun X, Altalhi W, Nunes SS. Vascularization strategies of engineered tissues and their application in cardiac regeneration. *Adv Drug Deliv Rev.* 2016;96:183-194.

131. Sasagawa T, Shimizu T, Yamato M, Okano T. Endothelial colony-forming cells for preparing prevascular three-dimensional cell-dense tissues using cell-sheet engineering. *J Tissue Eng Regen Med.* 2016;10(9):739-747.

132. Morrissette-McAlmon J, Blazeski A, Somers S, Kostecki G, Tung L, Grayson WL. Adipose-derived perivascular mesenchymal stromal/stem cells promote functional vascular tissue engineering for cardiac regenerative purposes. *J Tissue Eng Regen Med.* 2017.

133. Haug V, Torio-Padron N, Stark GB, Finkenzeller G, Strassburg S. Comparison between endothelial progenitor cells and human umbilical vein endothelial cells on neovascularization in an adipogenesis mouse model. *Microvasc Res.* 2015;97:159-166.

134. Madri JA, Williams SK. Capillary endothelial cell cultures: phenotypic modulation by matrix components. *Journal of Cell Biology.* 1983;97(1):153-165.

135. Jin E, Chae DS, Son M, Kim SW. Angiogenic characteristics of human stromal vascular fraction in ischemic hindlimb. *Int J Cardiol.* 2017;234:38-47.

136. Maijub JG, Boyd NL, Dale JR, Hoying JB, Morris ME, Williams SK. Concentration-Dependent Vascularization of Adipose Stromal Vascular Fraction Cells. *Cell Transplant.* 2015;24(10):2029-2039.

137. Wagner RC, Kreiner P, Barrnett RJ, Bitensky MW. Biochemical characterization and cytochemical localization of a catecholamine-sensitive adenylate cyclase in isolated capillary endothelium. *Proc Natl Acad Sci U S A.* 1972;69(11):3175-3179.

138. Wagner RC, Matthews MA. The isolation and culture of capillary endothelium from epididymal fat. *Microvasc Res.* 1975;10(3):286-297.

139. Leblanc AJ, Touroo JS, Hoying JB, Williams SK. Adipose stromal vascular fraction cell construct sustains coronary microvascular function after acute myocardial infarction. *Am J Physiol Heart Circ Physiol.* 2012;302(4):H973-982.

140. Shepherd BR, Hoying JB, Williams SK. Microvascular transplantation after acute myocardial infarction. *Tissue Eng.* 2007;13(12):2871-2879.

141. Hiscox AM, Stone AL, Limesand S, Hoying JB, Williams SK. An islet-stabilizing implant constructed using a preformed vasculature. *Tissue Eng Part A.* 2008;14(3):433-440.

142. Albini A. Extracellular Matrix Invasion in Metastases and Angiogenesis: Commentary on the Matrigel "Chemoinvasion Assay". *Cancer Res.* 2016;76(16):4595-4597.

143. Brown RM, Meah CJ, Heath VL, Styles IB, Bicknell R. Tube-Forming Assays. *Methods Mol Biol.* 2016;1430:149-157.

144. Nicosia RF, Ottinetti A. Modulation of microvascular growth and morphogenesis by reconstituted basement membrane gel in three-dimensional cultures of rat aorta: a comparative study of angiogenesis in matrigel, collagen, fibrin, and plasma clot. *In Vitro Cell Dev Biol.* 1990;26(2):119-128.

145. Antczak C, Mahida JP, Bhinder B, Calder PA, Djaballah H. A high-content biosensor-based screen identifies cell-permeable activators and inhibitors of EGFR function: implications in drug discovery. *J Biomol Screen.* 2012;17(7):885-899.

146. Heymach JV, Desai J, Manola J, et al. Phase II study of the antiangiogenic agent SU5416 in patients with advanced soft tissue sarcomas. *Clin Cancer Res.* 2004;10(17):5732-5740.

147. Nourse MB, Halpin DE, Scatena M, et al. VEGF Induces Differentiation of Functional Endothelium From Human Embryonic Stem Cells. Implications for Tissue Engineering. *Arterioscler Thromb Vasc Biol.* 2009.

148. Diaz-Flores L, Gutierrez R, Lizartza K, et al. Behavior of in situ human native adipose tissue CD34+ stromal/progenitor cells during different stages of repair. Tissue-resident CD34+ stromal cells as a source of myofibroblasts. *Anat Rec (Hoboken).* 2015;298(5):917-930.

149. Arnaoutova I, Kleinman HK. In vitro angiogenesis: endothelial cell tube formation on gelled basement membrane extract. *Nat Protoc.* 2010;5(4):628-635.

150. Staton CA, Reed MW, Brown NJ. A critical analysis of current in vitro and in vivo angiogenesis assays. *Int J Exp Pathol.* 2009;90(3):195-221.

151. Lin S, Xie J, Gong T, et al. Smad signal pathway regulates angiogenesis via endothelial cell in an adipose-derived stromal cell/endothelial cell co-culture, 3D gel model. *Mol Cell Biochem.* 2016;412(1-2):281-288.

152. Mildmay-White A, Khan W. Cell surface Markers on Adipose-Derived Stem Cells: A Systematic Review. *Curr Stem Cell Res Ther.* 2016.

153. Moore MC, Pandolfi V, McFetridge PS. Novel human-derived extracellular matrix induces in vitro and in vivo vascularization and inhibits fibrosis. *Biomaterials.* 2015;49:37-46.

154. Fercana GR, Yerneni S, Billaud M, et al. Perivascular extracellular matrix hydrogels mimic native matrix microarchitecture and promote angiogenesis via basic fibroblast growth factor. *Biomaterials.* 2017;123:142-154.

155. Mammoto T, Jiang E, Jiang A, Mammoto A. Extracellular matrix structure and tissue stiffness control postnatal lung development through the lipoprotein receptor-related protein 5/Tie2 signaling system. *Am J Respir Cell Mol Biol.* 2013;49(6):1009-1018.

156. Sacharidou A, Stratman AN, Davis GE. Molecular mechanisms controlling vascular lumen formation in three-dimensional extracellular matrices. *Cells Tissues Organs.* 2012;195(1-2):122-143.

157. Ebrahem Q, Chaurasia SS, Vasanji A, et al. Cross-talk between vascular endothelial growth factor and matrix metalloproteinases in the induction of neovascularization in vivo. *Am J Pathol.* 2010;176(1):496-503.

158. Hughes SE. Functional characterization of the spontaneously transformed human umbilical vein endothelial cell line ECV304: use in an in vitro model of angiogenesis. *Exp Cell Res.* 1996;225(1):171-185.

159. Carstens MH, Gomez A, Cortes R, et al. Non-reconstructable peripheral vascular disease of the lower extremity in ten patients treated with adipose-derived stromal vascular fraction cells. *Stem Cell Res.* 2017;18:14-21.

160. Zakhari JS, Zabonick J, Gettler B, Williams SK. Vasculogenic and angiogenic potential of adipose stromal vascular fraction cell populations in vitro. *In Vitro Cell Dev Biol Anim.* 2018;54(1):32-40.

161. Giltay JC, van Mourik JA. Structure and function of endothelial cell integrins. *Haemostasis.* 1988;18(4-6):376-389.

162. Ruoslahti E, Pierschbacher MD. New perspectives in cell adhesion: RGD and integrins. *Science.* 1987;238(4826):491-497.

163. Plow EF, Haas TA, Zhang L, Loftus J, Smith JW. Ligand binding to integrins. *J Biol Chem.* 2000;275(29):21785-21788.

164. Drake CJ, Cheresh DA, Little CD. An antagonist of integrin alpha v beta 3 prevents maturation of blood vessels during embryonic neovascularization. *J Cell Sci.* 1995;108 ( Pt 7):2655-2661.

165. Woodard AS, Garcia-Cardena G, Leong M, Madri JA, Sessa WC, Languino LR. The synergistic activity of alphavbeta3 integrin and PDGF receptor increases cell migration. *J Cell Sci.* 1998;111 ( Pt 4):469-478.

166. Borges E, Jan Y, Ruoslahti E. Platelet-derived growth factor receptor beta and vascular endothelial growth factor receptor 2 bind to the beta 3 integrin through its extracellular domain. *J Biol Chem.* 2000;275(51):39867-39873.

167. Cheresh DA, Stupack DG. Regulation of angiogenesis: apoptotic cues from the ECM. *Oncogene.* 2008;27(48):6285-6298.

168. Arnaout MA, Goodman SL, Xiong JP. Structure and mechanics of integrin-based cell adhesion. *Curr Opin Cell Biol.* 2007;19(5):495-507.

169. Mahabeleshwar GH, Feng W, Reddy K, Plow EF, Byzova TV. Mechanisms of integrin-vascular endothelial growth factor receptor cross-activation in angiogenesis. *Circ Res.* 2007;101(6):570-580.

170. Walser R, Metzger W, Gorg A, Pohlemann T, Menger MD, Laschke MW. Generation of co-culture spheroids as vascularisation units for bone tissue engineering. *Eur Cell Mater.* 2013;26:222-233.

171. Laschke MW, Mussawy H, Schuler S, Eglin D, Alini M, Menger MD. Promoting external inosculation of prevascularised tissue constructs by pre-cultivation in an angiogenic extracellular matrix. *Eur Cell Mater.* 2010;20:356-366.

172. Cao L, Arany PR, Kim J, et al. Modulating Notch signaling to enhance neovascularization and reperfusion in diabetic mice. *Biomaterials.* 2010;31(34):9048-9056.

173. Brooks PC, Clark RA, Cheresh DA. Requirement of vascular integrin alpha v beta 3 for angiogenesis. *Science.* 1994;264(5158):569-571.

174. Weis SM, Lindquist JN, Barnes LA, et al. Cooperation between VEGF and beta3 integrin during cardiac vascular development. *Blood.* 2007;109(5):1962-1970.

175. Mahabeleshwar GH, Feng W, Phillips DR, Byzova TV. Integrin signaling is critical for pathological angiogenesis. *J Exp Med.* 2006;203(11):2495-2507.

176. Mahabeleshwar GH, Byzova TV. Vascular integrin signaling. *Methods Enzymol.* 2008;443:199-226.

177. Mahabeleshwar GH, Chen J, Feng W, Somanath PR, Razorenova OV, Byzova TV. Integrin affinity modulation in angiogenesis. *Cell Cycle.* 2008;7(3):335-347.

178. Feng W, McCabe NP, Mahabeleshwar GH, Somanath PR, Phillips DR, Byzova TV. The angiogenic response is dictated by beta3 integrin on bone marrow-derived cells. *J Cell Biol.* 2008;183(6):1145-1157.

179. Sugahara KN, Teesalu T, Karmali PP, et al. Coadministration of a tumor-penetrating peptide enhances the efficacy of cancer drugs. *Science.* 2010;328(5981):1031-1035.

180. Sugahara KN, Teesalu T, Karmali PP, et al. Tissue-penetrating delivery of compounds and nanoparticles into tumors. *Cancer Cell.* 2009;16(6):510-520.

181. Tarui T, Miles LA, Takada Y. Specific interaction of angiostatin with integrin alpha(v)beta(3) in endothelial cells. *J Biol Chem.* 2001;276(43):39562-39568.

182. Magnon C, Galaup A, Mullan B, et al. Canstatin acts on endothelial and tumor cells via mitochondrial damage initiated through interaction with alphavbeta3 and alphavbeta5 integrins. *Cancer Res.* 2005;65(10):4353-4361.

183. Rehn M, Veikkola T, Kukk-Valdre E, et al. Interaction of endostatin with integrins implicated in angiogenesis. *Proc Natl Acad Sci U S A.* 2001;98(3):1024-1029.

184. Sudhakar A, Sugimoto H, Yang C, Lively J, Zeisberg M, Kalluri R. Human tumstatin and human endostatin exhibit distinct antiangiogenic activities mediated by alpha v beta 3 and alpha 5 beta 1 integrins. *Proc Natl Acad Sci U S A.* 2003;100(8):4766-4771.

185. Tabatabai G, Weller M, Nabors B, et al. Targeting integrins in malignant glioma. *Target Oncol.* 2010;5(3):175-181.

186. Delbaldo C, Raymond E, Vera K, et al. Phase I and pharmacokinetic study of etaracizumab (Abegrin), a humanized monoclonal antibody against alphavbeta3 integrin receptor, in patients with advanced solid tumors. *Invest New Drugs.* 2008;26(1):35-43.

187. Premaratne GU, Ma LP, Fujita M, Lin X, Bollano E, Fu M. Stromal vascular fraction transplantation as an alternative therapy for ischemic heart failure: anti-inflammatory role. *J Cardiothorac Surg.* 2011;6:43.

188. Granel B, Daumas A, Jouve E, et al. Safety, tolerability and potential efficacy of injection of autologous adipose-derived stromal vascular fraction in the fingers of patients with systemic sclerosis: an open-label phase I trial. *Ann Rheum Dis.* 2015;74(12):2175-2182.

189. Comella K, Parcero J, Bansal H, et al. Effects of the intramyocardial implantation of stromal vascular fraction in patients with chronic ischemic cardiomyopathy. *J Transl Med.* 2016;14(1):158.

190. Atalay S, Coruh A, Deniz K. Stromal vascular fraction improves deep partial thickness burn wound healing. *Burns.* 2014;40(7):1375-1383.

191. Menasche P. How close are we to using stem cells in routine cardiac therapy? *Can J Cardiol.* 2014;30(11):1265-1269.

192. Lai CY, Wu PJ, Roffler SR, et al. Clearance kinetics of biomaterials affects stem cell retention and therapeutic efficacy. *Biomacromolecules.* 2014;15(2):564-573.

193. Cai L, Dewi RE, Heilshorn SC. Injectable Hydrogels with In Situ Double Network Formation Enhance Retention of Transplanted Stem Cells. *Adv Funct Mater.* 2015;25(9):1344-1351.

194. Patel NM, Yazdi IK, Tasciotti E, Birla RK. Optimizing cell seeding and retention in a three-dimensional bioengineered cardiac ventricle: The two-stage cellularization model. *Biotechnol Bioeng.* 2016;113(10):2275-2285.

195. Huang CC, Pan WY, Tseng MT, et al. Enhancement of cell adhesion, retention, and survival of HUVEC/cbMSC aggregates that are transplanted in ischemic tissues by concurrent delivery of an antioxidant for therapeutic angiogenesis. *Biomaterials.* 2016;74:53-63.

196. Burdick JA, Mauck RL, Gerecht S. To Serve and Protect: Hydrogels to Improve Stem Cell-Based Therapies. *Cell Stem Cell.* 2016;18(1):13-15.

197. Follin B, Juhl M, Cohen S, et al. Human adipose-derived stromal cells in a clinically applicable injectable alginate hydrogel: Phenotypic and immunomodulatory evaluation. *Cytotherapy.* 2015;17(8):1104-1118.

198. Silva KR, Rezende RA, Pereira FD, et al. Delivery of Human Adipose Stem Cells Spheroids into Lockyballs. *PLoS One.* 2016;11(11):e0166073.

199. Chen YS, Hsueh YS, Chen YY, Lo CY, Tai HC, Lin FH. Evaluation of a laminin-alginate biomaterial, adipocytes, and adipocyte-derived stem cells interaction in

animal autologous fat grafting model using 7-Tesla magnetic resonance imaging. *J Mater Sci Mater Med.* 2017;28(1):18.

200. Natesan S, Baer DG, Walters TJ, Babu M, Christy RJ. Adipose-derived stem cell delivery into collagen gels using chitosan microspheres. *Tissue Eng Part A.* 2010;16(4):1369-1384.

201. Williams SK, Touroo JS, Church KH, Hoying JB. Encapsulation of adipose stromal vascular fraction cells in alginate hydrogel spheroids using a direct-write three-dimensional printing system. *Biores Open Access.* 2013;2(6):448-454.

202. Lin SD, Huang SH, Lin YN, et al. Injected Implant of Uncultured Stromal Vascular Fraction Loaded Onto a Collagen Gel: In Vivo Study of Adipogenesis and Long-term Outcomes. *Ann Plast Surg.* 2016;76 Suppl 1:S108-116.

203. Aijian AP, Garrell RL. Digital microfluidics for automated hanging drop cell spheroid culture. *J Lab Autom.* 2015;20(3):283-295.

204. Leung BM, Lesher-Perez SC, Matsuoka T, Moraes C, Takayama S. Media additives to promote spheroid circularity and compactness in hanging drop platform. *Biomater Sci.* 2015;3(2):336-344.

205. Chan BP, Hui TY, Wong MY, Yip KH, Chan GC. Mesenchymal stem cell-encapsulated collagen microspheres for bone tissue engineering. *Tissue Eng Part C Methods.* 2010;16(2):225-235.

206. Chan OC, So KF, Chan BP. Fabrication of nano-fibrous collagen microspheres for protein delivery and effects of photochemical crosslinking on release kinetics. *J Control Release.* 2008;129(2):135-143.

207. Keshaw H, Thapar N, Burns AJ, et al. Microporous collagen spheres produced via thermally induced phase separation for tissue regeneration. *Acta Biomater.* 2010;6(3):1158-1166.

208. Yao L, Phan F, Li Y. Collagen microsphere serving as a cell carrier supports oligodendrocyte progenitor cell growth and differentiation for neurite myelination in vitro. *Stem Cell Res Ther.* 2013;4(5):109.

209. Yao R, Zhang R, Luan J, Lin F. Alginate and alginate/gelatin microspheres for human adipose-derived stem cell encapsulation and differentiation. *Biofabrication.* 2012;4(2):025007.

210. Yeo M, Lee JS, Chun W, Kim GH. An Innovative Collagen-Based Cell-Printing Method for Obtaining Human Adipose Stem Cell-Laden Structures Consisting of Core-Sheath Structures for Tissue Engineering. *Biomacromolecules.* 2016;17(4):1365-1375.

211. Chang CC, Boland ED, Williams SK, Hoying JB. Direct-write bioprinting three-dimensional biohybrid systems for future regenerative therapies. *J Biomed Mater Res B Appl Biomater.* 2011;98(1):160-170.

212. Smith CM, Stone AL, Parkhill RL, et al. Three-dimensional bioassembly tool for generating viable tissue-engineered constructs. *Tissue Eng.* 2004;10(9-10):1566-1576.

213. Smith CM, Christian JJ, Warren WL, Williams SK. Characterizing environmental factors that impact the viability of tissue-engineered constructs fabricated by a direct-write bioassembly tool. *Tissue Eng.* 2007;13(2):373-383.

214. Klar AS, Guven S, Biedermann T, et al. Tissue-engineered dermo-epidermal skin grafts prevascularized with adipose-derived cells. *Biomaterials.* 2014;35(19):5065-5078.

215. Vernon RB, Lara SL, Drake CJ, et al. Organized type I collagen influences endothelial patterns during "spontaneous angiogenesis in vitro": planar cultures as models of vascular development. *In Vitro Cell Dev Biol Anim.* 1995;31(2):120-131.

216. Liu Y, Lu J, Li H, Wei J, Li X. Engineering blood vessels through micropatterned co-culture of vascular endothelial and smooth muscle cells on bilayered electrospun fibrous mats with pDNA inoculation. *Acta Biomater.* 2015;11:114-125.

217. Picardo NE, Khan WS. Tissue engineering applications and stem cell approaches to the skin, nerves and blood vessels. *Curr Stem Cell Res Ther.* 2012;7(2):115-121.

218. Kakisis JD, Liapis CD, Breuer C, Sumpio BE. Artificial blood vessel: the Holy Grail of peripheral vascular surgery. *J Vasc Surg.* 2005;41(2):349-354.

219. Stegemann JP, Kaszuba SN, Rowe SL. Review: advances in vascular tissue engineering using protein-based biomaterials. *Tissue Eng.* 2007;13(11):2601-2613.

220. Gong Z, Niklason LE. Blood vessels engineered from human cells. *Trends Cardiovasc Med.* 2006;16(5):153-156.

221. Debakey ME, Jordan GL, Jr., Abbott JP, Halpert B, O'Neal RM. The Fate of Dacron Vascular Grafts. *Arch Surg.* 1964;89:757-782.

222. Sayers RD, Raptis S, Berce M, Miller JH. Long-term results of femorotibial bypass with vein or polytetrafluoroethylene. *Br J Surg.* 1998;85(7):934-938.

223. Barnes CP, Sell SA, Boland ED, Simpson DG, Bowlin GL. Nanofiber technology: designing the next generation of tissue engineering scaffolds. *Adv Drug Deliv Rev.* 2007;59(14):1413-1433.

224. Leach MK, Feng ZQ, Tuck SJ, Corey JM. Electrospinning Fundamentals: Optimizing Solution and Apparatus Parameters. *Journal of Visualized Experiments : JoVE.* 2011(47).

225. Pu J, Yuan F, Li S, Komvopoulos K. Electrospun bilayer fibrous scaffolds for enhanced cell infiltration and vascularization in vivo. *Acta Biomater.* 2015;13:131-141.

226. de Valence S, Tille JC, Mugnai D, et al. Long term performance of polycaprolactone vascular grafts in a rat abdominal aorta replacement model. *Biomaterials.* 2012;33(1):38-47.

227. Nottelet B, Pektok E, Mandracchia D, et al. Factorial design optimization and in vivo feasibility of poly(epsilon-caprolactone)-micro- and nanofiber-based small diameter vascular grafts. *J Biomed Mater Res A.* 2009;89(4):865-875.

228. Inoguchi H, Kwon IK, Inoue E, Takamizawa K, Maehara Y, Matsuda T. Mechanical responses of a compliant electrospun poly(L-lactide-co-epsilon-caprolactone) small-diameter vascular graft. *Biomaterials.* 2006;27(8):1470-1478.

229. Mun CH, Jung Y, Kim SH, et al. Three-dimensional electrospun poly(lactide-co-varepsilon-caprolactone) for small-diameter vascular grafts. *Tissue Eng Part A.* 2012;18(15-16):1608-1616.

230. Mun CH, Jung Y, Kim SH, Kim HC, Kim SH. Effects of pulsatile bioreactor culture on vascular smooth muscle cells seeded on electrospun poly (lactide-co-epsilon-caprolactone) scaffold. *Artificial organs.* 2013;37(12):E168-178.

231. Theron JP, Knoetze JH, Sanderson RD, et al. Modification, crosslinking and reactive electrospinning of a thermoplastic medical polyurethane for vascular graft applications. *Acta Biomater.* 2010;6(7):2434-2447.

232. Uttayarat P, Perets A, Li M, et al. Micropatterning of three-dimensional electrospun polyurethane vascular grafts. *Acta Biomater.* 2010;6(11):4229-4237.

233. Dargaville BL, Vaquette C, Rasoul F, Cooper-White JJ, Campbell JH, Whittaker AK. Electrospinning and crosslinking of low-molecular-weight poly(trimethylene carbonate-co-(L)-lactide) as an elastomeric scaffold for vascular engineering. *Acta Biomater.* 2013;9(6):6885-6897.

234. Woodruff MA, Hutmacher DW. The return of a forgotten polymer—Polycaprolactone in the 21st century. *Progress in Polymer Science.* 2010;35(10):1217-1256.

235. McManus M, Boland E, Sell S, et al. Electrospun nanofibre fibrinogen for urinary tract tissue reconstruction. *Biomed Mater.* 2007;2(4):257-262.

236. Sun H, Mei L, Song C, Cui X, Wang P. The in vivo degradation, absorption and excretion of PCL-based implant. *Biomaterials.* 2006;27(9):1735-1740.

237. Lotfi M, Ghasemi N, Rahimi S, Vosoughhosseini S, Saghiri MA, Shahidi A. Resilon: A Comprehensive Literature Review. *Journal of Dental Research, Dental Clinics, Dental Prospects.* 2013;7(3):119-130.

238. Schantz JT, Hutmacher DW, Lam CX, et al. Repair of calvarial defects with customised tissue-engineered bone grafts II. Evaluation of cellular efficiency and efficacy in vivo. *Tissue Eng.* 2003;9 Suppl 1:S127-139.

239. Bagherzadeh R, Latifi M, Najar SS, Kong L. Three-dimensional pore structure analysis of Nano/Microfibrous scaffolds using confocal laser scanning microscopy. *Journal of Biomedical Materials Research Part A.* 2013;101(3):765-774.

240. Bagherzadeh R, Latifi M, Kong L. Three-dimensional pore structure analysis of polycaprolactone nano-microfibrous scaffolds using theoretical and experimental approaches. *Journal of Biomedical Materials Research Part A.* 2014;102(3):903-910.

241. Joshi VS, Lei NY, Walthers CM, Wu B, Dunn JC. Macroporosity enhances vascularization of electrospun scaffolds. *Journal of Surgical Research.* 2013;183(1):18-26.

242. Mikhalovska L, Grant P, Tomlins P, Mikhalovsky S, James S. Measurement of pore size and porosity of tissue scaffolds. *Journal of ASTM International.* 2004;1(1):1-8.

243. Rnjak-Kovacina J, Wise SG, Li Z, et al. Tailoring the porosity and pore size of electrospun synthetic human elastin scaffolds for dermal tissue engineering. *Biomaterials.* 2011;32(28):6729-6736.

244. Di Luca A, Szlazak K, Lorenzo-Moldero I, et al. Influencing chondrogenic differentiation of human mesenchymal stromal cells in scaffolds displaying a structural gradient in pore size. *Acta Biomaterialia.* 2016;36:210-219.

245. Park S-N, Park J-C, Kim HO, Song MJ, Suh H. Characterization of porous collagen/hyaluronic acid scaffold modified by 1-ethyl-3-(3-dimethylaminopropyl)carbodiimide cross-linking. *Biomaterials.* 2002;23(4):1205-1212.

246. Jin G, Lee S, Kim S-H, Kim M, Jang J-H. Bicomponent electrospinning to fabricate three-dimensional hydrogel-hybrid nanofibrous scaffolds with spatial fiber tortuosity. *Biomedical microdevices.* 2014;16(6):793-804.

247. Ho ST, Hutmacher DW. A comparison of micro CT with other techniques used in the characterization of scaffolds. *Biomaterials.* 2006;27(8):1362-1376.

248. Zhao YN, Fan JJ, Li ZQ, Liu YW, Wu YP, Liu J. Effects of Pore Size on the Osteoconductivity and Mechanical Properties of Calcium Phosphate Cement in a Rabbit Model. *Artificial organs.* 2016.

249. Aarvold A, Smith JO, Tayton ER, et al. The effect of porosity of a biphasic ceramic scaffold on human skeletal stem cell growth and differentiation in vivo. *J Biomed Mater Res A.* 2013;101(12):3431-3437.

250. Dahlin RL, Kasper FK, Mikos AG. Polymeric nanofibers in tissue engineering. *Tissue Engineering Part B: Reviews.* 2011;17(5):349-364.

251. Pham QP, Sharma U, Mikos AG. Electrospun poly (ε-caprolactone) microfiber and multilayer nanofiber/microfiber scaffolds: characterization of scaffolds and measurement of cellular infiltration. *Biomacromolecules.* 2006;7(10):2796-2805.

252. Nguyen TH, Padalhin AR, Seo HS, Lee BT. A hybrid electrospun PU/PCL scaffold satisfied the requirements of blood vessel prosthesis in terms of

mechanical properties, pore size, and biocompatibility. *Journal of biomaterials science Polymer edition.* 2013;24(14):1692-1706.

253. Giesche H. Mercury Porosimetry: A General (Practical) Overview. *Particle & Particle Systems Characterization.* 2006;23(1):9-19.

254. Drasler WJ, Wilson GJ, Jenson ML, et al. Venturi grafts for hemodialysis access. *ASAIO Trans.* 1990;36(3):M753-757.

255. Emery RW, Petersen R, Baumgard C, Nicoloff DM. First clinical use of the Possis synthetic coronary graft. *J Card Surg.* 1993;8(4):439-442.

256. Schoenenberger AD, Foolen J, Moor P, Silvan U, Snedeker JG. Substrate fiber alignment mediates tendon cell response to inflammatory signaling. *Acta Biomater.* 2018.

257. Tan Z, Gao X, Liu T, et al. Electrospun vein grafts with high cell infiltration for vascular tissue engineering. *Mater Sci Eng C Mater Biol Appl.* 2017;81:407-415.

258. Wang K, Zhu M, Li T, et al. Improvement of cell infiltration in electrospun polycaprolactone scaffolds for the construction of vascular grafts. *J Biomed Nanotechnol.* 2014;10(8):1588-1598.

CURRICULUM VITA

| | |
|---|---|
| NAME: | Joseph Samir Zakhari |
| ADDRESS: | Cardiovascular Innovation Institute<br>University of Louisville School of Medicine<br>302 E. Muhammad Ali Boulevard<br>Suite 204<br>Louisville, KY 40202 |
| DOB: | Cheverly, Maryland – April 27, 1987 |
| EDUCATION & TRAINING: | M.D. (expected May 2020)<br>University of Louisville School of Medicine<br>2013-present<br><br>Ph.D. (expected May 2018)<br>Physiology and Biophysics<br>University of Louisville School of Medicine<br>2015-2018<br><br>M.A., Medical Science<br>Boston University School of Medicine<br>2011-2013<br><br>B.S., Biology<br>Wake Forest University<br>2005-2009 |
| AWARDS & HONORS: | IFATS Best Poster Presentation<br>2017<br><br>IFATS Best Poster Presentation<br>2016<br><br>Honors Thesis Presentation: “The Mechanism of Histatin 5 Induced Cell Death in Saccharomyces Cerevisiae”<br>2013 |

Dean's List
2009

SCHOLARSHIPS & FELLOWSHIPS:

Integrated Programs in the Biomedical Science(IPIBS) Graduate Fellowship
2015-2016

Summer Research Scholars Program (SRSP)
2013, 2014

Physician-Scientist Training Program (M.D./Ph.D.) Scholarship
2013-present

PROFESSIONAL SOCIETIES:

American Heart Association
2015-present

American Physician Scientists Association
2013-present

Greater Louisville Medical Societies
2013-present

PUBLICATIONS:

1. **Zakhari JS**, Zabonick J Gettler B, Williams SK. Vasculogenic and angiogenic potential of adipose stromal vascular fraction cell populations in vitro. *In Vitro Cellular Development Biology*. January 2018.

2. Gettler BC, **Zakhari JS**, Gandhi PS, Williams SK. Formation of adipose stromal vascular fraction cell-laden spheroids using a three-dimensional bioprinter and superhydrophobic surfaces. *Tissue Engineeering Part C.* September 2017.

3. Stowe GN, Shlosburg JE, Vendruscolo LF, Edwards S, Misra KK, Schulteis G, **Zakhari JS**, Koob GF, and Janda KD. Developing a Vaccine Against Multiple Psychoactive Targets: A Case Study of Heroin. *CNS and Neurological Disorders Drug Targets*. January 2012.

4. **Zakhari JS,** Zorrilla EP, Zhou B, Mayorov AV, and Janda KD. Oligoclonal Antibody Targeting Ghrelin Increases Energy Expenditure and Reduces Food Intake in Fasted Mice. *Molecular Pharmaceutics*. December 2011.

5. **Zakhari JS,** Kinoyama I, Hixon MS, Di Mola A, Globisch D, and Janda KD. Formulating A New Basis For the Treatment Against Botulinum Neurotoxin Intoxication: 3,4-Diaminopyridine Prodrug Design and Characterization. *Bioorganic and Medicinal Chemistry.* November 2011.

6. Garner AL, Park J, **Zakhari JS,** Lowery CA, Struss AK, Sawada D, Kaufmann GF, and Janda KD. A Multivalent Probe For AI-2 Quorum-Sensing Receptors. Journal of the American Chemical Society. October 2011.

7. Stowe GN, Vendruscolo LF, Edwards S, Schlosburg JE, Misra KK, Schelteis G, Mayorov AV, **Zakhari JS,** Koob GF, and Janda KD. A Vaccine Strategy That Induces Protective Immunity Against Heroin. *Journal of Medicinal Chemistry.* July 2011.

8. Garner AL, Gloeckner C, Tricoche N, **Zakhari JS**, Samje M, Cho-Ngwa F, Lustigman S, and Janda KD. Design, Synthesis and Biological Activities of Closantel Analogues: Structural Promiscuity and its Impact on Onchocerca volvulus. Journal of Medicinal Chemistry. June 2011.

9. **Zakhari JS,** Kinoyama I, Struss AK, Pullanikat P, Lowery CA, Lardy M, and Janda KD. Synthesis and Molecular Modeling Provide Insight into a *Pseudomonas aeruginosa* Quorum Sensing Conundrum. *Journal of the American Chemical Society*. February 2011.

10. Salzameda NT, Eubanks LM, **Zakhari JS,** Tsuchikama K, DeNunzio NJ, Allen KN, Hixon MS, and Janda KD. A cross-over inhibitor of the botulinum neurotoxin light chain B: a natural product implicating an exosite mechanism of action. *Chemical Communications.* December 2010.

11. Eubanks LM, Silhar P, Salzameda NT, **Zakhari JS,** Xiaochuan F, Barbieri JT, Shoemaker CB, Hixon MS, and Janda KD. Identification of a Natural Product Antagonist against the Botulinum Neurotoxin Light Chain Protease. *American Chemical Society Medicinal Chemistry Letters*. June 2010.

ABSTRACT ORAL & POSTER PRESENTATIONS:

1. "Piroxicam reduces residual collagenase activity in enzymatically-derived stromal vascular fraction." **J.S. Zakhari**, S.K. Williams. 15th Annual IFATS Meeting, Miami FL (11/2017).

2. "3D bioprinting the cardiac purkinje system using human adipogenic mesenchymal stem cell derived purkinje cells." E. Tracy, B Gettler, **J.S.**

**Zakhari**, S.K. Williams, R. Birla, R. Schwartz. Research! Louisville 2017 Annual Meeting, University of Louisville, Louisville KY (10/2017)

3. "Stromal vascular fraction undergoes vasculogenesis and angiogenesis in a novel in vitro assay." **J.S. Zakhari**, S.K. Williams. 32nd Annual MD/PhD National Student Conference, Keystone CO (07/2017)

4. "Automated stromal vascular fraction spheroid production using 3D bioprinting in conjunction with a combination hydrophobic/hydrophilic surface treatment." B.C. Gettler, P.S. Gandhi, **J.S. Zakhari**, S.K. Williams. 14th Annual IFATS Meeting, San Diego CA (11/2016)

5. "An in vitro functional assay of vasculogenesis and angiogenesis using freshly isolated adipose stromal vascular fraction cells." **J.S. Zakhari**, J.A. Zabonick, B.C. Gettler, B. Tweed, B. Apakalai, S.K. Williams. 14th Annual IFATS Meeting, San Diego CA (11/2016)

6. "An in vitro functional assay of vasculogenesis and angiogenesis using freshly isolated adipose stromal vascular fraction cells." **J.S. Zakhari**, J.A. Zabonick, B.C. Gettler, B. Tweed, B. Apakalai, S.K. Williams. Research! Louisville 2016 Annual Meeting, University of Louisville, Louisville KY (10/2016)

7. "Porcine extracellular matrix injection in ischemic myocardium as mechanical therapy for heart failure." **J. S. Zakhari**, K. Soucy, M.S. Slaughter, and S.C. Koenig. Research! Louisville 2015 Annual Meeting, University of Louisville, Louisville KY (10/2015)

PATENTS: "Spheroids including biologically-relevent materials and related methods"
S.K. Williams, B.C. Gettler, **J.S. Zakhari**, P.S. Gandhi.
Publication # WO2018005477A1
Application # PCT/US2017/039483
2016

INVITED PRESENTATIONS:

1. "An in vitro functional assay of vasculogenesis and angiogenesis using freshly isolated adipose stromal vascular fraction cells." Cardiovascular Innovation Institute, University of Louisville School of Medicine, (05/2017)